AFML-TR-76-222

RESEARCH TOWARD DEVELOPING AN UNDERSTANDING OF CRYSTALLOGRAPHIC TEXTURE ON MECHANICAL PROPERTIES OF TITANIUM ALLOYS

DEL WEST ASSOCIATES, INC.
6324 VARIEL AVENUE
WOODLAND HILL, CA 91367

JANUARY 1977

TECHNICAL REPORT AFML-TR-76-222
FINAL REPORT FOR PERIOD JUNE 1974 - AUGUST 1976

AIR FORCE MATERIALS LABORATORY
AIR FORCE WRIGHT AERONAUTICAL LABORATORIES
AIR FORCE SYSTEMS COMMAND
WRIGHT-PATTERSON AIR FORCE BASE, OHIO 45433

NOTICE

When Government drawings, specifications, or other data are used for any purpose other than in connection with a definitely related Government procurement operation, the United States Government thereby incurs no responsibility nor any obligation whatsoever; and the fact that the government may have formulated, furnished, or in any way supplied the said drawings, specifications, or other data, is not to be regarded by implication or otherwise as in any manner licensing the holder or any other person or corporation, or conveying any rights or permission to manufacture, use, or sell any patented invention that may in any way be related thereto.

This final report was submitted by Del West Associates, Inc. 6324 Variel Avenue, Woodland Hills, CA 91367 under Contract F33615-74-C-5107, Job Order 73510568 with the Air Force Materials Laboratory, Wright-Patterson Air Force Base, Ohio 45433. Dr. S. Fujishiro, AFML/LLS was the laboratory project engineer.

This technical report has been reviewed and is approved for publication.

Shiro Fujishiro

SHIRO FUJISHIRO
Project Engineer
Structural Metals Branch
Metals and Ceramics Division

FOR THE COMMANDER

Nathan G. Tupper

NATHAN G. TUPPER
Acting Chief
Structural Metals Branch
Metals and Ceramics Division

Copies of this report should not be returned unless return is required by security considerations, contractual obligations, or notice on a specific document.

UNCLASSIFIED

SECURITY CLASSIFICATION OF THIS PAGE (When Data Entered)

REPORT DOCUMENTATION PAGE

READ INSTRUCTIONS BEFORE COMPLETING FORM

1. REPORT NUMBER: AFML-TR-76-222	2. GOVT ACCESSION NO.
3. RECIPIENT'S CATALOG NUMBER	
4. TITLE (and Subtitle): RESEARCH TOWARD DEVELOPING AN UNDERSTANDING OF CRYSTALLOGRAPHIC TEXTURE ON MECHANICAL PROPERTIES OF TITANIUM ALLOYS.	5. TYPE OF REPORT & PERIOD COVERED: FINAL TECHNICAL REPORT JUN 74 — AUG 76
	6. PERFORMING ORG. REPORT NUMBER: DW12-1
7. AUTHOR(s): Sommer, A. W. / Sommer; Kroeger, M. / Kroeger	8. CONTRACT OR GRANT NUMBER(s): F33615-74-C-5107
9. PERFORMING ORGANIZATION NAME AND ADDRESS: Del West Associates, Inc. 6324 Variel Avenue Woodland Hills, CA 91367	10. PROGRAM ELEMENT, PROJECT, TASK AREA & WORK UNIT NUMBERS: 73510568
11. CONTROLLING OFFICE NAME AND ADDRESS: Air Force Materials Laboratory Air Force Systems Command Wright-Patterson Air Force Base, OH 45433	12. REPORT DATE: Jan 77
	13. NUMBER OF PAGES: 229 (12) 226p
14. MONITORING AGENCY NAME & ADDRESS (if different from Controlling Office): Same as Block 11	15. SECURITY CLASS. (of this report): Unclassified
	15a. DECLASSIFICATION DOWNGRADING SCHEDULE: NA

16. DISTRIBUTION STATEMENT (of this Report)

Approved for public release; distribution unlimited.

17. DISTRIBUTION STATEMENT (of the abstract entered in Block 20, if different from Report)

Same as Block 16

18. SUPPLEMENTARY NOTES

391217

19. KEY WORDS (Continue on reverse side if necessary and identify by block number)

Crystallographic Texture; Ti Alloys; Thermomechanical Processing; Mechanical Properties, Fatigue Crack Growth, Corrosion Fatigue, R-Curves, Fracture Toughness, Creep, Cyclic Stress: Strain; Fractography, 6Al-4V Ti; 6Al-2Sn-4Zr-6Mo Ti.

20. ABSTRACT (Continue on reverse side if necessary and identify by block number)

Research was conducted during this effort to define the relationship(s) between mechanical properties and crystallographic texture development in three commonly used $\alpha + \beta$ Ti alloys compositions. Texture development was monitored during the conversion of production ingot stock to one quarter inch thick rolled plate as a function of thermomechanical processing. The three alloy compositions were: 6Al-4V Ti ELI Grade, 6Al-4V Ti Standard Grade, and 6Al-2Sn-4Zr-6Mo Ti. Sufficient quantities of one specific textural type, basal transverse, were produced for all three compositions to permit extensive mechanical and

DD FORM 1 JAN 73 1473 EDITION OF 1 NOV 65 IS OBSOLETE

UNCLASSIFIED

SECURITY CLASSIFICATION OF THIS PAGE (When Data Entered)

20. ABSTRACT: (Continued)

fracture property testing at room and elevated temperature as a function of product orientation. Material properties evaluated were: elastic modulus, monotonic stress: strain behavior, cyclic stress: strain behavior, notched and unnotched fatigue, fracture toughness (Resistance Curves), K_{ISCC} and da/dN vs. ΔK. The last two properties were evaluated in both lab air and 3.5% NaCl in H_2O as a function of final thermal practice.

Results of this study include the establishment of the conditions required for the production of either a basal transverse texture or an isotropic basal pole array in equiaxed microstructures of all three alloy chemistries. Additionally, the uniaxial unnotched mechanical properties of strongly basal transverse textured 6Al-4V Ti and 6Al-2Sn-4Zr-6Mo Ti have been shown to be highly anisotropic in the temperature range 70°F to 1000°F. Crack growth velocities induced by either static or fatigue loading in basal transverse textures 6Al-4V Ti and 6Al-2Sn-4Zr-6Mo Ti alloys are not only a strong function of alpha phase crystallography but are as well significantly dependent on final thermal practice and detailed alloy chemistry.

PREFACE

This report was prepared by Del West Associates, Inc., Woodland Hills, Ca under USAF Contract No. F33615-74-C-5107. The contract work was performed under Project 7351 administered under the Air Force Material Laboratory, Air Force Systems Command, Wright-Patterson AFB, Ohio with Dr. S. Fujishiro as Project Engineer.

Dr. A. W. Sommer served as Program Manager for Del West Associates, Inc., and directed all activities. Dr. M. Creager of Del West served as Principal Investigator. This report has been assigned Del West No. DW12-1 for internal control purposes.

The reporting period extends from June, 1974 to August, 1976.

The authors wish to acknowledge several members of the Crucible Steel Materials Research Center, Pittsburgh, Pa whose help, patience and whole-hearted cooperation were pivotal in providing not only the raw material required for the Program but also many of the measurements and observations recorded in Part I of this

report. They are Mr. Vincent Peterson, Dr. F. R. Froes, Dr. M. G. H. Wells, and Mr. Frank Malone. Additionally, we wish to thank Professor Kanji Ono of UCLA and Dr. G. A. Alers of the Rockwell Science Center, Thousand Oaks, Ca for making all the dynamic Young's Modulus measurements required for our textural determinations as well as the Boeing Co. for their X-ray pole figure measurements. Finally we wish to thank Dr. Fujishiro not only for his encouragement and helpful suggestions during the course of the study but also for making the creep measurements reported in Part II.

This report was released by the authors on December, 1976

TABLE OF CONTENTS

LIST OF TABLES

LIST OF TABLES (Cont.)

LIST OF FIGURES

PART I

LIST OF FIGURES (Cont.)

LIST OF FIGURES (Cont.)

LIST OF FIGURES (Cont.)

PART III (Cont.) PAGE

LIST OF FIGURES (Cont.)

PART III (Cont.) PAGE

FIGURE

INTRODUCTION

The research conducted during this Program involved substantial efforts in primary production process metallurgy; conventional physical metallurgy/mechanical property evaluations; and fracture property/microstructure interactions employing three widely used $\alpha + \beta$ Ti alloy compositions. We considered the diversity of results obtained here and assumed that certain readers may only be interested in say process metallurgy results as opposed to conventional physical/mechanical metallurgy evaluations and/or fracture/microstructure behavior patterns. On this basis, we decided to partition the total sum of results obtained here by principal subject matter under one of the three following subsections:

PART I - CRYSTALLOGRAPHIC TEXTURE DEVELOPMENT IN $\alpha + \beta$ TITANIUM ALLOYS

PART II - ON THE MECHANICAL BEHAVIOR OF BASAL TRANSVERSE TEXTURED TITANIUM ALLOYS

PART III - ON THE GROWTH OF CRACKS IN BASAL TRANSVERSE TEXTURED $\alpha + \beta$ TITANIUM ALLOYS AS A FUNCTION OF CHEMICAL ENVIRONMENT

Each Part is a complete entity containing its own set of relevant Tables, Figures, References, etc. Thus, the reader

who is only interested in the details associated with a portion of this rather broad ranged study can easily by-pass those portions of the work which are of lesser interest to him. In order that all readers may have the opportunity to overview the total sum of results obtained here, we have also included a Section labelled SUMMARY.

SUMMARY

Research was conducted during this effort to define the relationship(s) between mechanical properties and crystallographic texture development in three commonly used $\alpha + \beta$ Ti alloy compositions. Texture development was monitored during the conversion of production ingot stock to one quarter inch thick rolled plate as a function of thermomechanical processing. The three alloy compositions were: 6Al-4V Ti ELI Grade, 6Al-4V Ti Standard Grade, and 6Al-2Sn-4Zr-6Mo Ti. Sufficient quantities of one specific textural type, basal transverse, were produced for all three compositions to permit extensive mechanical and fracture property testing at room and elevated temperature as a function of product orientation. Material properties evaluated were: elastic modulus, monotonic stress: strain behavior, cyclic stress:strain behavior, notched and unnotched fatigue, fracture toughness (Resistance Curves), K_{ISCC} and da/dn vs. ΔK. The last two properties were evaluated in both lab air and 3.5% NaCl in H_2O as a function of final thermal practice.

Results of this effort include the establishment of the conditions required for the production of either a basal transverse texture

or an isotropic basal pole array in equiaxed microstructures of all three alloy chemistries. The role played by post rolling thermal practice in altering and/or intensifying α Ti crystallographic textures has been modelled and experimentally corroborated. Experimentally verified deformation mechanisms are presented to elucidate the over-riding role played by prior thermomechanical billet/plate rolling process history in determining the final crystallogrphic textures a given product will exhibit. This rationale extends even to the case where the starting perferredly oriented material is additionally worked an additional 90% (reduction in thickness) under a wide variety of conditions.

The uniaxial unnotched mechanical properties of strongly basal transverse textured 6Al-4V Ti and 6Al-2Sn-4Zr-6Mo Ti have been shown to be highly anisotropic in the temperature range 70°F to 1000°F. All three alloy chemistries showed a 20% improvement in Young's Modulus at 70°F when results obtained in the long transverse direction were compared with data taken parallel to the rolling direction. For example, the two 6Al-4V Ti chemistries achieved Young's Moduli in excess of 20 x 10^6 psi in the long transverse direction at 70°F. Similarly, 25% improvements in both monotonic and cyclic tensile properties were also observed at 70°F when long transverse direction oriented samples of all three

materials were compared to their rolling direction counterparts. Moreover, the cyclic compression yield strength of the 6Al-4V Ti ELI Grade composition at 70°F in the long transverse direction was 188 Ksi vs. 94 Ksi in the rolling direction. All of the above quoted 70°F strength and Young's Moduli differences with orientation increased significantly when the above measurements were remade at 700°F. Smooth fatigue lives in 6Al-4V Ti were also improved in the long transverse direction at all stress levels. Notched fatigue S-N data (K_t=4) were the same for both orientations in all three alloy chemistries. In the temperature range 700°F - 1000°F, the creep resistance parallel to the long transverse direction in 6Al-4V Ti was always found to be significantly better than its rolling direction counterpart. The creep resistance of the 6Al-4V Ti composition was also found to be a function of test environment with the material in both orientations observed to be significantly more creep resistant in vacuum (3 x 10^{-6} mm of H_g) than in lab air. Microstructural/crystallographic mechanisms are offered to rationalize the several mechanical property improvements noted in this work.

Crack growth velocities induced by either static or fatigue loading in basal transverse textured 6Al-4V Ti and 6Al-2Sn-4Zr-6Mo Ti alloys are not only a strong function of alpha phase crystallography, but are as well significantly dependent on final thermal

practice and detailed alloy chemistry. Working with strongly basal transverse textured versions of both generic alloy compositions, two crystallographically distinct modes of cleavage fracture have been identified during fatigue at low ΔK. These are (1) the well known "near basal" cleavage observed in both lab air and 3.5% NaCl in H_2O and (2) cleavage on or near the prism plane of the alpha phase which only occurred during salt water testing. The velocity of cracks propagating via a "near basal" cleavage mode is very sensitive to minor changes in final thermal processing and alloy chemistry. Combinations of such small changes can alter the observed crack growth rates by a factor of 100 during fatigue in 3.5% NaCl in H_2O. In contrast to the extreme velocity sensitivity of "near basal" cleavage to minor metallurgical changes, prism cleavage is virtually insensitive to such changes.

For example, the fatigue crack growth rates (in lab air and salt water) associated with "near basal" cleavage in 6Al-4V Ti were found to be very sensitive functions of the final cooling rate the product sees the last time it is stabilized at a temperature of 1400°F or above. This alloy composition cracked 10 times faster at 2 hertz in 3.5 NaCl in H_2O when it was furnace cooled from 1400°F to 70°F (<100°F/hr.) than when it was air cooled through this same temperature (>2000°F/hr.) In this regard, several new cost saving Ti fabrication methods (diffusion bonding, superplastic

forming and isothermal forging) effect their cost saving by producing a virtually "net part" through metal flow above 1400°F in the case of 6Al-4V Ti. These "net parts" are then slowly cooled in their tooling to room temperature for use in this final heat treatment state. Recognizing the potential problems that could arise as these novel manufacturing practices are adopted for use in the aerospace industry, recommendations are presented for their avoidance and specific tasks are suggested for additional research in this important area.

A hypothesis is proposed to account for "near basal" cleavage crack growth observed under static and fatigue loadings in lab air and 3.5% NaCl in H_2O environments. The model predicts that the velocity of such "near basal" cleavage cracks is a product of some function of the alloy's hydrogen concentration times some function related to the degree of short/long range ordering of Al and O in the alpha phase. The metallurgical origins of prism cleavage are unclear at this time.

PART I

CRYSTALLOGRAPHIC TEXTURE DEVELOPMENT IN $\alpha + \beta$ TITANIUM ALLOYS

Textures arise as a result of extensive plastic deformation usually in one direction, and may be modified or strengthened by subsequent recrystallization annealing. In titanium alloys where the hexagonal phase predominates, the textures which develop are usually described in terms of the orientation of the basal plane (0001). The basal textures which develop in titanium alloys during deformation operations can be broadly classified as those in which the basal planes are parallel with the rolling plane (Figure 1(a)) and those in which the basal planes are normal to the rolling plane (Figure 1(b)). The former textures are well documented to result in improved biaxial strength properties (References 1-4). The latter textures, by contrast, produce mechanical property anisotropy in the rolling plane (References 5-7).

Development of rolling practices suitable for generation of biaxially strengthened 6Al-4V titanium alloy products (i.e., Figure 1(a) textures) has been studied extensively (References 1-4). In order to produce a strong Figure 1(a) type texture

SCHEMATIC VIEW OF ALPHA PHASE TEXTURED PLATES & THEIR CORRESPONDING BASAL PLANE POLE FIGURES

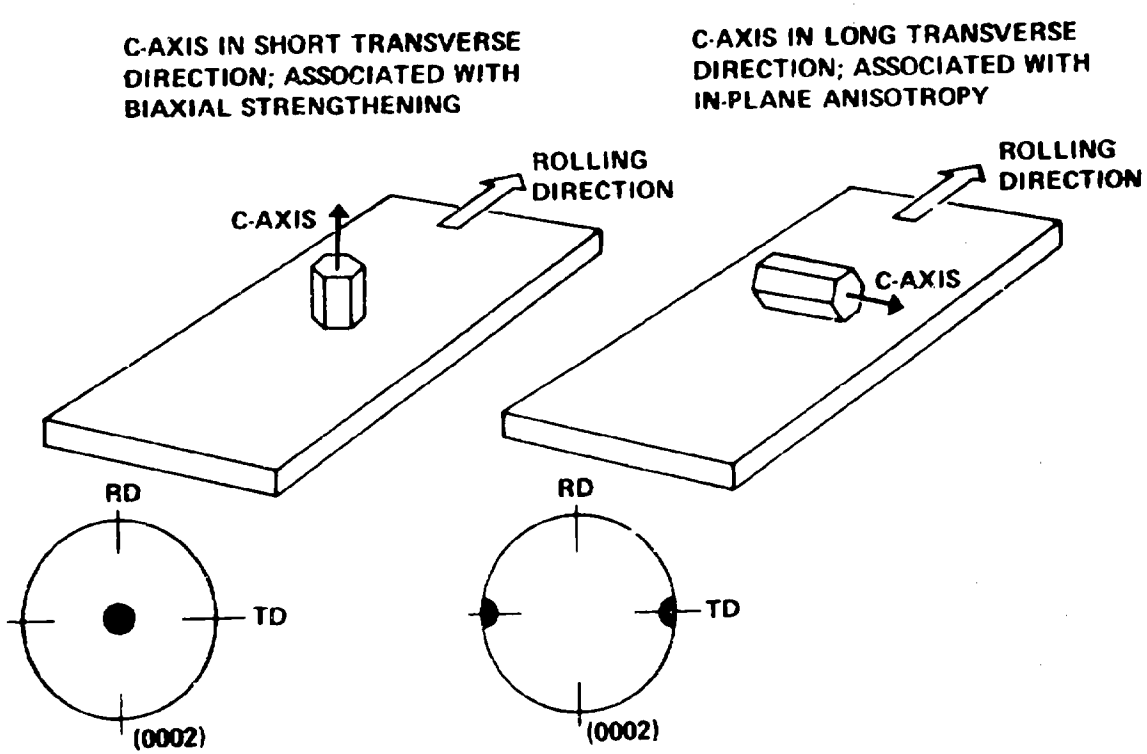

Figure 1

texture in 6Al-4V Ti, one requires that a substantial amount of deformation (>85% reduction in area, see References 1-4) be imparted to the metal in the temperature range 1000°F - 1500°F. In this temperature range, the alpha phase volume fraction always exceeds 85%.

Texture development for biaxial strength thus controlled by the deformation behavior of the alpha phase. Moreover, the equilibrium chemical composition of the alpha phase in 6Al-4V Ti approximates that of the binary alloy Ti 6.6 wt.% Al. In this regard, Paton et al (Reference 8) have studied the temperature and alloy composition dependence of plastic flow in Ti-Al single crystals. Their work indicates that the critical resolved shear stresses (crss) for basal and prism slip modes with a $\langle 11\bar{2}0 \rangle$ vector are equal above 500°F. By contrast, the crss for $\langle \vec{c} + \vec{a} \rangle$ vector slip is uniformly a factor of 5 higher than that for $\langle \vec{a} \rangle$ vector slip between 500°F and 1400°F. One thus expects the extensive deformation associated with a rolling mill campaign involving alpha Ti to be controlled by $\langle \vec{a} \rangle$ vector slip. Elementary textbooks generally describe slip controlled deformation texture evolution in terms of rotation of the active slip plane into an orientation normal to the axis of rolling compression with the active slip direction parallel to the rolling tensile axis (or rolling direction). Based on the above

one would predict that extensive unidirectional rolling of an $\alpha + \beta$ Ti alloy such as 6Al-4V Ti below 1500°F should produce basal pole texture wherein the <0001> vectors are uniformly distributed along a great circle connecting the short transverse and width directions of the rolled product.

Support for the above texture development model can be found in the works of Harrigan et al (Reference 4) and Fitzpatrick and Crossley (Reference 1). In both works, extensive unidirectional rolling of 6Al-4V Ti sheet at 1300°F from previously isotropic billets resulted in a preferred orientation of basal poles distributed along the great circle connecting the thickness and width directions of the sheet product. Fitzpatrick and Crossley (Reference 1) demonstrated this same pole figure was also obtainable on the unidirectional rolling of 7Al-2.5Mo Ti sheet in the temperature range.

In order to obtain the perfect biaxial strengthening texture shown in Figure 1(a), Fitzpatrick and Crossley (Reference 1) and Fredericks (Reference 3) extensively cross-rolled their 6Al-4V Ti sheet and plate products in the temperature range

$1000^{\circ}F$ - $1500^{\circ}F$. By continually changing rolling direction between reduction passes, the slip anisotropy of the hexagonal phase ($\tau_{crss}^{basal} = \tau_{crss}^{prism} = 1/5 \times \tau_{crss}^{<c+a>}$, Reference 8) forces rotation of all basal poles previously in the rolling plane to a direction parallel to the products thickness direction in order to provide the metal with continued deformation capability as opposed to cracking. This latter observation provides yet another bit of evidence attesting to the validity of the "alpha phase slip anistropy" model for Figure 1(a) texture development.

Figure 1(b) presents an ideal basal transverse pole figure. In contrast with our relatively high level of understanding of the production methods required to generate the Figure 1(a) texture, no general agreement exists as to the mechanism by which this textural type evolves. Nor has any investigator begun his rolling campaign with billet whose crystallographic texture was demonstrated to be random initially and generated a strong basal transverse texture from scratch, as it were. Two investigators, Fredericks (Reference 3) and Zarkades and Larson References 6 and 7), have proposed models to account for this textural type often found in commercially rolled $\alpha + \beta$ Ti alloy and plate.

Fredericks hypothesized that the basal transverse alpha phase texture results from a strain controlled beta to alpha transformation. Specifically, he points out that if one transforms the conventional bcc coldwork texture, (100) [110], via the Burgers relation with the additional constraint that the only permissible alpha variant formed is that which introduces transformation strains compatible with the ongoing rolling deformation (i.e., a large tensile strain in the rolling direction, a large compression strain in the thickness direction and a very small tensile strain in the width direction), his result is an alpha phase product with a basal transverse texture. Consequently, he argues that this texture will most readily form when 50% or more of the metal volume is bet (i.e., roll near the beta transus in $\alpha + \beta$ alloys). Zarkades and Larson (Reference 6) also recommend rolling near but below the beta transus in order to obtain our desired basal transverse texture. However, their concept of the manner in which this texture is formed is quite different than that of Fredericks. The latter authors postulate the texture forms as a result of increased $\{11\bar{2}2\}$ twinning which these authors theorize occurs preferentially in the alpha phase when at least 25% of the overall microstructural volume is occupied by the beta phase (see Figure 2).

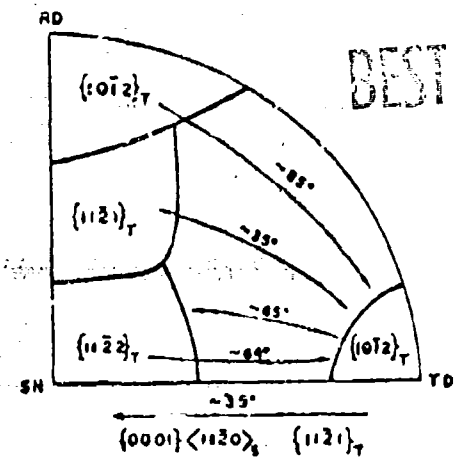

Figure 2: Rotations of the (0001) pole due to various twin and slip modes (taken from Reference 6).

It thus appears that one should be able to control the basal deformation texture of α + β Ti alloys by simply controlling rolling temperature and extent of cross-rolling. That is to say extensive unidirectional rolling at temperatures near the beta transus should produce a strong basal transverse texture. Recall that similar rolling campaigns begun below 1500°F have been shown to defocus the basal pole concentration along a great circle connecting the width and thickness directions of the product.

A third category of deformation induced basal pole distribution in rolled plate is random. Commercial mill rolled plate product is more often than not produced with a random array of basal poles (i.e., mechanical property isotropy exists in three orthogonal directions.) However, no published manufacturing methods describe how this textural mode can be

generated nor are there any analytical models in existence which predict the conditions required to generate a well worked fine grain $\alpha + \beta$ equiaxed microstructure in isotropic rolled sheet and plate products.

One objective of the current work is to determine the plate rolling campaign parameters required to produce basal transverse texture having begun with a plate billet whose basal pole distribution is known to be random. Once these parameters are defined experimentally, one should be able to distinguish between the Fredericks and Zarkades and Larson hypotheses for its generation. Another objective is to define the rolling parameters required to produce equiaxed, mechanically isotropic plate. Three distinct $\alpha + \beta$ Ti alloy compositions will be employed in this study to examine the generality of our texture generation findings. These are:

- 6Al-4V Ti ELI Grade
- 6Al-4V Ti Standard Grade
- 6Al-2Sn-4Zr-6Mo Ti

EXPERIMENTAL PROCEDURE

Melting and forging descriptions for all three alloys, employed in this work are given in Tables I - III. Alloy chemistries and beta transi can also be found for all three in these Tables. All heats were unidirectionally forged to cross sections of approximately 6" x 4½". A majority of the forging deformation was carried out below the beta transi of the respective alloys.

All rolling campaigns in this work involved unidirectional working of the individual 4½" thick billet stock to ¼" thickness (i.e., ≈ 94% reduction in thickness). The rolling mill employed in this work was of the two high variety. Its roll diameter was 12" and its face width was 16". It was driven by a 75 h.p. motor and was capable of a maximum speed of 100 linear ft/minute. Its maximum opening was 5" and its maximum width was 10".

Prior to rolling, the billets were heated in a laboratory furnace located adjacent to the mill to minimize heat losses associated with transfer of the work pieces from the furnace to the mill. The laboratory furnace temperature was controlled to ±10°F and the metal was normally soaked in the furnace for at least 1 hour prior to rolling in order to assure its temperature uniformity.

TABLE I

Ti-6Al-4V ELI MATERIAL

Supplier: Crucible Steel Corporation

Heat No: R51645

Ingot Description: 29" diameter x 39.7" long, 4060 lbs. Double consumable arc melted.

Chemistry:

	Al	V	O_2	C	N	Fe	H
Aim	5.9±0.3	4.0±0.5	0.10±0.02	-	-	-	-
Actual	6.0	3.8	0.095	0.013	0.01	0.05	0.0027

Beta Transus: 1760°F

Process Sequence:

1. Straight out forge from 29" diameter to 15" square by length, one reheat at 19" round.
2. Straight out forge from 15" square to 12" x 10" x length bloom at 2050°F.
3. Straight out forge to 8" square x length at 2050°F.
4. Straight out forge to 6" x 4½" x length. Forged in the 1500°F - 1700°F range.
5. Conditioned all over. Sonic test.

TABLE II

Ti-6Al-4V STANDARD GRADE MATERIAL

Supplier: International Titanium Corporation

Melter: Ti Tech International, Inc.

Heat No.: A-290

Ingot Description: 24" diameter x 118" long, 8700 lbs.
Double consumable vacuum arc melted.

Chemistry:

	Al	V	O_2	C	N	Fe	H
Aim	5.9±0.3	4.0±0.5	0.17±0.02	-	-	-	-
Actual	5.94	3.83	0.162	0.030	0.012	0.17	0.0044

Beta Transus: 1830°F

Process Sequence:

1. Straight draw out forge from 24" round to 17" square at 2000°F.
2. Straight out forge to 10" square at 1850°F.*
3. Straight out forge to 6" square at 1750°F.*
4. Straight out forge to 6 1/8" x 4 3/8" x length at 1750°F.*
5. Condition all over. Sonic test.

*Reheat at 1450°F.

TABLE III

Ti-6Al-2Sn-4Zr-6Mo MATERIAL

Supplier: Oregon Metallurgical Corporation

Heat No.: 784-004

Ingot Description: 24" diameter x 50" long, 3690 lbs.
Double consumable vacuum arc melted.

Chemistry:

	Al	Sn	Zr	Mo	O_2
Aim	5.9±0.3	2.0±0.2	4.0±0.4	6.0±0.5	0.10±.02
Actual	5.75	2.07	4.16	6.2	0.127

	C	N	Fe	H
Aim	-	-	-	-
Actual	0.030	0.008	0.06	0.0068

Beta Transus: 1735°F

Process Sequence:

1. Upset forge from 24" diameter x 5" long to 31" diameter x 30" length at 2050°F.
2. Straight draw out forge to 25" square at 2050°F.
3. Straight out cog to 20" square at 1650°F.*
4. Beta anneal at 1850°F.
5. Straight out cog to 9½" round at 1560°F.
6. Straight out forge to 6 1/8" x 4 1/2" x length at 1650°F.*
7. Condition all over. Sonic test.

*Reheat when metal wouldn't hone (∿ 1400°F)

Slab temperature following individual passes during a given rolling campaign were determined rapidly with a Ray-O-Tube device. Tempil sticks were used to confirm the Ray-O-Tube determinations at the completion of each rolling schedule.

Individual pieces of the various rolled products were subjected to various post rolling thermal practices. These heat treatments are catalogued in Table IV.

The degree and type of texture obtained with the thermomechanical treatment (TMT) schedules employed in this work was determined in terms of both Young's Modulus anisotropy and X-Ray pole figures. Young's Modulus in a given direction was measured dynamically by pinning a ¼" diameter 4" long bar at the center of its length and measuring the frequency required to resonate the bar at its fundamental frequency. The frequency of the configuration's first and second overtones were also established in order to assure that the fundamental resonance measurement was proper. Young's Modulus can be calculated with these data and the use of equation (1):

TABLE IV

POST ROLLING HEAT TREATMENT SCHEDULE

Alloy	Designation	Heat Treatment
6Al-4V Ti ELI Grade	"Mill Annealed"	1350°F/1 hour + furnace cool at less than 100°F/hour
	"Recrystallized"	1710°F/4 hours + furnace cool at less than 100°F/hour to room temperature
	"Beta Annealed"	1710°F/4 hours + 1900°F/10 minutes + 1710°F/1 hour + 1400°F/air cool
	"Duplex Annealed"	1710°F/4 hours + furnace cool at less than 100°F/hour to 1400°F/1 hour + air cool
6Al-4V Ti Standard Grade	"Recrystallized"	1780°F/4 hours + furnace cool at less than 100°F/hour to room temperature
6Al-2Sn-4Zr-6Mo Ti	"Mill Annealed"	1200°F/1 hour + air cool
	"Recrystallized"	1700°F/8 hours + furnace cool + 1200°F/1 hour + air cool

$$E = 4\rho\nu_r^2 l^2 \qquad (1)$$

Where E = Young's Modulus

ν_r = fundamental mode resonant frequency

l = length of bar

ρ = density of metal

= 0.160 lbs/in^3 for 6Al-4V Ti

= 0.169 lbs/in^3 for 6Al-2Sn-4Zr-6Mo Ti

The X-Ray pole figures were obtained from the Boeing Co. employing a modification of the Kula-Lopata technique as described in Reference 9.

RESULTS

In this section, we shall present detailed accounts of the methods and procedures required to generate either a basal transverse texture or a random array of basal poles in each alloy. To characterize the impact that forging practice has on texture development, basal pole figures were assessed upon completion of the forging procedures described in Tables I - III. Samples were taken from both the surface and center of each 4½" thick billet. Results for 6Al-4V Ti and 6Al-2Sn-4Zr-6Mo Ti samples taken from the surface position are shown in Figures 3 and 4. As one can note, both billets exhibit virtually a random array of basal poles despite a significant amount of unidirectional forging in the $\alpha + \beta$ field. Beta transi determinations for 6Al-4V Ti ELI Grade and 6Al-2Sn-4Zr-6Mo Ti are shown in Figure 5. To simplify the presentation of our findings, let us review rolling induced texture generation in each of the three distinct alloy compositions separately. It should be noted that rolling deformation was unidirectional throughout the work.

6Al-4V Ti ELI Grade

Nine types of thermomechanical treatment procedures were applied to 4½" thick billet stock in order to convert the billet to

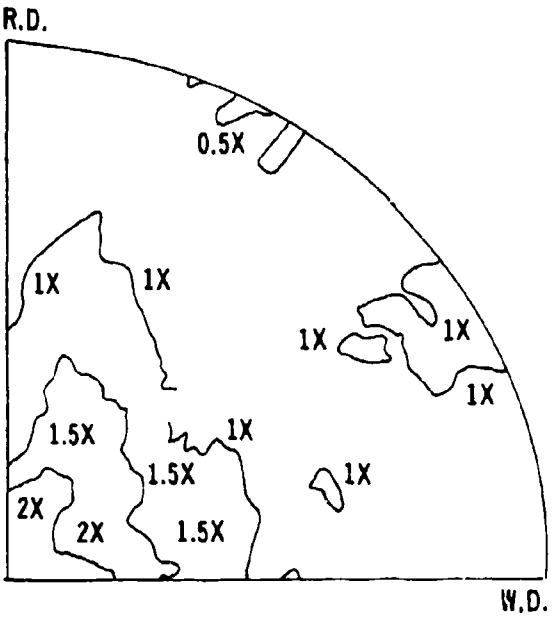

Figure 3
Basal Pole Figure for 4¼" thick 6Al–4V Ti Forge Billet–Sample Taken From Surface Location.

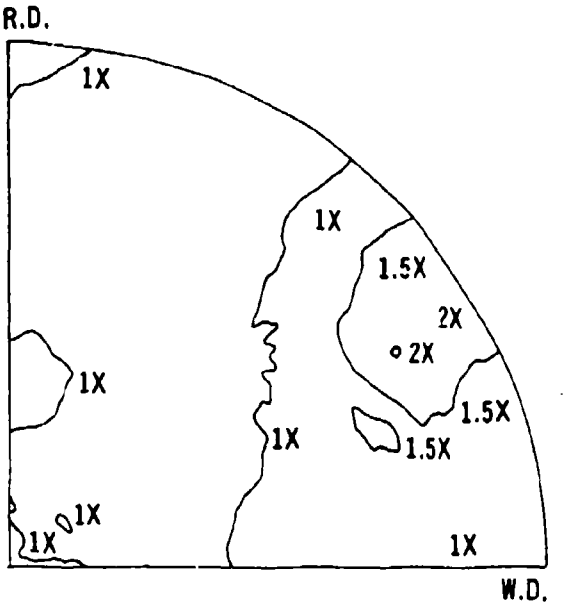

Figure 4
Basal Pole Figure for 4¼" thick 6Al–2Sn–4Zr–6Mo Ti Forge Billet–Sample Taken from Surface Location.

Figure 5

Beta Transus Determination

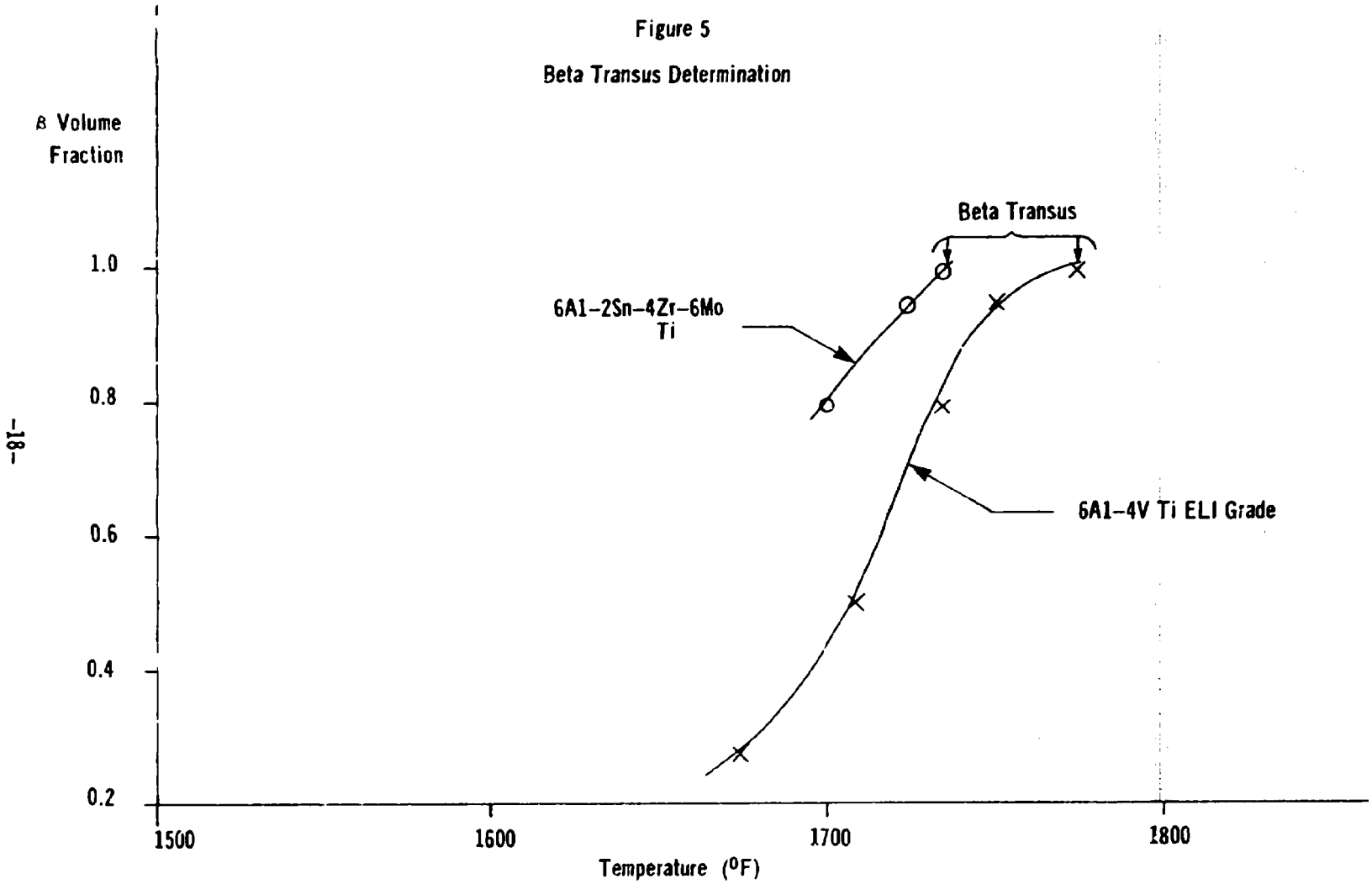

1/4" thick plate. Table V describes each of these procedures in some detail. As one can note from Table V, three distinct types of rolling campaign were conducted here. Methods 1 and 2 involved reducing the metal's thickness isothermally (i.e., the workpiece was reheated after each reduction pass). Methods 3 - 5 involved reheating the workpiece several times during the operation as detailed in the Table. Methods 6 - 9 involved continuous thickness reduction on a reversing mill without intermediate reheats. Details of the deformation%/instantaneous slab temperature/elapsed time during rolling relation for Methods 6 and 7 are given in Figure 6. Also shown in this Figure is the equilibrium beta transus temperature for this alloy composition determined from Figure 5.

Preferred orientations of basal and prism poles following the thermomechanical processing described in Table V were assessed by two independent methods. Basal and prism pole figure quadrants were determined employing an X-Ray diffraction technique. Additionally Young's moduli were assessed for the rolling and width directions of all products. The moduli measurements relate to preferred orientation, in that the elastic properties of the alpha phase are anisotropic (see Figure 7).

TABLE V

THERMOMECHANICAL TREATMENTS FOR 6Al-4V Ti ELI GRADE

Processing Type	Method	% Reduction in thickness	No. of Passes	Furnace Temp.	Slab Temperature After Last Pass	Time in Furnace (min.)	Time to Roll (sec.)	Post Rolling Heat Treatment*
Isothermal Rolling @ β - 50°F	1	94	-	1710°F	1650°F**	-	-	Mill Annealed
	2	94	-	1710°F	1650°F**	-	-	Recrystallization Annealed
Thermal Cascade Rolling With Designated Reheats	5	60	6	1800°F	1500°F	75	65	Mill Annealed
	Reheat	81	6	1700°F	1390°F	35	40	
	Total thickness reduction for Method #5 = 92%							
	4	60	6	1800°F	1500°F	75	65	Mill Annealed
	Reheat	Unk.	2	1750°F	1525°F	23	12	
	Reheat	Unk.	2	1625°F	1435°F	21	11	
	Reheat	25	2	1500°F	1230°F	23	12	
	Total thickness reduction for Method #4 = 92%							
	3	60	6	1800°F	1500°F	75	65	Mill Annealed
	Reheat	Unk.	2	1700°F	1525°F	38	10	
	Reheat	Unk.	2	1535°F	1300°F	8	12	
	Reheat	37.5	2	1370°F	1150°F	22	18	
	Reheat	24	2	1200°F	950°F	32	13	
	Total thickness reduction for Method #3 = 93%							
Thermal Cascade Rolling Without Reheats	6***	82.5	12	1800°F	1275°F	50	125	Mill Annealed
	7***	92.5	12	1800°F	1275°F	50	125	Recrystallization Annealed
	8***	92.5	12	1800°F	1275°F	50	125	Beta Anneal
	9***	92.5	12	1800°F	1275°F	50	125	Duplex Anneal
	10***	92.5	12	1800°F	1275°F	50	125	1710°F/4 hrs. + air cool to 70°F

* For definition of terms, please see Table IV

** Plate billet was reheated to 1710°F after each pass

*** Rolled without reheat

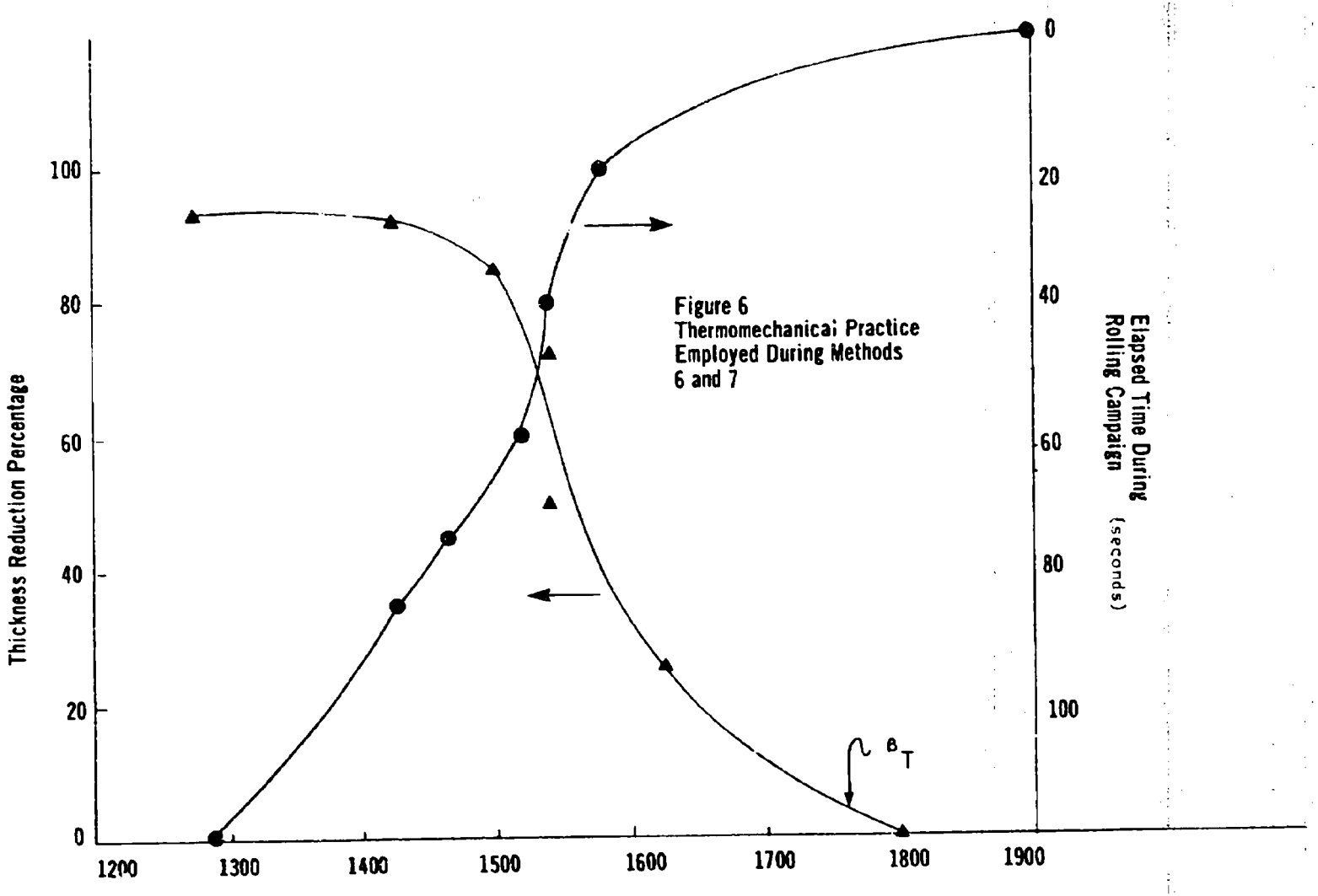

Figure 6
Thermomechanical Practice
Employed During Methods
6 and 7

SLIP & TWIN DEFORMATION PLANES IN ALPHA TITANIUM

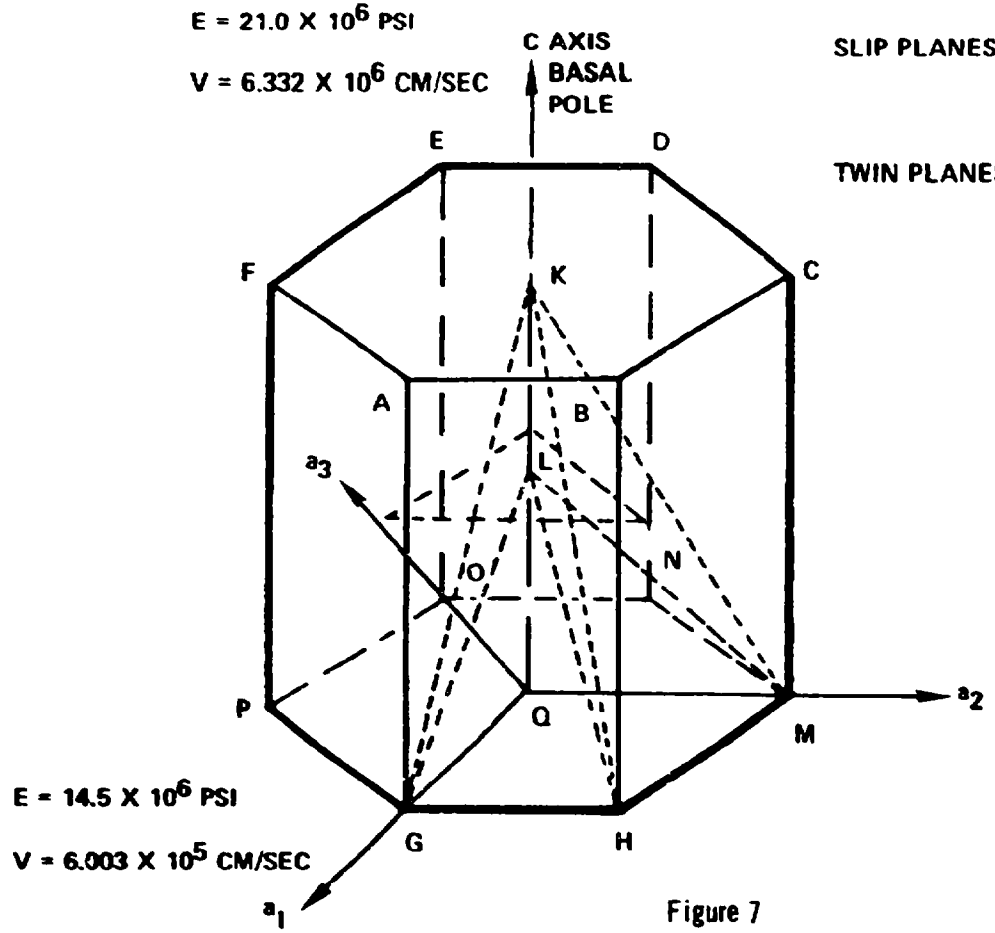

SLIP PLANES IN	TI	$(000\bar{1})$	ABCDEF BASAL PLANE
		$(10\bar{1}0)$	ABHG PRISM PLANE
		$(10\bar{1}1)$	GHK
TWIN PLANES IN	TI	$(10\bar{1}2)$	GHL
		$(11\bar{2}1)$	GMK
		$(11\bar{2}2)$	GML

Figure 7

In Table VI, we present data describing the variation in Young's modulus anisotropy with thermomechanical processing. In Figures 8 - 14, we present basal and prism pole figure quadrants developed for metal processed via Methods 1, 2, 5, 6, and 7 respectively.

Examination of the elastic modulus data (Table VI) and the basal/prism pole figures (Figures 8 - 11) associated with Methods 1 and 2 indicate that extensive isothermal rolling just below the alloy's beta transus produces a very weak basal transverse texture when the metal is subsequently mill annealed (heat treatment details are given in Table IV) as in Method 1. This basal pole preferred orientation can be further randomized to the point where the metal is virtually isotropic by simply exposing the metal to its initial rolling temperature (1710°F) for an additional four hours (see Method 2). The latter observation can be seen either from the X-Ray pole figures referred to above or the elastic modulus anisotropy shown in Table VI.

If one permits the workpiece temperature to decline from β_T + 40°F to the vicinity of 1500°F while the metal is rapidly reduced in thickness (60% reduction in 75 seconds) prior to reheating to β_T - 50°F, the width direction of the metal develops a significant concentration of basal poles. This texture development assertion

TABLE VI

VARIATION IN YOUNG'S MODULUS ANISOTROPY
WITH THERMOMECHANICAL PROCESSING
OF
6Al-4V Ti ELI GRADE

Method*	$E_{\text{Roll Direction}}$ ($\times 10^6$ psi)	$E_{\text{Width Direction}}$ ($\times 10^6$ psi)	ΔE_{W-R} ($\times 10^6$ psi)
1	16.50	[illegible].70	2.[illegible]
2	17.35	18.25	0.8
3	15.25	19.00	3.45
4	15.96	19.20	3.24
5	15.96	[illegible]72	3.76
6	15.20	19.50	4.30
7	15.75	[illegible]0.18	4.43
8	17.25	[illegible].65	-0.55
9	15.45	20.25	4.80
10	15.55	19.65	4.10

*For thermomechanical process history, please see Table V

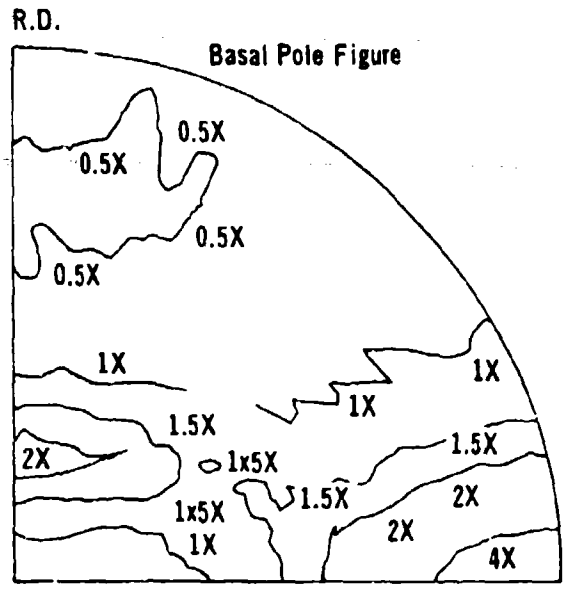

Figure 8: Material–6A1–4V Ti
ELI Grade
TMT Process Method:1

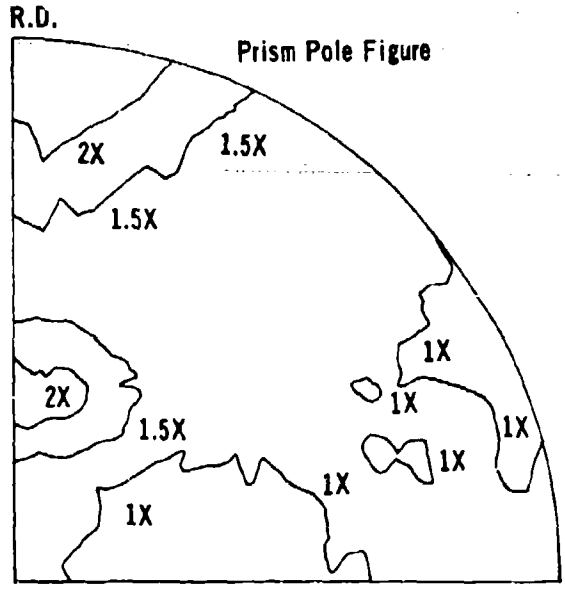

Figure 9: Material–6A1–4V Ti
ELI Grade
TMT Process Method:1

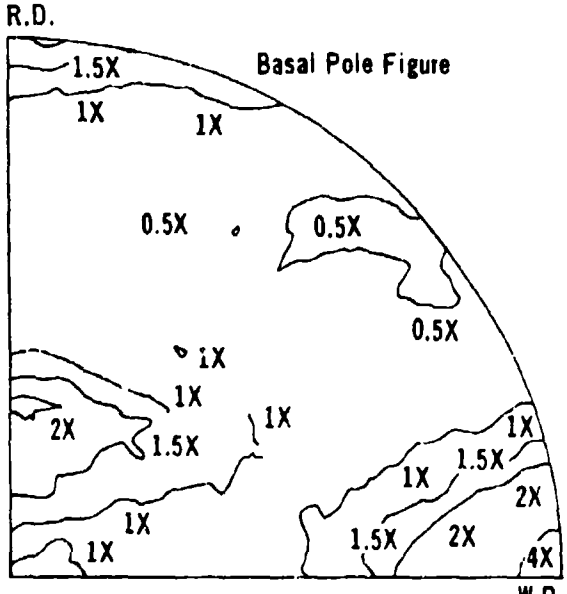

Figure 10: Material–6A1–4V Ti
ELI Grade
TMT Process Method:2

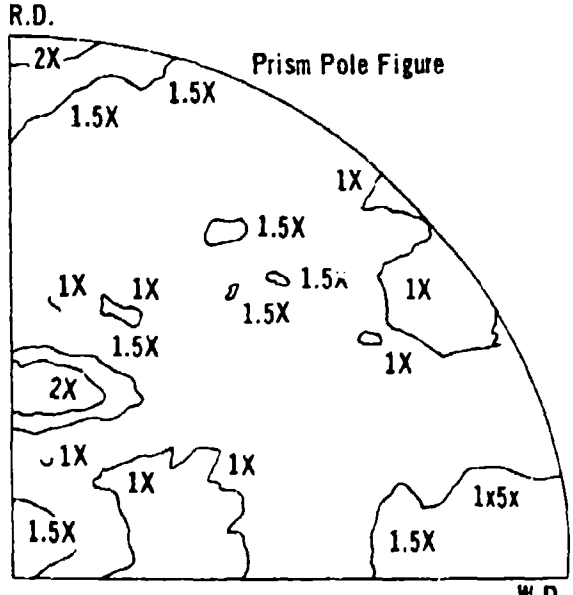

Figure 11: Material–6A1–4V Ti
ELI Grade
TMT Process Method:2

can be seen in terms of the Young's modulus anisotropy shown for Methods 3 and 4 in Table VI. The basal transverse texture can be intensified if one only reheats the metal once as opposed to several times. For example, compare elastic modulus anisotropy results shown in Table VI for Methods 3 and 4 versus Method 5. The basal pole figure associated with Method 5 metal is shown in Figure 12.

Based on the results obtained in Method 5 where the number of reheats was reduced to one, it was decided to process an 1800°F metal billet from 4 ½" in thickness to ½" thickness without reheating. The results of this work are shown as Methods 6 - 10 in terms of elastic constants in Table VI and in terms of basal pole figures in Figures 13 and 14. To gauge the impact of eliminating the single reheat during the texture rolling campaign one should compare the results for Methods 5 and 6 wherein the metal is placed in a common heat treat condition after rolling. Basal pole figures for the two Methods (compare Figures 12 and 13) are virtually identical as are the width direction Young's moduli. Recrystallizing the strongly textured Method 6 metal causes the basal transverse texture to become even more intense. Compare the results for Method 7 metal with that of Method 6 (for comparable basal pole figures, see Figures 13 and 14; for comparable $E_{\text{WIDTH DIRECTION}}$ values, see Table VI).

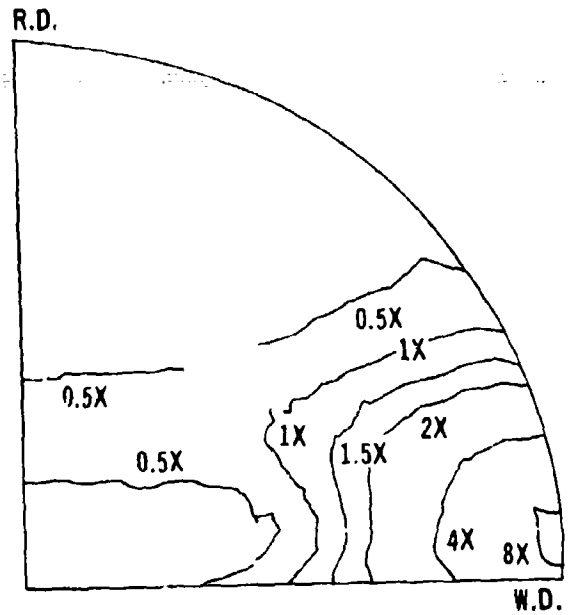

Figure 12: Material–6A1–4V Ti
ELI Grade
TMT Process Method:5

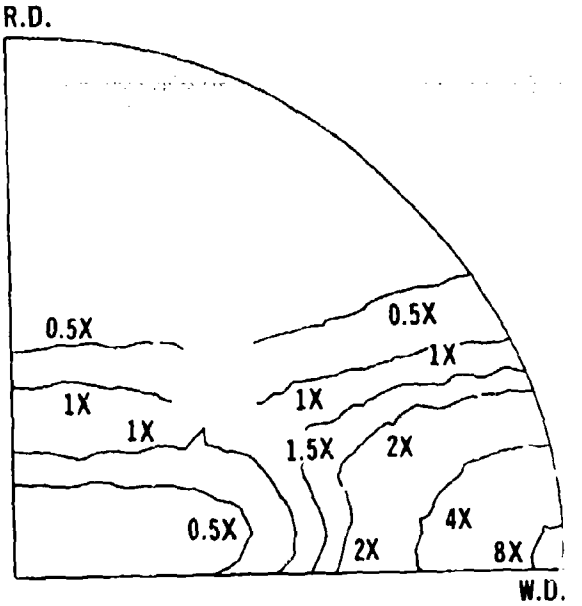

Figure 13: Material–6A1–4V Ti
ELI Grade
TMT Process Method:6

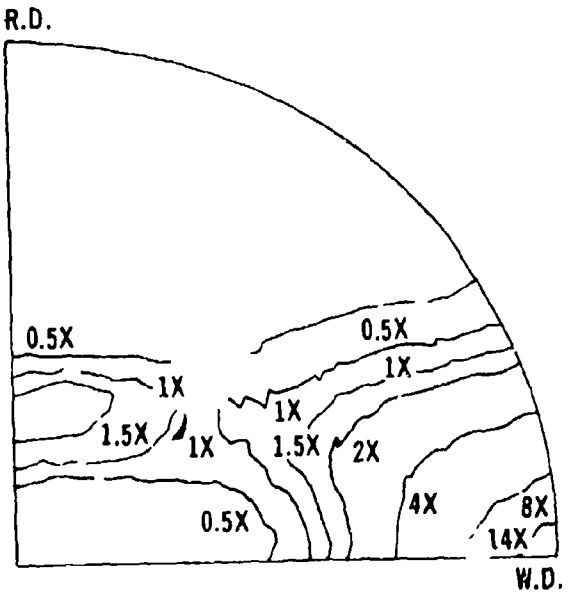

Figure 14: Material–6A1–4V Ti ELI Grade
TMT Process Method:7

In order to ascertain how reproducibly Method 7 would generate an intense basal transverse texture, three independent 4¼" thick billets of metal were rolled to ¼" thick plate employing this method on three separate occasions. The results of this study are given in Table VII in terms of Young's Modulus anisotropy.

TABLE VII
ON THE RELIABILITY OF METHOD
7 TO PRODUCE A STRONG BASAL
TRANSVERSE TEXTURE

Method	$E_{Rolling}$ ($\times 10^6$ psi)	E_{Width} ($\times 10^6$ psi)	ΔE_{W-R}
7(original)	15.75	20.18	4.43
7(a)	15.65	20.25	4.60
7(b)	15.62	20.11	4.49

In addition to studying the relationship between rolling practice and basal pole texture development, we have also studied the response of the strong basal pole transverse texture generated by thermal cascade rolling (see Table V) to post rolling thermal practice. Results obtained in this effort are summarized in Table VIII in terms of elastic modulus anisotropy.

TABLE VIII

THE EFFECT OF POST ROLLING THERMAL PRACTICE ON BASAL TRANSVERSE TEXTURE INTENSITY

6Al-4V Ti ELI Grade

Method	Heat Treatment	E_{Roll} ($\times 10^6$ psi)	E_{Width} ($\times 10^6$ psi)	ΔE_{W-R} ($\times 10^6$ psi)
6	Mill Anneal*	15.20	19.50	4.30
7	Recrystallization*	15.75	20.18	4.43
8	Beta Anneal*	17.25	16.65	-0.55
9	Duplex Anneal*	15.45	20.25	4.80
10	1710°F/4 hr. + air cool to 70°F	15.55	19.65	4.10

*as defined in Table IV

Employing the magnitude of the width direction modulus as an arbiter of basal pole intensity in that direction, one can conclude, as noted earlier, that recrystallizing a strongly basal transverse product below its beta transus and cooling the product slowly from its recrystallization temperature intensifies the preference of basal poles in the width direction (compare Methods 6 and 7). Standard optical metallography was employed to ascertain that the warm worked structure present in the Method 6 metal recrystallized during the 1710°F/4 hour treatment applied to Method 7. material. Once intensified by subtransus recrystallization, the metal can be subsequently processed at lower temperatures and cooled rapidly in air without adversely affecting the texture

of the product. These results are marked contrast with our earlier report that recrystallization of weakly textured metal tended to randomize the distribution of basal poles (review results in Table VI for Methods 1 and 2). Cooling the metal rapidly in air from its subtransus recrystallization temperature produced a small dimunition in transverse basal pole population (compare results for Methods 7 and 10). Once the metal was heated over its beta transus, all semblance of the deformation induced basal transverse texture was lost (compare results for Methods 7 and 8).

6Al-4V Ti - Standard Grade

The role played by oxygen content in basal transverse texture generation was assessed by subjecting a 4½" thick billet of this oxygen richer alloy to a thermomechanical process scheme similar to Method 2 (detailed in Table V) for the ELI Grade of this alloy. Comparison of actual alloy chemistries listed in Tables I and II demonstrate that the only significant difference between the two heats of metal is the 72% higher oxygen level in the Standard Grade metal. The only significant changes between Method 7 and the thermomechanical practice applied to the Standard Grade of the alloy (hereafter known as Method 11) were to increase the workpiece temperature prior to rolling to 1855°F (β_T + 25°F) and increase its post rolling recrystallization temperature to 1780°F (β_T - 50°F). In Figure 15, we summarize

the Method 11 practice. If one compares Figures 15 and 6 on the basis of beta transi equivaleuce, he recognizes that both oxygen grades of this alloy were given identical thermomechanical processing procedures. Texture development upon application of Method 11 was assessed via elastic constant anisotropy (Table IX) and X-Ray basal pole figure determination (Figure 16). Examination

TABLE IX

EFFECT OF THERMOMECHANICAL PROCESSING ON THE ELASTIC CONSTANT ANISOTROPY OF 6Al-4V Ti STANDARD GRADE

Method	$E_{Rolling}$ ($\times 10^6$ psi)	E_{Width} ($\times 10^6$ psi)	ΔE_{W-R} ($\times 10^6$ psi)
11	16.00	21.20	5.20
11(a)*	16.05	20.65	4.60

*Same as 11 but produced on a separate occasion.

of the data in Table IX and Figure 16 indicates that Method 11 will consistently produce a very strong basal transverse texture in 6Al-4V Ti Standard Grade. Comparison of the basal pole figure for the higher oxygen grade (Figure 16) with its lower oxygen counterpart (Figure 14) shows the two figures to be qualitatively similar. However, the specific basal pole intensity in the width direction

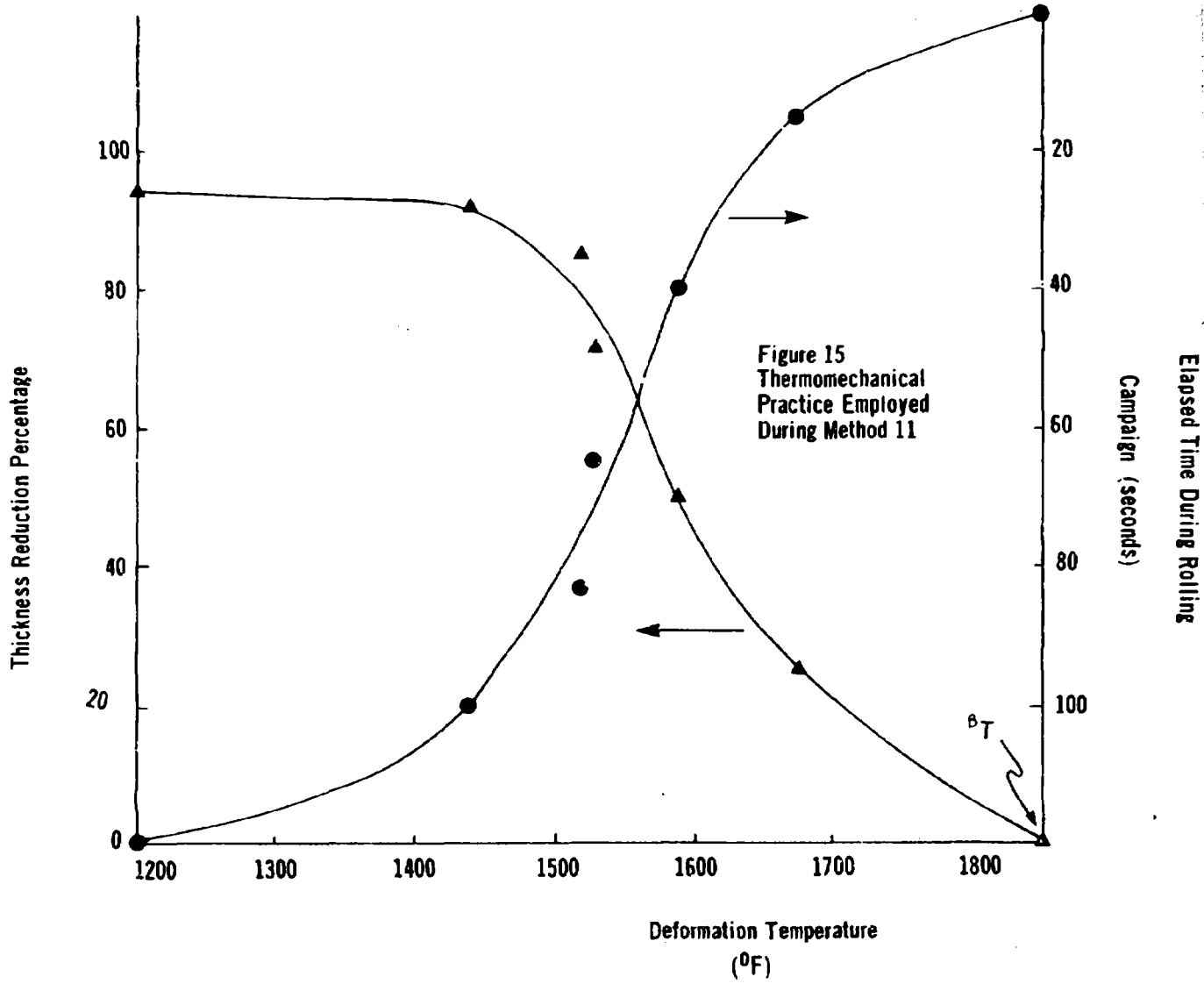

Figure 15
Thermomechanical
Practice Employed
During Method 11

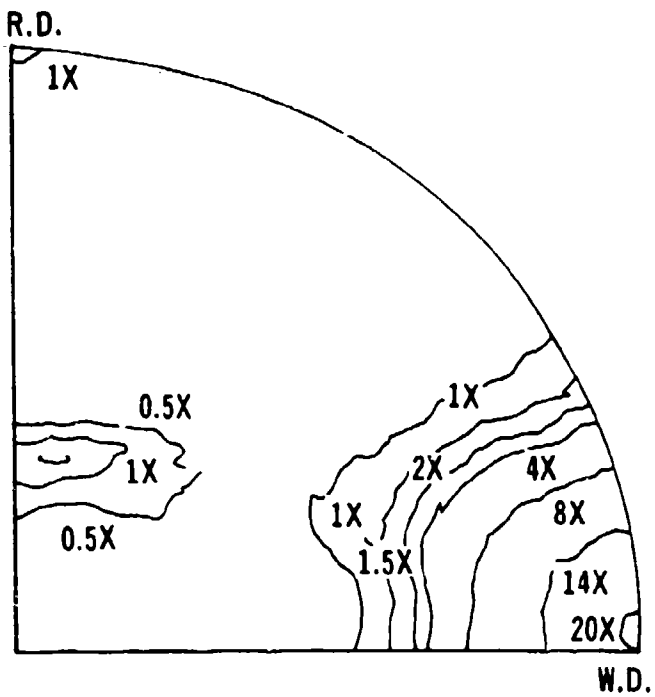

Figure 16: Material–6Al–4V Ti
Standard Grade
TMT Method 11

in Figure 16 is larger than that observed in Figure 14. Correspondingly ΔE_{W-R} in Table IX for the higher oxygen metal on the average exceeds that reported in Table VII for the ELI Grade. Another significant effect of raising the oxygen content of 6Al-4V Ti however is to increase the overall stiffness of the alloy by approximately 0.4×10^6 psi in an isotropic sense. For example, compare Tables VII and IX with respect to E_{Roll} as well as E_{Width}.

6Al-2Sn-4Zr-6Mo Ti

Six types of thermomechanical treatment procedures were applied to 4½" thick billet stock in order to convert it to ¼" thick plate. Table X describes each of these procedures in some detail. Here again, as was previously done with 6Al-4V Ti ELI Grade, we examined the texture induced in 6Al-2Sn-4Zr-6Mo Ti plate rolled in one of three ways, isothermally just below the alloy's beta transus as well as thermal cascade with or without intermediate reheating. It should be noted that a significant difference in roll force requirements exists between the 6Al-4V Ti alloy and its 6Al-2Sn-4Zr-6Mo Ti counterpart when similar billet geometries are worked rapidly and allowed to cool from temperatures within 25°F of the alloys' respective beta transi employing similar reductions per pass. On initial billet breakdown in the rolling mill under these conditions, the rolling force required to deform the 6Al-2Sn-4Zr-6Mo Ti alloy rapidly is considerably higher than that required for 6Al-4V Ti. This difference was considerable enough that it

TABLE X

THERMOMECHANICAL TREATMENTS FOR 6Al-2Sn-4Zr-6Mo Ti

Method	% Reduction in Thickness	No. of Passes	Furnace Temperature (^{o}F)	Slab Temperature after last pass (^{o}F)	Time in Furnace (min.)	Time to Roll (Sec.)	Post Rolling Heat Treatment*
Isothermal Rolling							
12	94	-	1700	1650**	-	-	Mill Anneal
13	94	-	1700	1650**	-	-	Recrystallization Anneal
Thermal Cascade Rolling with Designated Reheats							
14	90	9	1850	1500	50	-	Recrystallization Anneal
	38	3	1400	1200	15	-	
15	38	3	1760	1510	50	120	Mill Anneal
	90	9	1760	1300	15	85	
16	38	3	1760	1510	50	120	Recrystallization Anneal
	90	9	1760	1300	15	85	
Thermal Cascade Rolling Without Reheat							
17	92	12	1850	1200	50	120	Recrystallization Anneal

*As defined in Table IV

** Reheated to 1700^{o}F after each pass

constrained our choices of rolling campaign parameters noted below. This constraint was dictated because our work was performed entirely on a laboratory mill of limited capacity which was described in an earlier section of this paper. Normally production mills have a much larger roll force capacity per linear inch of billet width so that this difference is not expected to be a major problem in a manufacturing sense.

The basal pole preferred orientations introduced by these six Methods detailed in Table X are expressed in terms of elastic modulus anisotropy in Table XI and shown as basal pole figures in Figures 17 - 20. As one can observe from Table XI, extensive

TABLE XI

RELATION BETWEEN ELASTIC CONSTANT ANISOTROPY AND THERMOMECHANICAL PROCESSING

6Al-2Sn-4Zr-6Mo Ti

Method	$E_{Rolling}$	E_{Width}	ΔE_{W-R}
12	16.90	17.90	1.0
13	16.75	18.05	1.3
14	16.10	18.48	2.4
15	16.60	18.10	1.5
16	15.81	19.04	3.23
17	15.50	18.32	2.80

isothermal roll processing just below the alloy's 1735°F beta transus (i.e., reheating after each pass) produces a product that is nearly isotropic (see Method 12). This relative isotropy

is unaffected by additional post rolling exposure at 1710°F (compare Methods 12 and 13 results in Table XI).

Ignoring Method 15 momentarily, let us consider results obtained with materials subjected to various types of thermal cascade rolling (i.e., those with and without intermediate reheats) combined with recrystallizing the product prior to making a textural observation, that is to say, Methods 14, 16 and 17 metal. Of these three the most highly basal transverse textured product by far is Method 16 according to both the elastic anisotropy data in Table XI and the basal pole figures in Figures 17, 19 and 20. Another interesting point to note is that Method 16 was initially heated to 1760°F (β_T + 25°F) prior to roiling whereas the initial rolling temperatures for Methods 14 and 17 was 1850°F (β_T + 115°F). It is interesting to observe that Method 17 was rolled from 1850°F without any reheat in about the same time interval as was employed earlier in developing the strongest basal transverse textures found for 6Al-4V Ti. Yet this Method was not nearly as effective in concentrating a large number of basal poles in the width direction of the plate as was Method 16 which involved an intermediate reheat above the beta transus of the alloy (compare the magnitude of E_{Width} for the two Methods or Figures 19 and 20). In fact, reviewing the processing given

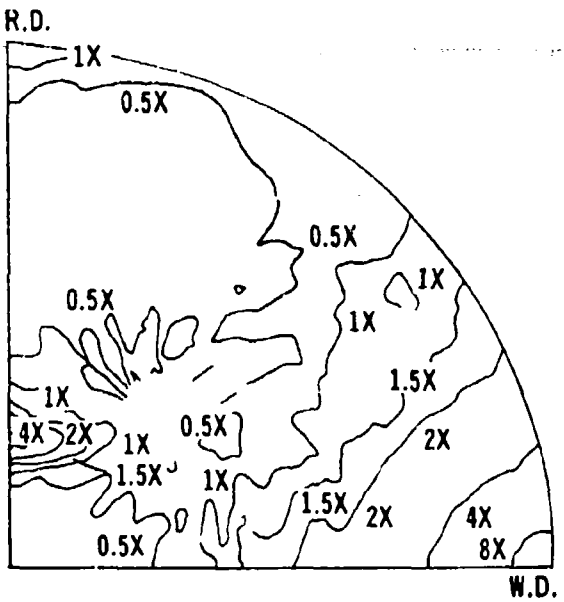

Figure 17: Material–6Al–2Sn–4Zr–6Mo Ti
TMT Method – 14

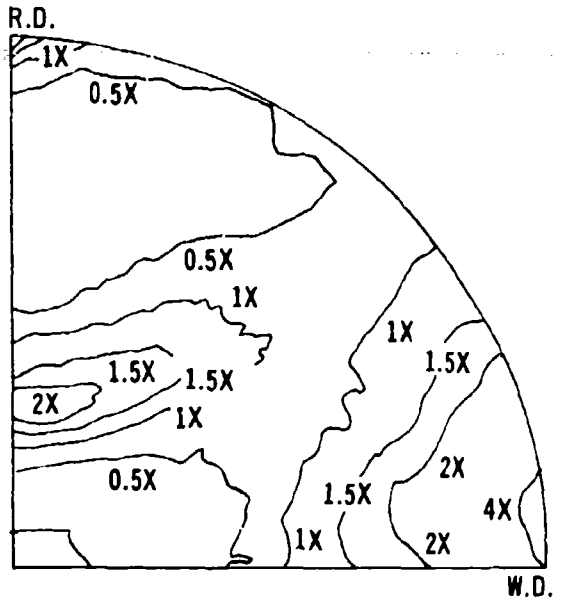

Figure 18: Material 6Al–2Sn–4Zr–6Mo Ti
TMT Method – 15

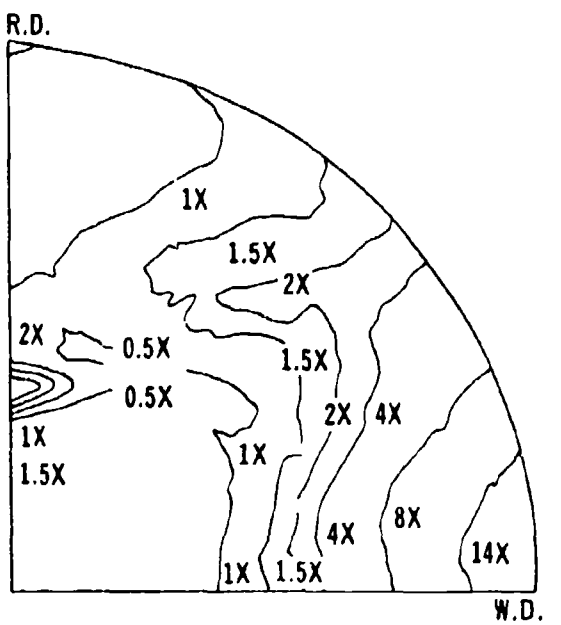

Figure 19: Material–6Al–2Sn–4Zr–6Mo Ti
TMT Method – 16

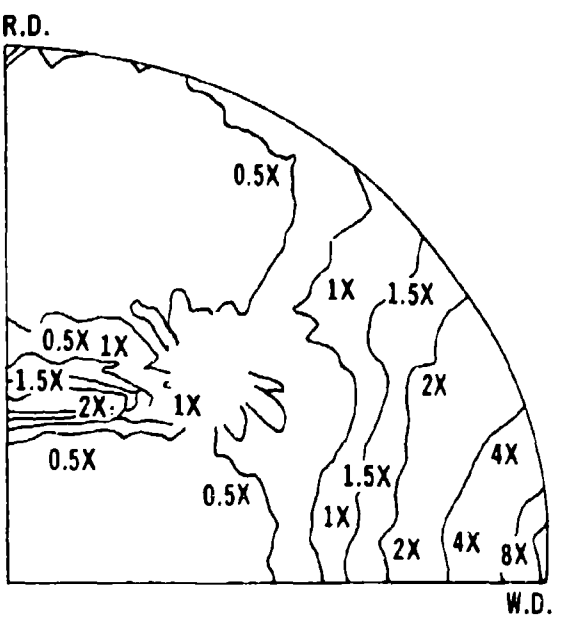

Figure 20: Material–6Al–2Sn–4Zr–6Mo Ti
TMT Method –17

for Method 16 in Table XI, it is entirely reasonable to conclude that the first 38% reduction in area accomplished little towards establishing the final strong basal transverse texture one now observes in this metal as the metal was reheated 250°F to 25°F above the beta transus after this reduction was accomplished and held there for 15 minutes prior to reinitiating rolling reduction. A majority of this initial 38% rolling reduction probably took place between 1500°F and 1600°F because logistical difficulties involved with forcing the metal into the rolling mill occurred during the 120 seconds it took to accomplish 3 passes for 35% reduction. A detailed report of the second phase of thermomechanical processing experienced during Method 16 where the metal was reduced another 90% in thickness is given in Figure 21. Summarizing our findings with respect to Methods 14, 16 and 17, one concludes that obtaining a strong basal transverse texture not only requires thermal cascade rolling (or rapid rolling reduction without intermediate reheats to the vicinity of β_T or above) but also requires that one begin his reduction with the metal heated to $\beta_T \pm 25°F$ (if one begins too far below the beta transus with unidirectional rolling, he runs the risk of scattering basal poles along the great circle connecting the width and short transverse direcions).

In addition to examining the basal transverse texture of Method 16 metal after recrystallizing the rolled plate, the results

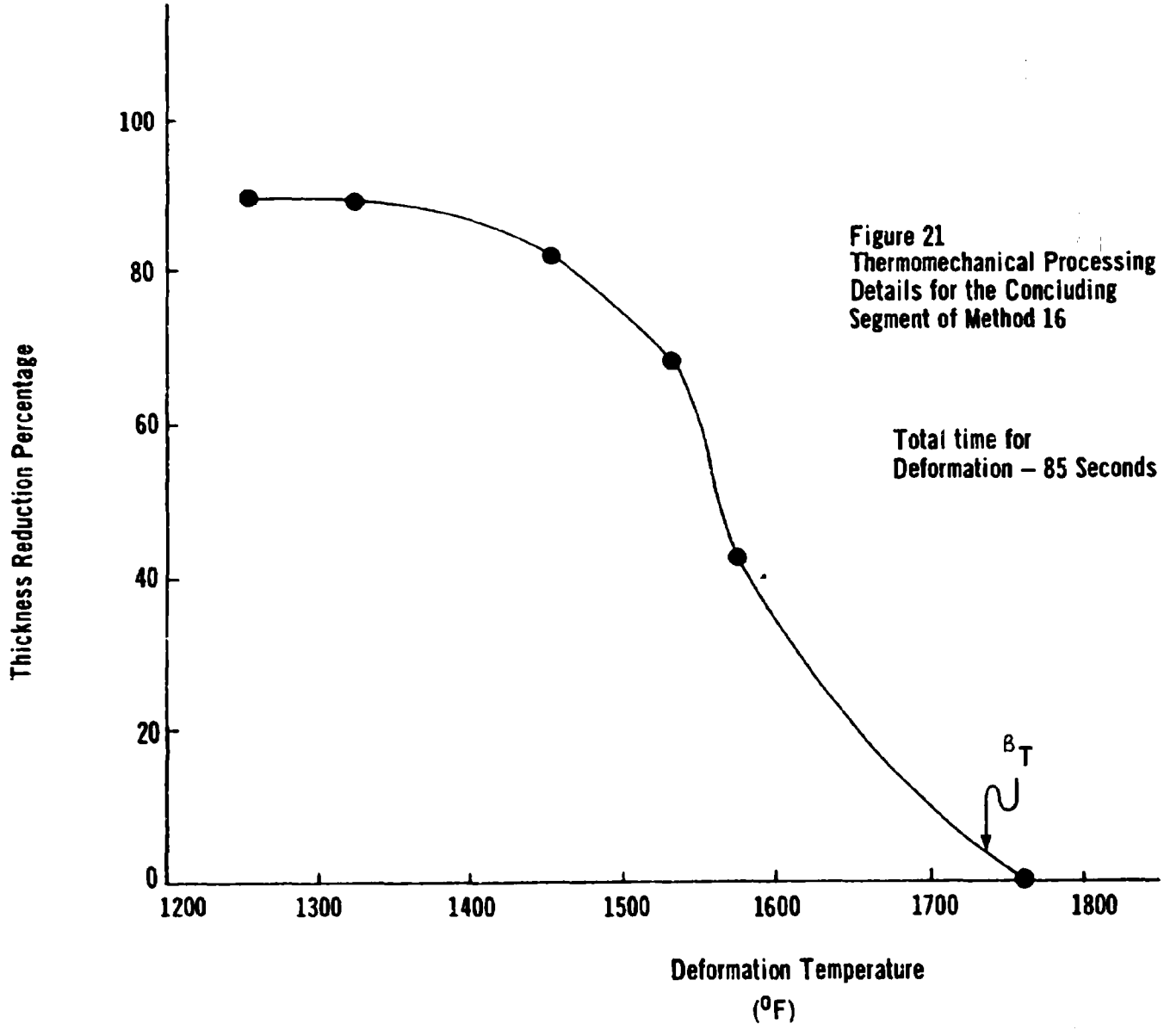

Figure 21
Thermomechanical Processing
Details for the Concluding
Segment of Method 16

Total time for
Deformation – 85 Seconds

of this rolling process were also assessed with respect to elastic constant anisotropy when the metal was still in virtually its "as rolled" condition (i.e., Method 15). The surprising result seen in Table XI is that the rolling procedure by itself resulted in a very small elastic anisotropy with the E_{Width} for Method 15 being hardly greater than that observed in Method 13 wherein the recrystallized metal was virtually isotropic. Recrystallizing Method 15 metal to form Method 16 metal led to an extremely large concentration of basal poles in the width direction relatively speaking (E_{Width} for Method 16 exceeds E_{Width} for Method 15 by $\sim 1.0 \times 10^6$ psi). Thus at least in the case of 6Al-2Sn-4Zr-6Mo Ti it is not only necessary to properly roll the metal in a thermal cascade manner beginning within 25°F of β_T but one must recrystallize the final rolled product if he desires the alpha phase fraction of the metal to exhibit a stong basal transverse texture.

In order to test the reproducibility of the basal transverse texture induced by Method 16, the entire Method was practiced on 4" thick billet stock on two separate occasions. The results obtained here are given in Table XII.

TABLE XII

ON THE REPRODUCIBILITY OF

METHOD 16 FOR BASAL

TRANSVERSE TEXTURE GENERATION

Method	$E_{Rolling}$ ($\times 10^6$psi)	$E_{Transverse}$ ($\times 10^6$psi)	ΔE_{W-R} ($\times 10^6$psi)
16	15.81	19.04	3.23
16(a)*	16.02	18.95	2.93

*Repeat of Method 16 on a separate occasion.

DISCUSSION

The experimental phase of this work has established the reproducibility and efficacy of the following TMT procedures:

(1) Production of isotropic $\alpha + \beta$ Ti alloy products with equiaxed microstructures requires isothermal rolling just below the alloy's beta transus followed by completion of the recrystallization process at the same temperature.

(2) Employ unidirectional thermal cascade rolling (initiated at a temperature within 25°F of the alloy's transus) to reduce the product's thickness by 90% and temperature by 500°F - 600°F in less than two minutes and generate a basal transverse texture.

(3) Subsequent recrystallization of such thermally cascade rolled metal intensifies the deformation induced basal transverse texture. The extent of this intensification is a function of alloy chemistry as well as deformation practice.

(4) Beta annealing of basal transverse textured products results in the total annihilation of the basal transverse texture.

(5) Unidirectional thermal cascade rolling results in a basal transverse texture of greater intensity with increasing oxygen content in the 6Al-4V Ti composition.

One objective of our discussion will be to compare the observations summarized above with the various models for α Ti texture generation reviewed in the Introduction to this work. Secondly, all of these current laboratory observations will be combined with the experimental texture development results of earlier investigators in an attempt to provide a single unified picture for the various preferred basal pole orientations that develop in the alpha phase as a function of thermomechanical process techniques.

The two principal models for basal transverse texture generation reviewed earlier (References 3, 6, and 7) emphasize the importance of prolonged high temperature rolling in order to maintain a large beta phase volume fraction during the entire texture rolling campaign. Based on the experimental results quoted above, it would appear at first that these earlier basal transverse texture generation models are not appropriate here. Recall the equilibrium beta volume fraction for both 6Al-4V Ti and 6Al-2Sn-4Zr-6Mo Ti exceeded 50% in Methods 1, 2, 12 and 13 where the two alloy compositions were unidirectionally worked isothermally at β_T - 50^0F (See Figure 15). The results of this thermomechanical processing mode were equiaxed isotropic products exhibiting random arrays of basal poles. The difficulty with these earlier models (References 3, 6, and 7) is that they ignore the possibility that the product worked continuously at just under the beta transus will continuously recrystallize

leaving the basal pole distribution randomized. Additional evidence to support this ascertion can be seen in Table VI (compare results of Methods 1 and 2) and Figures 8 and 10 in the case of 6Al-4V Ti. Here we note that low intensity basal transverse textures are not particularly stable when the product is simply held at just below the beta transus for any appreciable time after the rolling operation is complete. Similar data comparisons exist for 6Al-2Sn-4Zr-6Mo Ti in Table XI (see results from Methods 12 and 13). Metallographic examination of both the 6Al-4V Ti and 6Al-2Sn-4Zr-6Mo Ti plate products rolled isothermally, moreover, showed both to be nearly recrystallized as they exited from the hot rolls at the ¼" thickness level. Thus, it is highly likely that premature recrystallization as the product is heavily worked just below the beta transus prevents intense textural development. Additional recrystallization further degrades the textural intensity of the metal and the overall thermomechanical scheme is a convenient means of producing virtually isotropic metal.

Having concluded that continuous recrystallization during isothermal hot working (just below the beta transus) probably is responsible for lack of a strong texture in products generated by Methods 1 and 2 and 12 and 13, one must now postulate by what mechanism a

strong basal transverse texture may be generated in order to design a suitable production method. In searching for a reasonable mechanism, it would be easiest to simply modify one of the existing hypotheses (i.e., References (3) and (6)). Of the two, Frederick's proposal is the easier with which to work. Actually, his basic mechanism of a strain controlled transformation of a (100) [110] b.c.c. texture to the basal transverse texture may still be close to correct. In order to appreciate how his approach can be modified to conform with our current observations, let us briefly review his hypothesis. He assumed that if one were to unidirectionally roll an $\alpha + \beta$ Ti alloy extensively at a temperature where it was predominantly beta, his result would be an (001) [110] b.c.c. texture as shown in Figure 22. If one permits this b.c.c. textured product to transform to its alpha counterpart on cooling via the well known Burger's Relation, $(110)_\beta \,||\, (0002)_\alpha$ and $\langle 111 \rangle_\beta \,||\, \langle 11\bar{2}0 \rangle$, then each $(110)_\beta$ plane shown in Figure 22 would be replaced by a (0002) basal plane and the resultant α phase product would be virtually isotropic with regard to basal pole distribution. However, as Frederick noted only one of the four possible basal plane orientations produces a beta to alpha transformation strain matrix which is compatible with the rolling strains generated during the deformation operation (i.e., that labelled A or Simple Basal Transverse in Figure 22). Assuming the β to α

transformation occurs as the product continues to be rolled and begins to cool, the only permissable basal plane orientation is shown as A in Figure 22 or basal transverse. If the Frederick hypothesis were strictly appropriate, the isothermally rolling campaign for 6Al-4V Ti should have produced a strongly basal transverse texture since the metal was cooled repeatedly from 1700°F (50% Beta) to 1650°F (< 25% Beta) during the rolling process.

In order to eliminate recrystallization and randomization of the b.c.c. phase prior to its being heavily enough deformed to form a strong (100) [110] texture, one must not only have a large volume fraction of beta present during the rolling operation but also one must perform a majority of his deformation in a temperature range where the sluggishness of the beta recrystallization process does not permit this phenomenon to interfere with the buildup of a cold work texture in the b.c.c. phase. Thermal cascade rolling accomplishes this by allowing the product to cool so rapidly that a large volume fraction of metastable beta can be maintained while the metal is worked in the temperature range 1500°F - 1600°F. It is in this temperature range where a majority of the overall deformation imparted to the product is rapidly introduced (see Figures 15 and 16 in the case of 6Al-4V Ti and Figure 21 in the case of 6Al-2Sn-4Zr-6Mo Ti.).

A CRYSTALLOGRAPHIC RATIONALE
FOR BASAL TRANSVERSE
TEXTURE IN α TITANIUM
(Ref. Frederick, S. F., AFML-TR-73-265)

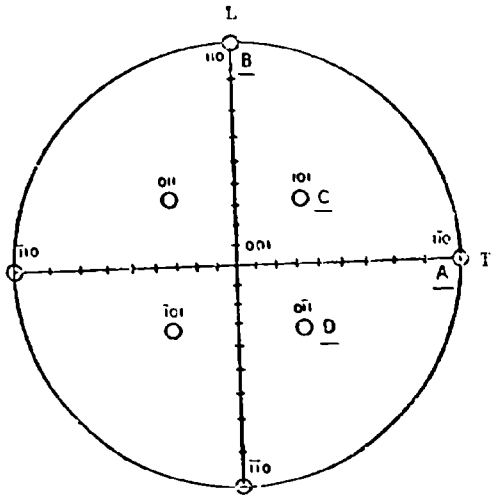

IDEAL BASAL PLANE ORIENTATION FOR TRANSFORMED
BETA WITH A (001) [110] INITIAL TEXTURE

Summary of Orthogonal Transformation
Strains for the β→α Reaction in
Titanium

Basal Pole Orientation	TRANSFORMATION STRAINS Longitudinal	Transverse	Thickness
Type A*	+9.7%	+1.1%	-10.5%
Type B**	+1.1%	+9.7%	-10.5%
Type C	-3.2%	-1.9%	+5.4%
Type D	-1.9%	-3.2%	+5.4%

*Simple Basal Transverse
**Basal Longitudinal

Figure 22

The metastable beta phase can, of course, lower the system's free energy by simply transforming to any one of six hexagonal alpha variants allowed by the Berger's Relation. If one manages to introduce sufficient cold work into the b.c.c. beta phase to texture the phase prior to its transformation, then Frederick's suggested removal of degeneracy from the Burger's Relation (see Figure 22) in order to provide compatibility between the transformation and rolling strains suggests an additional means for further decreasing the free energy of the system. If all the textured beta grains transform to alpha in a manner described as Type A (simple beta transverse), then the shape assumed by the new alpha grain (longer in the rolling direction and thinner than its beta parent) will be in keeping with the further release of stored cold work in the old beta grain. It should also be recognized the Type A crystallographic $\beta \rightarrow \alpha$ transformation is the only means by which this additional dimunition of free energy is available assuming that the product's temperature is too low to permit long range diffusion to drive a conventional recrystallization process. In this regard Shibata and Ono have shown that the equilibrium $\beta \rightarrow \alpha$ transformation is of the Martensitic type and is predictable from elastic strain energy considerations (Reference 10). Thus one expects the kinetics of this transformation to be considerably faster below say 1600°F in 6Al-4V Ti than are the kinetics for conventional recrystallization. Therefore,

the applicability of Frederick's suggestion is broadened in the sense that once one cold works and textures the beta phase by rolling, its transformation via a Type A process (Figure 22) is ensured at any later date when the temperature of the product is high enough to permit the transformation to occur, even if this occurs on a subsequent reheat of the product once the rolling process is complete as opposed to its happening only during the rolling operation itself.

The above texture model makes the following predictions. One can assure that his unidirectionally rolled product will be elastically isotropic (i.e., basal poles are randomly distributed) if he hot works the metal at high enough temperatures where the beta phase recrystallizes in a conventional manner rather than storing the applied deformation and becoming textured. In order to generate a strong basal transverse texture in a previously isotropic material, one must satisfy the following requirements:

(1) A large volume fraction of beta phase must be present during the rolling operation itself.

(2) The beta phase must adopt a (110) <111> cold work texture as opposed to conventionally recrystallizing during the working operation.

(3) At some point in time, either during the rolling operation or during a later post rolling heat treatment, the beta phase must be permitted to transform to its hexagonal alpha counterpart.

Once the basal transverse texture is formed, the metal on continued rolling at all temperatures between 70°F and the two phase alloy's beta transus is expected to deform almost exclusively in a prism mode due to the geometric orientation of this plane with respect to the product's rolling plane. Recall, Paton et al's report of that mode and basal slip exhibiting the lowest crss over the above noted temperature range (Reference 8) in Ti-Al alpha phase alloys. Thus a strong basal transverse texture is extremely stable when additional rolling deformation is accomplished well below the beta transus.

As noted in the Introduction to the current effort, extensive unidirectional rolling of previously isotropic 6Al-4V Ti products at 1500°F and below results in a preferential spread of basal poles along a great circle connecting the short transverse and width directions of the product and round or crossrolling under the same conditions results in a perfect basal short transverse of Figure 1(a) texture. The essential reason why these results are possible on the one hand and cascade rolling from the alloy's beta transus into the 1500°F and below temperature regime can also be applied to generate a basal transverse texture is the instantaneous difference in phasal volume fraction of the isotropic billet at initiation of the rolling campaign. In the former situation the thermally

equilibrated product is both isotropic and predominantly alpha in phasal volume fraction (see Figure 5). In the latter, the major phase volume fraction is more than likely metastable beta. Moreover, additional unidirectional rolling deformation applied to a strongly basal transverse textured product at 1500°F or below is expected to enhance the basal transverse texture in part through the residual beta phase texture rationale already presented. A second source for textural enhancement relate to completing the alighment of basal poles in the width direction associated with those grains so aligned with respect to the perfect basal transverse texture that the applied crss on basal planes for geometric reasons is well below the applied crss on prise planes (i.e., the basal planes here are just not oriented properly for easy slip during rolling). Proof of these assertions with respect to the effect of continued deformation at temperatures below 1500°F on the basal transverse texture can be found both in the current work as well as in the work of Frederick (Reference 3) where he initiated a rolling campaign with a product he denoted as one quarter inch thick "Hot Band" 6Al-4V Til As Frederick received this metal, it exhibited a strong basal transverse texture. He continued to unidirectionally roll this metal isothermally at a whole series of temperatures from 1600°F to 70°F. His only result was that the basal transverse texture became more intense.

One interesting result of our current effort is the finding that post rolling subtransus recrystallization of the alloy compositions studied actually caused strongly basal transverse textured products to become even more intensely textured in the basal transverse mode. Moreover, the effect of post rolling recrystallization was much more effective in sharpening the basal transverse texture of 6Al-2Sn-4Zr-6Mo Ti than its 6Al-4V ti counterpart. In terms of basal pole intensity in the width direction of the former alloy composition, the texture in the as rolled condition was more than doubled on recrystallizing the rolled product as opposed to the much more modest textural sharpening exhibited by the 6Al-4V Ti composition subjected to the same post rolling thermal practice (compare results in Table VIII and XI). A probable rationale for this difference in behavior involves the ability of each alloy composition to retain an excessive volume fraction of metastable beta on rapid cooling to room temperature. 6Al-4V Ti is a moderately beta stabilized two phase alloy and has little capacity for retaining excess metastable beta phase at room temperature. By contrast Williams and Rhodes (Private Communication, July, 1976) have studied the metallography of 6Al-2Sn-4Zr-6Mo Ti in some detail recently and report that this more heavily beta stabilized alloy has a large capacity for retaining excessive amounts of metastable beta phase at 70^{o}F if

it is air cooled from high in its $\alpha + \beta$ range (as occurs after rolling). If one retains any significant volume fraction of cold work textured beta phase at room temperature, our basal pole alpha texture measurements (in terms of elastic properties of X-Ray pole figures) would report the solid to be less anisotropic than it would be after the product was reheated to a high enough temperature to allow the beta to transform to alpha in the strain controlled mode described earlier. It is expected that the transformation would occur as the metal was being heated to its subtransus recrystallization temperature. Moreover, it would occur at a temperature significantly lower than the temperature for diffusion controlled recrystallization.

Recrystallization below the beta transus only served to enhance the strong "as rolled" basal transverse texture in both alloys. In Figure 5, we note that the equilibrium beta phase volume fraction obtained during our 4-8 hour post rolling recrystallization heat treatment was on the order of 50% for 6Al-4V Ti and 80% for 6Al-2Sn-4Zr-6Mo Ti. Thus, at first, one might expect that when these fully annealed beta grains transform to alpha in the fully recrystallized product on furnace cooling, they should be able to pick any one of 6 normally equivalent variants of hexagonal alpha at random as their transformed orientation and thus randomize or destroy the prior basal transverse texture. However, it is well known that subtransus recrystallization of the alpha phase in such two

phase alloys has virtually no effect on grain shape or size, the process simply significantly lowers the dislocation density within the α grains themselves. So long as the grain shapes remain constant as $\alpha \xrightarrow[\text{temperature}]{\text{at high}} \beta \xrightarrow[\text{cooling}]{\text{on}} \alpha$, a strong basal transverse texture is recaptured on cooling the product in order to minimize the free energy of the system and not have neighboring grains store excessive amounts of elastic strain energy. This additional elastic strain energy would be associated with neighboring beta grains adopting different α variant orientations on cooling chen they had on heating. If new α variant orientations did occur on cooling then grain to grain shape changes would be required (i.e., here again the β → α transformation strain matrix forces the Burger's relation to function as if only one α variant orientation were possible).

Annealing recrystallized 6Al-4V Ti above the beta transus eliminated the basal transverse texture as seen in Table VI. In this case, it is well known that exceeding the beta transus by 150°F in 6Al-4V Ti as was done here permits excessive grain growth and extensive grain shape changes to take place. Thus it is not surprising that this thermal treatment eliminates the basal transverse texture. Although no X-Ray pole figures were made during this work on the beta annealed metal and our elastic modulus measurements were all

in the rolling plane of the product, it should be pointed out that the metal may not be without a significant basal pole texture as a result of this treatment. For example, Frederick (Reference 3) reports that if one heats a strongly basal transverse textured 6Al-4V Ti product above its beta transus, his result is a basal texture of the "split longitudinal" type. Major basal pole concentrations are found at $\pm 25^{\circ}$ from the short transverse product direction. No crystallographic mechanisms to account for the formations of this annealing texture have yet been proposed.

Finally let us consider the role played by alloy chemistry in mandating the intensity of the basal transverse texture. Examination of Figures 6, 15 and 21 demonstrate that all three alloy compositions were subject to similar cascade rolling processes assuming the beta transus temperature of each alloy is employed as a common base. It is not surprising that the 6Al-2Sn-4Zr-6Mo Ti alloy did not exhibit as intense a basal transverse texture after cascade rolling as did the other two compositions. Firstly, the former alloy is more heavily beta stabilized and thus is probably not capable of attaining the ultimate basal transverse textural intensity available in its lesser beta stabilized counterparts. In the current effort, we employed Method 16 to obtain an $E_{Width} = 19.0 \times 10^{6}$ psi. In an earlier work, where the initial texture and rolling

campaign schedule of the starting ½" thick 6Al-2Sn-4Zr-6Mo Ti plate were unknown, Harrigan et al (Reference 11) continued to roll the ½" thick plate isothermally at 1300°F to a thickness of 0.060" (net thickness reduction 88%) and reported E_{Width} = 19.5 x 10^6psi. They also measured the highest basal pole intensity in the width direction to be 30 times greater than random employing an X-Ray technique identical to that used in this work. Thus, if one were to modify Method 16 by eliminating the reheat above the beta transus after the initial 34% reduction, one might be able to obtain the earlier more highly textured result that Harrigan et al reported.

One notes in Tables VI and IX (in terms of elastic anisotropy) and Figures 14 and 16 (in terms of X-Ray pole figures) that increasing the oxygen content of 6Al-4V Ti ELI Grade by 78% has two effects on the textured metal one obtains by similar cascade rolling procedures. Firstly, the basal pole concentration in the width direction is increased as a result of the additional oxygen as can be seen by comparing Figures 14 and 16. This is a somewhat surprising result in that all the deformation applied to create these textures was imparted at temperatures well above 500°F. The significance of 500°F here is that it is generally well accepted that all effects of oxygen content on the

mechanical behavior of $\alpha + \beta$ Ti alloys vanish above this test temperature.

A second effect that increasing oxygen content has on 6Al-4V Ti is non-textured related. In Table IX we see that both E_{Roll} and E_{Width} of the higher oxygen grade material exceed their counterparts in Table VII by at least 300,000 psi to 400,000 psi. Thus, a portion of the total increase in elastic moduli seen in the above referenced Tables is due to the fact that adding oxygen is simply a potent means of stiffening the basis hexagonal closed packed lattice as opposed to assuming further enhancement of the basal transverse texture.

CONCLUSIONS

Conditions for the production of either a basal transverse texture or isotropic basal pole array in $\alpha + \beta$ Ti alloys have been established. The role of alloy chemistry was ascertained by employing two oxygen grades of 6Al-4V Ti in this study as well as 6Al-2Sn-4Zr-6Mo Ti. The importance of beta phase recrystallization in promoting basal pole randomization during the rolling operation itself is described in detail. Slip deformation processes are employed in concert with a knowledge of the $\beta \rightarrow \alpha$ transformation strain matrix to model the production of basal pole arrays that are either random, basal long transverse or basal short transverse. It is shown that these models are capable of not only accounting for texture generation but also for basal transverse texture intensification when the metal is recrystallized under subtransus conditions or basal transverse texture annihilation on beta annealing. Slip mechanistic arguments and experimental verification are presented to elucidate the over-riding role played by prior thermomechanical billet/plate rolling process history in determining the final crystallographic textures a given product will exhibit even in the case where the starting material is additionally worked to reduce its thickness by another 90% under a wide variety of conditions.

BIBLIOGRAPHY

1. Fitzpatrick, J. M. and F. A. Crossley, " Development of Improved Biaxial Strength in Titanium Alloy Rocket Motor Cases Through Texture Hardening," Phase 1 AFRPL-TR-67-302, December, 1967.

2. Hatch, A. J., "Texture Strengthening of Titanium Alloys," Trans Met Soc AIME, Vol. 288, January 1965, pp 44-50

3. Frederick, S. F., "Manu. Methods for Production Process for Titanium Sheet with Controlled Texture," AFML-TR-73-265, Nov., 1973.

4. Harrigan, M. J., Sommer, A. W., and Alers, G. A., "The Effect of Textures on the Mechanical Properties of Titanium Alloys," Rockwell Int'l Rep't, NA-69-909, Dec., 1969.

5. Roberts, W. T., " Preferred Orientation and Anisotropy in Titanium," Journal of the Less Common Metals, Vol. 4, 1962, pp 345-361.

6. Zarkades, R. and Larson, F. R., "Sheet Tensile Properties of Titanium Alloys as Affected by Texture," AMMRC TR-68-03, January, 1968, DDC No. AD666765.

7. Larson, F. R., "Textures in Titanium Sheet and Its Effect on Plastic Flow Properties," Report No. AMRA-TR-65 24, Octover, 1965, DDC No. AD 626410

8. Paton, N. E., Baggerly, R. G. and Williams, J. C., "Deformation and Solid Solution Strengthening of Titanium Aluminum Single Crystals," Final Rep't on AFOSR Contract F44620-72-C-0043, Jan., 1976.

9. Olsen, R. H., Metallography, 5, pg. 369-71, 1972.

10. Shibata, M. and Ono, K., "The Strain Energy of a Spheroidal Inclusion and Its Application to bcc-hcp Martensitic Transformation,", Tech. Rep't #10, Contract No. N00014-67-C-4039.

11 Harrigan, M. J., Sommer, A. W., Reimers, P. A. and Alers, G. A., 2nd International Conference on Ti, Plenum Press, N. Y., N. Y., 1973, J. Jaffee and H. Burte, Editors.

PART II

ON THE MECHANICAL BEHAVIOR OF BASAL TRANSVERSE TEXTURED TITANIUM ALLOYS

It is well known that some metals can be strengthened by texture hardening. Moreover, considerable experimental and prototype production efforts have already been completed which successfully demonstrated that alpha rich alloys such as 6Al-4V Ti and 7Al-2.5 Mo Ti sheet can be texture hardened for biaxially strengthened pressure vessel applications (References 1 and 2). The specific crystallographic alpha phase texture required for biaxial strenghthening is shown in Figure 1(a). Biaxial hardening here is relatable to the facts that the elastic stiffness and critical resolved shear stress for plastic flow of α single crystals are considerably higher when loads are applied parallel to $\langle 0001 \rangle_\alpha$ as compared to the situation where the loading direction lies in the basal plane of these single crystals (see Figure 2 and Reference 3).

Another crystallographic alpha texture which sometimes occurs accidentally during commercial production of $\alpha + \beta$ Ti alloys wrought flat products is shown in Figure 1(b). In this case,

SCHEMATIC VIEW OF ALPHA PHASE TEXTURED PLATES & THEIR CORRESPONDING BASAL PLANE POLE FIGURES

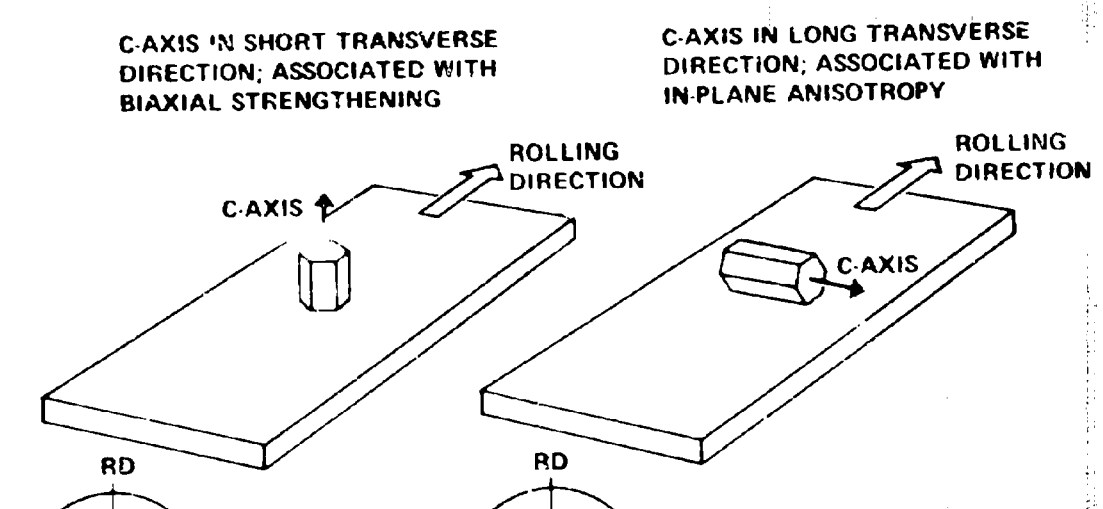

Figure 1

SLIP & TWIN DEFORMATION PLANES IN ALPHA TITANIUM

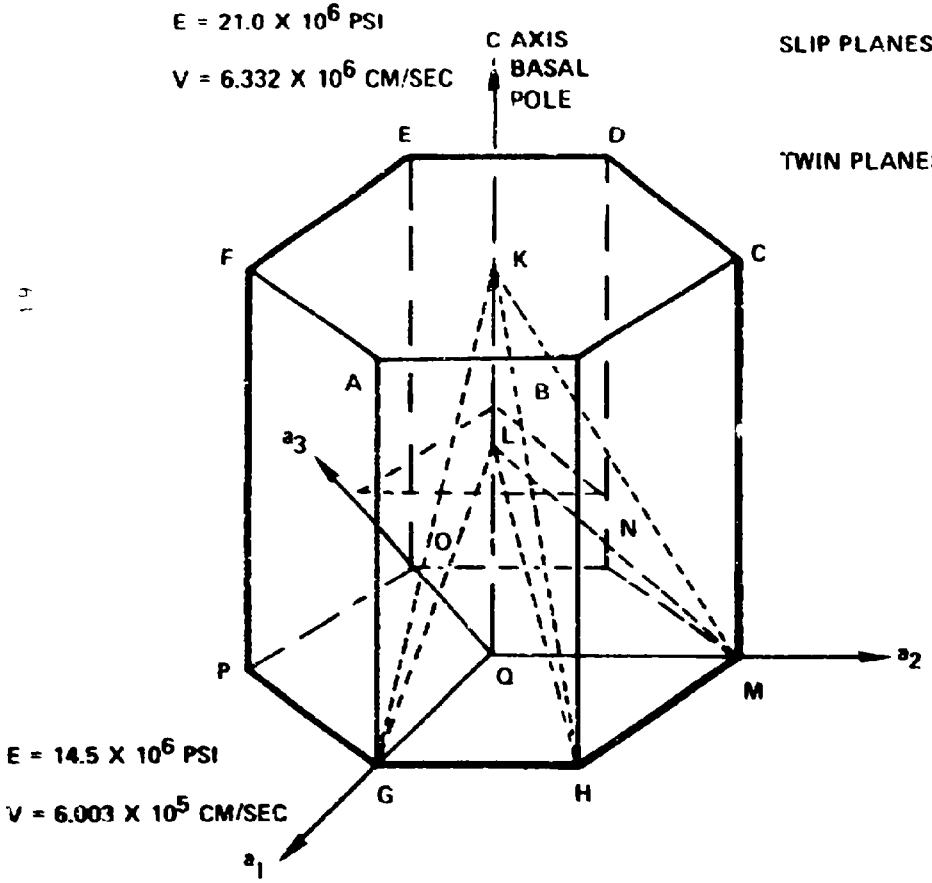

SLIP PLANES IN	TI	(0001)	ABCDEF BASAL PLANE
		$(10\bar{1}0)$	ABHG PRISM PLANE
		$(10\bar{1}1)$	GHK
TWIN PLANES IN	TI	$(10\bar{1}2)$	GHL
		$(11\bar{2}1)$	GMK
		$(11\bar{2}2)$	GML

Figure 2

the c axes or basal poles of the individual alpha grains are preferredly oriented in the long transverse direction of the product (i.e., a basal transverse texture). Based on the information cited in Figure 2 and Reference 3, one expects the long transverse direction of such textured plate to be considerably stiffer and stronger (in terms of static tensile properties) than all other directions in the product. Indeed, there is strong evidence to validate these expectations in the cases of both static tension and compression properties associated with basal transverse textured 6Al-4V Ti and 6Al-2Sn-4Zr-6Mo Ti at room temperature (References 4-7). In contrast to these static property improvements, in the long transverse direction of such textured $\alpha + \beta$ Ti materials, Zarkades and Larson (Reference 6) have reported a substantial decrease in fatigue crack initiation resistance in basal transverse textured 4Al-4V Ti (i.e. S-N sample life in the long transverse direction was significantly poorer than in the longitudinal direction).

However, 4Al-4V Ti is not a common used alloy composition and there is no reason to believe apriori that the alpha crystallography associated loss of fatigue life observed in its case should also apply to such industry work horse compositions as 6Al-4V Ti. The potential applications for basal transverse textured $\alpha + \beta$ Ti alloys are numerous and include all structural

members where loads are principally uniaxial. Examples of such aircraft structure embrace wing skins, spars, longerons, turbine blades horizontal stabilizer planks, etc. Thus, the objective of the current research is to fully characterize the mechanical behavior of basal transverse textured versions of three currently employed Ti alloy compositions:

- 6Al-4V Ti - ELI Grade
- 6Al-4V Ti - Standard Grade
- 6Al-2Sn-4Zr-6Mo Ti

EXPERIMENTAL PROCEDURE

Three distinct $\alpha + \beta$ Ti alloy chemistries were employed in this work. Two of these were of the basic 6Al-4V Ti composition differing only in their oxygen contents. The ELI version of this alloy contained 0.095 wt% oxygen. The Standard Grade 6Al-4V Ti composition contained 0.162 wt% oxygen. The wt% of all other alloy constituents in both heats were identical. The third alloy composition employed was 6Al-2Sn-4Zr-6Mo Ti. All materials used in this work were derived from production melting stock. They were thermomechanically processed to one quarter inch thick, six and one half inch wide plate stock. The metal process schemes employed were all designed to produce a plate product which exhibited an intense basal transverse crystallographic texture. X-Ray diffraction basal pole figures for each of the three alloy compositions are given in Figures 3 - 5. Another method for expressing basal pole preferred orientation is elastic constant anisotropy. Young's moduli for all three alloy products are given in Table I. Detailed accounts of the individual alloy chemistries thermomechanical process schemes employed and experimental procedures to obtain the X-Ray pole figures and Young's moduli can be found in Part I.

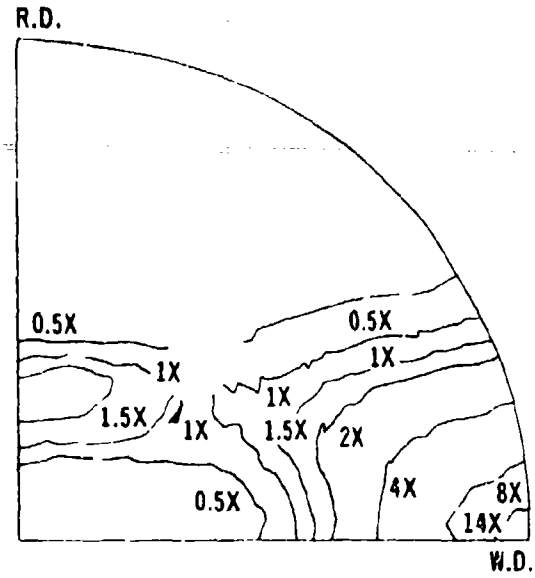

Figure 3: Material–6A1–4V Ti ELI Grade
TMT Process Method:7

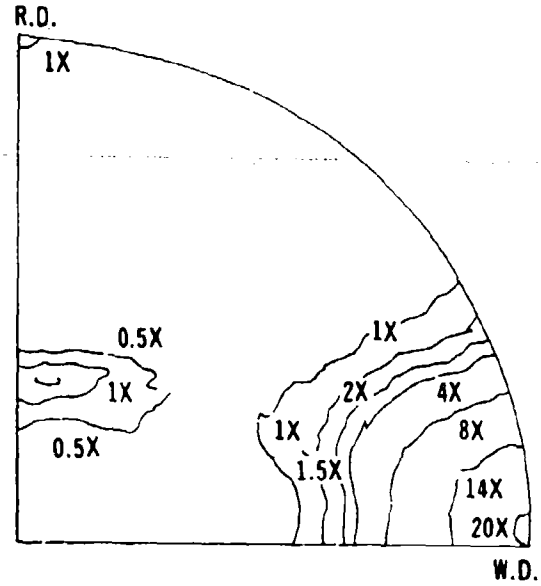

Figure 4: Material–6A1–4V Ti
Standard Grade
TMT Method 11

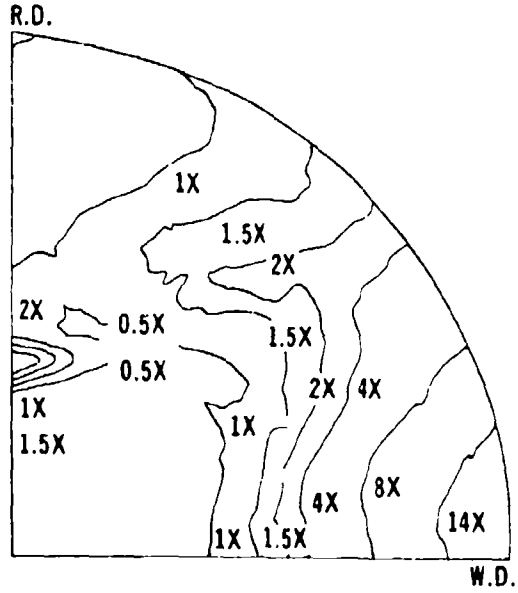

Figure 5: Material–6A1–2Sn–4Zr–6Mo Ti
TMT Method – 16

TABLE I

BASAL TRANSVERSE TEXTURE DETERMINATIONS

VIA YOUNG'S MODULUS ANISOTROPY

Alloy Composition	Heat Treatment*	E_{Width} ($\times 10^6$ psi)	$E_{Rolling}$ ($\times 10^6$ psi)	E_{W-R} ($\times 10^6$ psi)
6Al-4V Ti: ELI Grade	Rex'l I	20.18	15.75	4.43
	Rex'l II	19.65	15.55	4.10
	Duplex	20.25	15.45	4.80
6Al-4V Ti: Standard Grade	Rex'l	21.20	16.00	5.20
6Al-2Sn-4Zr-6Mo Ti	Rex'l	19.04	15.81	3.23
α Ti Single Crystal	Annealed	21.00 ($\vec{c}$ axis)	14.50 ($\vec{a}$ axis)	6.50

*For details of these treatments, please see Table II

Table II details the heat treatments our various alloy compositions were subjected to prior to test. As one can note, the ELI or low oxygen grade of 6Al-4V Ti was examined in three conditions and the other compositions in only one each. The elastic moduli of the variously heat treated alloys are given in Table I.

TABLE II

POST ROLLING THERMAL PROCESS SCHEDULES

Alloy Chemistry	Heat Treat Designation	Heat Treatment*
6Al-4V Ti-ELI Grade	Rex'l I	1710°F/4 hrs. + furnace cool at less than 100°F/ hour to 70°F.
	Rex'l II	1710°F/4 hrs. + air cool to 70°F
	Duplex	1710°F/4 hrs. + furnace cool at less than 100°F/ hour to 1400°F/ 1 hr. + air cool to 70°F.
6Al-4V Ti- Standard Grade	Rex'l	1780°F/4 hrs. + furnace cool at less than 100°F/ hour to 70°F
6Al-2Sn-4Zr-6Mo Ti	Rex'l	1700°F/8 hrs. + furnace cool to 1200°F/1 hr. + air cool to 70°F.

*Microstructurally, all three materials have ∿ 10 μ grain size and are fully recrystallized and equiaxed.

Mechanical property measurements performed to evaluate these basal transverse texture products included:

- monotonic stress:strain at room and elevated temperature
- cyclic stress:strain at room and elevated temperature
- S-N fatigue at K_t=1 and K_t=4 at room temperature in tension (R = 0.1)
- creep at elevated temperature only.

In all cases properties were obtained in two orthogonal directions (longitudinal and long transverse). Adopting pseudo single crystal nomenclature for these highly basal transverse products, these orthogonal directions referred to above become $\langle 10\bar{1}0 \rangle_\alpha$ and $\langle 0001 \rangle_\alpha$ respectively. Since all three alloy compositions have been processed to possess a primary alpha volume fraction greater than 85%, the use of tne pseudo single crystal terminology is relevant in describing the mechanical behavior of these two phase alloys.

All of the mechanical property data reported here was obtained employing MTS Corporation "closed loop" electro hydraulic equipment. Stress:strain and creep measurements were made with round bar dog-bone type samples (diameter - 0.160"). Monotonic stress: strain measurements at room and elevated temperatures were obtained in accordance with ASTM E8-69 and E21-70 respectively.

Creep measurements at elevated temperature followed the dictates of ASTM E139-70 with the exception that the samples were incrementally loaded. That is to say, the load was increased to the next higher level at a given test temperature after the creep rate reached its steady state value (a minimum slope of ε vs time was always attained within 100 hours and that minimum rate always occurred after less than 1% creep strain). All fatigue testing was conducted at room temperature in accordance with ASTM E466-72T. Sample designs required for K_t's of 1 and 4 were produced in accordance with requisites of Peterson (Reference 8).

All elevated temperature tests were performed in air except several creep experiments which were performed in a vacuum of 3×10^{-6} Torr. Temperature control during elevated temperature testing was always maintained within $\pm 3^{\circ}F$.

No ASTM Standards currently exist for cyclic stress:strain measurements and thus we shall discourse in greater detail here. The design of our cyclic stress:strain test fixture, test specimen and test setup required some departures from the more commonly found configurations used in such testing. The reasons for this lie in the difficulties associated with testing, in fully reversed loading, a specimen machined from stock which was 0.25

inches thick as well as the need for testing at 700°F. The thickness of the raw stock was chosen so as to insure a highly textured material and still be capable of being used for the other various mechanical tests described in Parts II and III.

Small size (i.e., 1/4" thickness) becomes a problem because of the increased possibility of specimen buckling under compression loads. Thus every attempt was made to maintain as large a test section thickness as possible. On the other hand, the specimen test section must be smaller than the grip area to insure that grip area failures do not occur. In order to simultaneously satisfy the above requirements, the specimen design shown in Figure 6 was successfully used. Note that the use of a partial thread in the grip area allows us to have a large net section area in the grip vicinity. It, moreover, allows us to have positive gripping even as we pass through zero load and does not require us to reduce the specimen test section thickness below .25 inches. The use of a circular cross section in the test section and the use of gripping threads which lie on a circular arc aided in minimizing misalignment problems.

In order to protect the MTS load cell and actuator from excessive temperatures we employed a fixture to hold the specimen which significantly separates the test machine from the heated

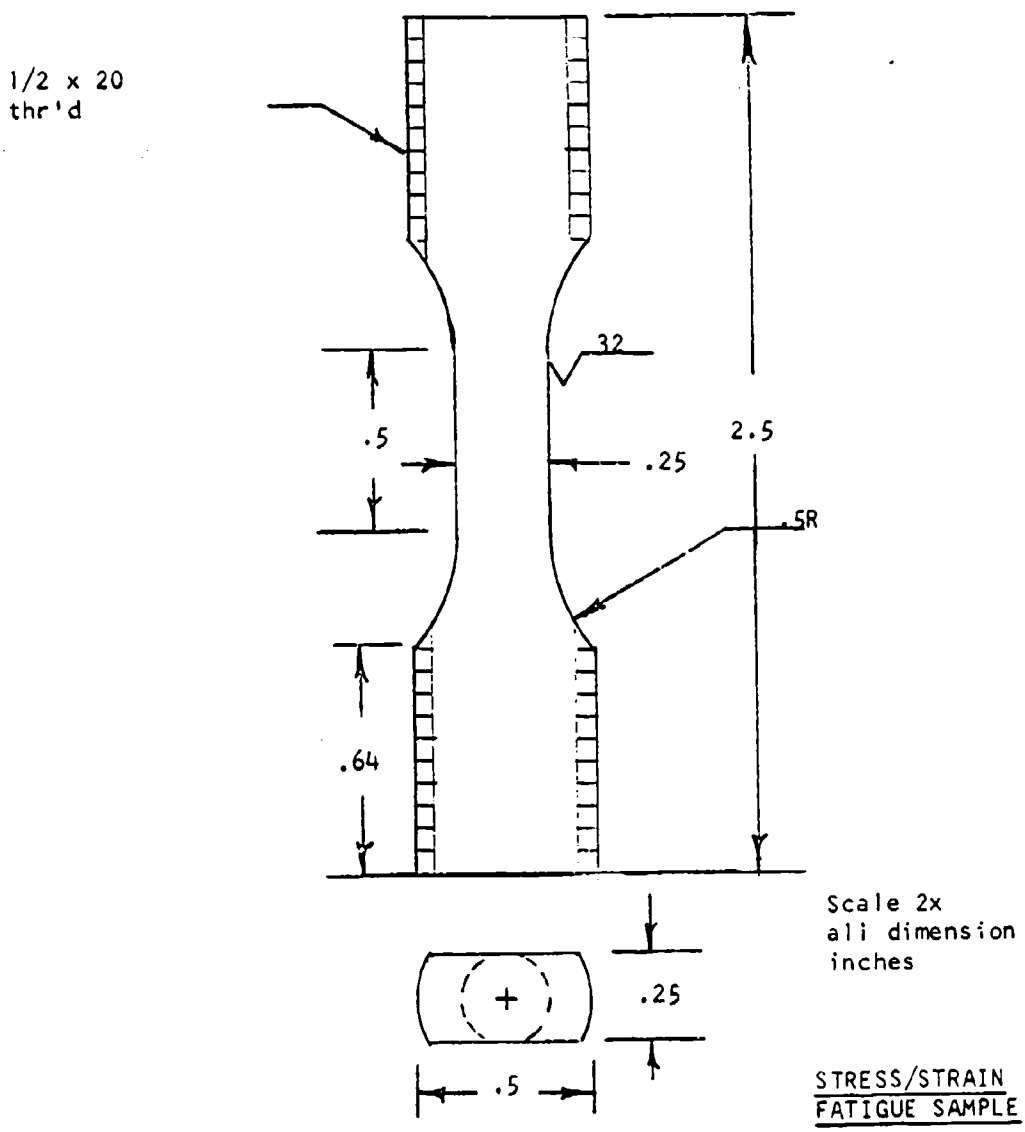
1/2 x 20
thr'd
32
.5
2.5
.25
.5R
.64
.25
.5
Scale 2x
ali dimension
inches
STRESS/STRAIN
FATIGUE SAMPLE

FIGURE 6

test area. The fixture is hollow and is cooled by flowing water through it. See Figure 7.

The additional buckling propensity brought about by the longer fixture length was minimized by careful attention to the machining of the fixture. The overall alignment error of the 20 inch fixture is less than .002 inches. The upper end of the fixture is to be attached to the load cell by a threaded connection. The lower end is attached to the actuator by a Woods metal pot.

Strain was monitored by measuring the relative displacement of the extension tubes shown in Figure 12. These tubes are attached to the specimen through the use of a split mounting plate which is precisely matched to the shoulder contour of the test specimen. The displacement was measured with a double cantilever beam clip gauge in the chamber at the top of the test fixture. Tests of the strain control system indicated that accuracies of 2% were maintained.

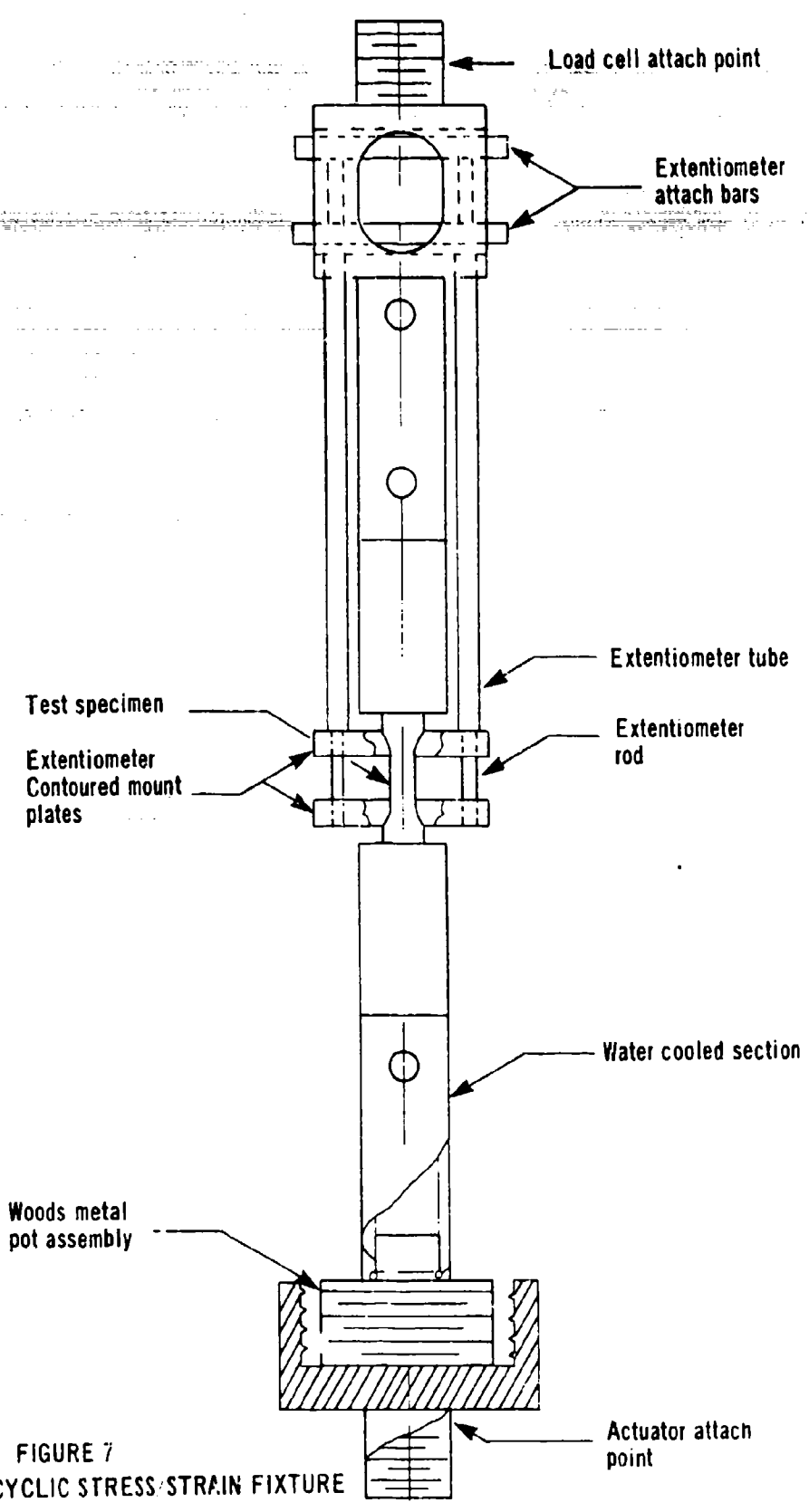

FIGURE 7
CYCLIC STRESS-STRAIN FIXTURE

RESULTS AND DISCUSSION

The monotonic mechanical behavior of polycrystalline alpha rich Ti alloys is strongly dependent on the state of preferred crystallographic orientation of the individual alpha grains (see Table III).

TABLE III

MONOTONIC STRENGTH OF BASAL TRANSVERSE TEXTURED α + β Ti ALLOYS AS A FUNCTION OF TEST TEMPERATURE

Test Direction	Test Temperature (°F)	Young's Modulus ($\times 10^6$ psi)	σ_y (ksi)	σ_u (ksi)	ε (%)	R/A (%)
6Al-4V Ti ELI Grade (Rex'l I Process)						
Rolling*	70	15.65	104	112	18	43
Transverse**	70	20.25	130	138	15	36
Rolling	700	11.60***	57	70	18	69
Transverse	700	17.90***	91	93	16	74
6Al-4V Ti ELI Grade (Duplex Process)						
Rolling	70	15.45	99.3	117.3	12.0	27.5
Transverse	70	20.25	131.0	140.6	13.5	38.4
6Al-4V Ti Standard Grade (Rex'l Process)						
Rolling	70	16.00	128	133	13	32
Transverse	70	21.20	154	164	16	33
Rolling	700	N.D.†	66	82	19	43
Transverse	700	N.D.†	95	109	15	63

TABLE III (Cont.)

6Al-2Sn-4Zr-6Mo Ti (Rex'l Process)

Test Direction	Test Temperature (^{o}F)	Young's Modulus (x10^{6}psi)	σ_y (ksi)	σ_u (ksi)	ε (%)	R/A (%)
Rolling	70	15.81	137.4	141.2	13	45.5
Transverse	70	19.04	153.3	162.1	13	36
Rolling	800	N.D.	86.5	101.5	17	53
Transverse	800	N.D.	109.5	123.5	15	51

*or $<10\bar{1}0>_{\alpha}$

**or $<0001>_{\alpha}$

***estimated from stress:strain relation; all other moduli were measured dynamically

† not determined

Studying Table III, one notes that the stiffer product direction is always the stronger direction regardless of alloy chemistry (both substitutional and interstitial), final thermal practice, and test temperature, at least up to 700^{o}F in 6Al-4V Ti and 800^{o}F in 6Al-2Sn-4Zr-6Mo Ti. Moreover, monotonic tensile property anisotropy on a percentage basis was always higher at elevated temperature than it was at 70^{o}F (see Table IV).

TABLE IV

BASAL TRANSVERSE TEXTURED

$\alpha + \beta$ Ti ALLOY MECHANICAL PROPERTY ANISOTROPY

Test Temperature	Alloy	$\frac{\sigma_y(<000\bar{1}>_{\alpha})}{\sigma_y(<10\bar{1}0>_{\alpha})}$	$\frac{\sigma_u(<000\bar{1}>_{\alpha})}{\sigma_u(<10\bar{1}0>_{\alpha})}$
70^{o}F	6Al-4V Ti/ELI	1.25	1.23
70^{o}F	6Al-4V Ti/St'd	1.20	1.23
70^{o}F	6Al-2Sn-4Zr-6Mo Ti	1.20	1.23
700^{o}F	6Al-4V Ti/ELI	1.60	1.33
700^{o}F	6Al-4V Ti/St'd	1.44	1.33
800^{o}F	6Al-2Sn-4Zr-6Mo Ti	1.46	1.33

The increase in mechanical property anisotropy with increasing temperature numerically results because on a percentage basis the strength (and stiffness in the case of 6Al-4V Ti/ELI, see Table III) in the $\langle 0001 \rangle_\alpha$ direction is less temperature sensitive than it is in the $\langle 10\bar{1}0 \rangle_\alpha$ direction. The essential reasons for the strength anisotropy noted above are the very low Schmidt factor for $\langle 11\bar{2}0 \rangle_\alpha$ slip in $\langle 0001 \rangle_\alpha$ or transverse oriented samples and the much higher crss for $\langle \bar{c} + \bar{a} \rangle$ as compared to $\langle \bar{a} \rangle$ slip shown by Paton et al (Reference 3) for the basic Ti-6.6Al solid solution. Interestingly enough, Paton et al (ibid) also report that the crss of 6.6Al-Ti single crystals on a percentage basis is less sensitive to increasing temperature (from 70°F to 700°F) in the case of $\langle \bar{c} + \bar{a} \rangle$ slip than it is in the case of $\langle \bar{a} \rangle$ slip. Alloying alterations (either interstitial or substitutional) produce changes in strength as expected but these changes occur in both directions equally (see Tables III and IV) leaving the mechanical property anisotropy unaltered. At both test temperatures, the ductility of the metal is quite reasonable and invariant with test temperature.

The fatigue behavior of our strongly basal transverse textured products has also been explored in terms of cyclic stress:strain diagrams in order to infer differences in low cycle fatigue performance (Reference 9) as a function of orientation as well as

conventional S-N curves in order to observe high cycle fatigue performance. Cyclic stress:strain curves were created in this investigation by connecting the tips of hysteresis loops saturated by repeated full stress reversals. After hysteresis loop saturation occurred at one amplitude, the next datum was always obtained by increasing the load amplitude. Typical cyclic stress:strain curves observed in this way for both 6Al-4V Ti and 6Al-2Sn-4Zr-6Mo Ti are shown in Figures 8 and 9. Tension and compression stress:strain curves are presented separately here in order to illustrate the role played by alpha phase crystallography in their generation. For example, the cyclic stress:strain behavior along $<10\bar{1}0>_\alpha$ in 6Al-4V Ti ELI Grade at 70^oF is nearly the same in both tension and compression loading (see Figure 8). The yield strengths in both testing directions are equal with the work hardening exponent in compression being somewhat higher than it is in tension. By contrast, cyclic stress:strain behavior parallel to $<0001>_\alpha$ is highly asymmetric when room temperature tension and compression results are compared for 6Al-4V Ti ELI Grade. The cyclic yield strength in compression in this product direction exceeds its tension counterpart by 45% and the plastic work hardening exponent in compression is a factor of 6 higher than it is in tension. Similar mechanical property asymmetry along $<0001>_\alpha$ has

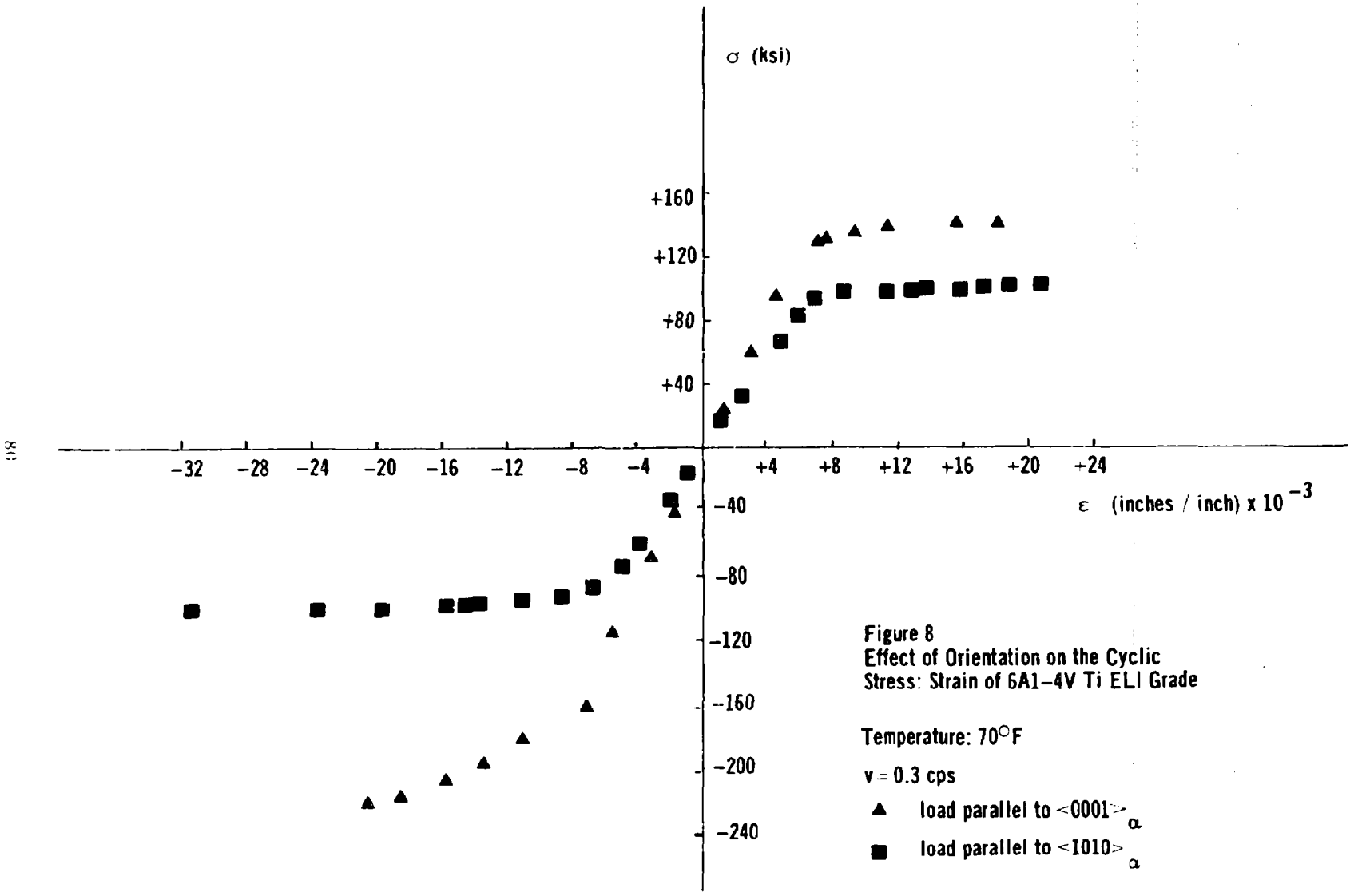

Figure 8
Effect of Orientation on the Cyclic Stress: Strain of 6A1–4V Ti ELI Grade

Temperature: 70°F

v = 0.3 cps

▲ load parallel to $<0001>_\alpha$

■ load parallel to $<1010>_\alpha$

been reported in terms of monotonic yield loci for highly basal transverse textured 6Al-4V Ti (Reference 7). A summary of our cyclic stress:strain data for all three alloy chemistries as a function alpha phase crystallography and temperature is given in Table V.

TABLE V

CYCLIC STRESS:STRAIN BEHAVIOR

OF BASAL TRANSVERSE TEXTURED $\alpha + \beta$ Ti ALLOYS

Test Direction	Test Temperature (^{o}F)	Static Behavior Tensile σ_y (ksi)	Cyclic Behavior Tensile σ_y (Ksi	Work Hard. Exp.	Compressive σ_y (ksi)	Work Hard. Exp.
6Al-4V Ti ELI Grade (Rex'l I Process)						
$<10\bar{1}0>_\alpha$	70	104	98	0.05	94	0.14
$<0001>_\alpha$	70	130	132	0.09	188	0.56
$<10\bar{1}0>_\alpha$	700	57	47	0.10	44	0.32
$<0001>_\alpha$	700	91	93	0.16	100	0.52
6Al-4V Ti Standard Grade (Rex'l Process)						
$<10\bar{1}0>_\alpha$	700	66	64	0.22	56	0.41
$<0001>_\alpha$	700	95	94	0.46	118	0.67
6Al-2Sn-4Zr-6Mo Ti (Rex'l Process)						
$<10\bar{1}0>_\alpha$	70	137.4	128	0	104	0.36
$<0001>_\alpha$	70	153.3	148	0.11	152	0.48

For the sake of convenience, we have also recapped the monotonic tensile yield behavior given in Table III for these metals. A comparison of monotonic and cyclic tensile yield strengths indicates that cyclic softening occurs at both room and elevated temperature (700°F) parallel to $<10\bar{1}0>_\alpha$ in 6Al-4V Ti ELI Grade. Loading parallel to $<0001>_\alpha$ in 6Al-4V Ti ELI Grade produces no change in yield strength when monotonic and cyclic tensile properties are compared at either listed test temperature. Moreover, at 700°F, the magnitude of the yield strength asymmetry along $<0001>_\alpha$ is vastly reduced (compare cyclic tensile and compression yield strength at 700°F vs 70°F) but the large asymmetry in working hardening coefficient between tension and compression modes remains when the metal is tested parallel to $<0001>_\alpha$ at 700°F.

Increasing the interstitial content of the 6Al-4V Ti composition produces little change in either the monotonic or cyclic stress: strain behavior at 700°F (compare results for 6Al-4V Ti ELI Grade and Standard Grade in Table V). It does appear from this comparison that whatever interstitial induced strengthening does remain at this temperature it is primarily associated with yielding due to loads applied along $<10\bar{1}0>_\alpha$.

Figure 9 presents 70°F cyclic stress:strain curves for orthogonally oriented samples of basal transverse textured 6Al-2Sn-4Zr-6Mo Ti. A summary of this behavior is also included in Table V. Cyclic strain softening is more apparent when loads are applied along $<10\bar{1}0>_\alpha$ than it is in the case of 6Al-4V Ti (compare monotonic and cyclic tensile yield strengths for the two materials). A modest degree of cyclic strain softening is even exhibited for tensile loads applied along $<0001>_\alpha$ in 6Al-2Sn-4Zr-6Mo Ti. The cyclic compression yield properties of this metal differ significantly from those just presented for 6Al-4V Ti. For example, the cyclic compression yield for loads applied along $<10\bar{1}0>_\alpha$ is distinctly lower than its tensile counterpart and the strong yield loci asymmetry noted in the case of 6Al-4V Ti loaded along $<0001>_\alpha$ virtually does not exist here. However, these differences in flow stress at plastic strains of 2×10^{-3} between the two material chemistries are minimized at higher flow stresses or plastic strains due to the large work hardening coefficients observed cyclicly when loads were applied in both the $<10\bar{1}0>_\alpha$ and $<0001>_\alpha$ directions. In fact, two of the more significant conclusions one can draw from Table V is that work hardening is much more extensive in compression in $\alpha + \beta$ Ti alloys than it is in tension and that compression along $<0001>_\alpha$ produces a significantly higher degree of work hardening than does similar loading along $<10\bar{1}0>_\alpha$.

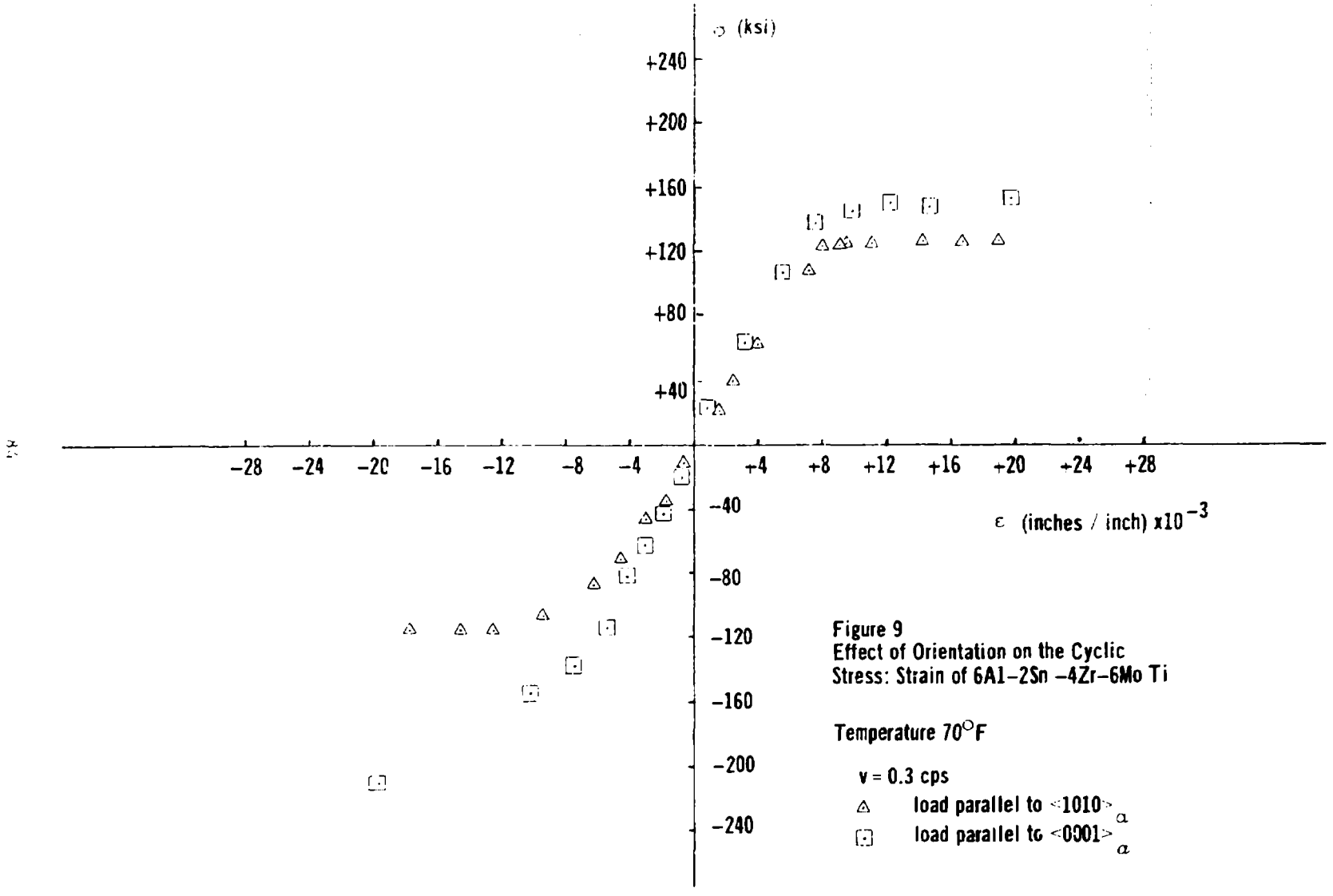

Figure 9
Effect of Orientation on the Cyclic Stress: Strain of 6Al–2Sn –4Zr–6Mo Ti

Temperature 70°F

v = 0.3 cps

△ load parallel to $\langle 10\bar{1}0 \rangle_\alpha$

⊡ load parallel to $\langle 0001 \rangle_\alpha$

Recognizing from Table V that cyclic strain softening does not occur to an appreciable enough extent in either orientation in 6Al-4V Ti to reduce the basic tensile yield strength differences observed monotonically between samples loaded in $<0001>_\alpha$ and $<10\bar{1}0>_\alpha$, one could well expect the S-N fatigue behavior of samples whose long axis is oriented parallel to $<0001>_\alpha$ to be superior to that associated with samples whose long axis was oriented parallel to $<10\bar{1}0>_\alpha$. Such an expectation is bourne out in Figure 10 where one notes the "smooth" fatigue lives of $<0001>_\alpha$ oriented 6Al-4V Ti ELI Grade samples exceed their $<10\bar{1}0>_\alpha$ counterparts by a factor of ten at all stress levels. In "notched" fatigue, the difference in life with alpha crystallographic orientation observed at $K_t = 1$ in Figure 10 for 6Al-4V Ti ELI Grade virtually disappears (see Figure 11). This result is not totally unexpected and can be rationalized based on the fact that a $K_t = 4$ notch creates a triaxial stress state which tends to average fatigue life performance in the two orthogonal loading directions. Increasing the oxygen and hydrogen levels of 6Al-4V Ti ELI Grade by 70% and 125% respectively produced no change in its notched fatigue S-N performance (compare S-N data presentations in Figures 11 and 12).

The S-N fatigue performance of basal transverse textured 6Al-2Sn-4Zr-6Mo Ti at a $K_t = 1$ is shown in Figure 13. As noted previously

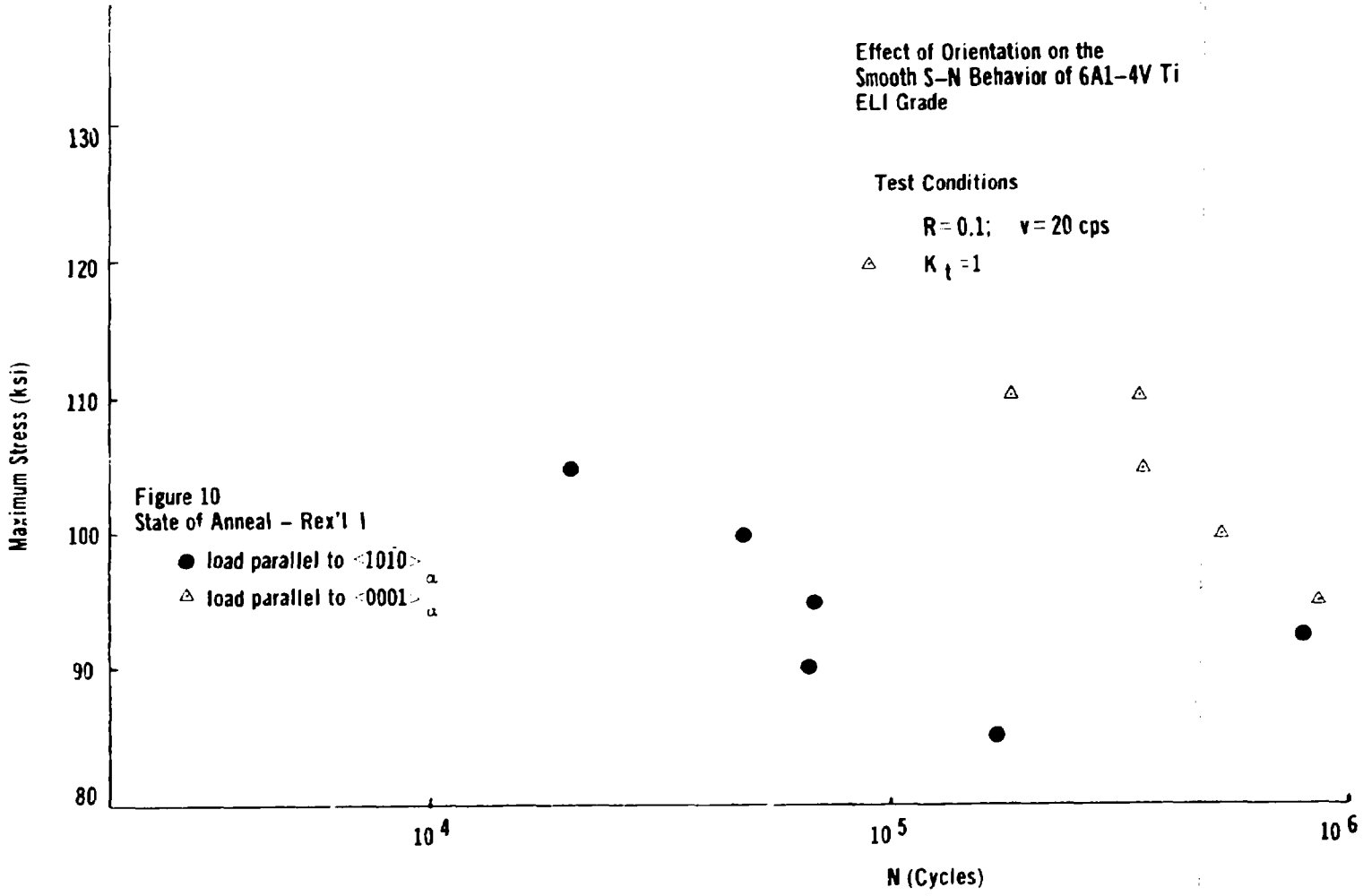
Effect of Orientation on the
Smooth S–N Behavior of 6Al–4V Ti
ELI Grade
Test Conditions
R = 0.1; v = 20 cps
△ K_t = 1
Maximum Stress (ksi)
130
120
110
100
90
80
10^4
10^5
10^6
N (Cycles)
Figure 10
State of Anneal – Rex'l I
● load parallel to $\langle 10\bar{1}0 \rangle_\alpha$
△ load parallel to $\langle 0001 \rangle_\alpha$

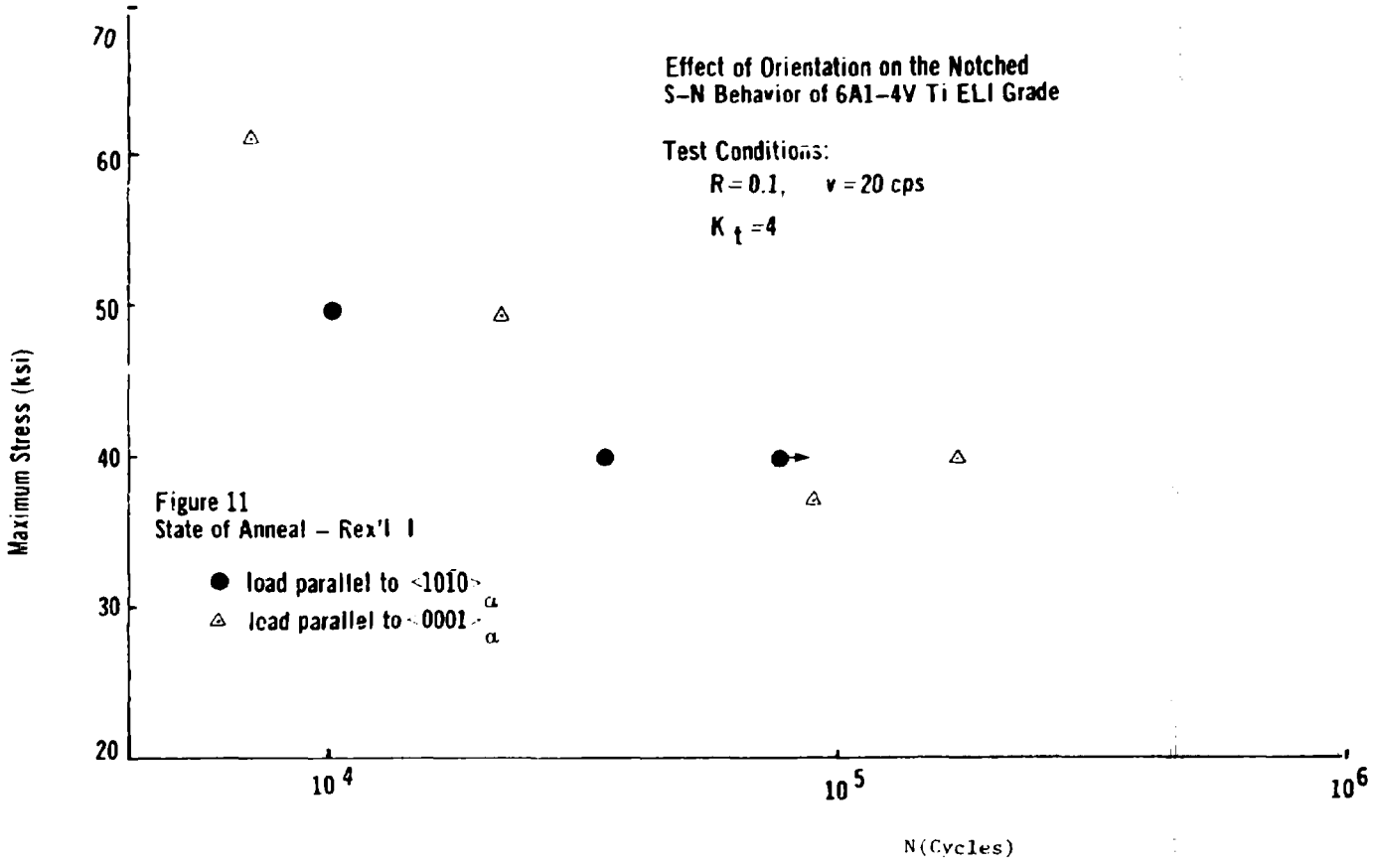

Figure 11
State of Anneal – Rex'l I

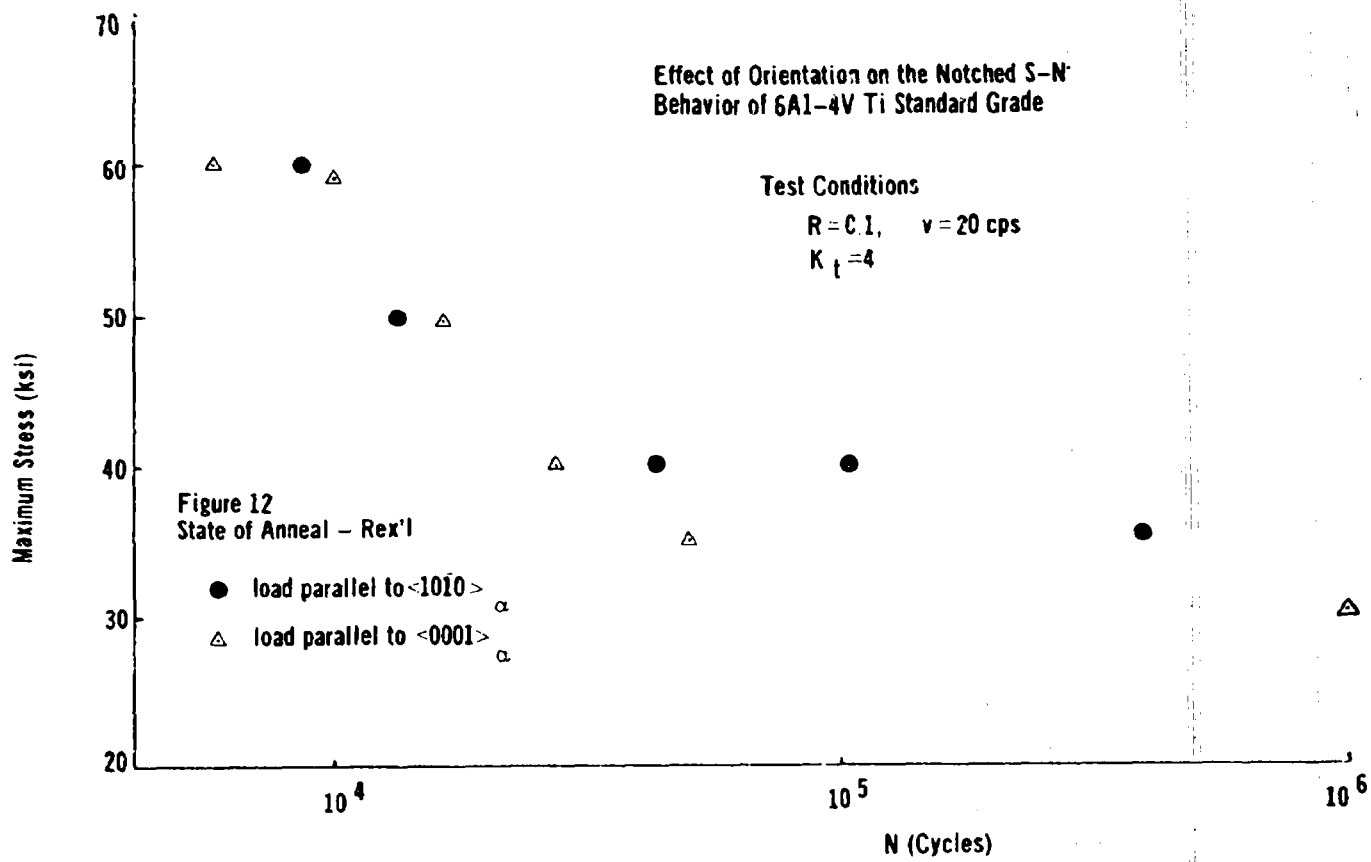

Figure 12
State of Anneal – Rex'l

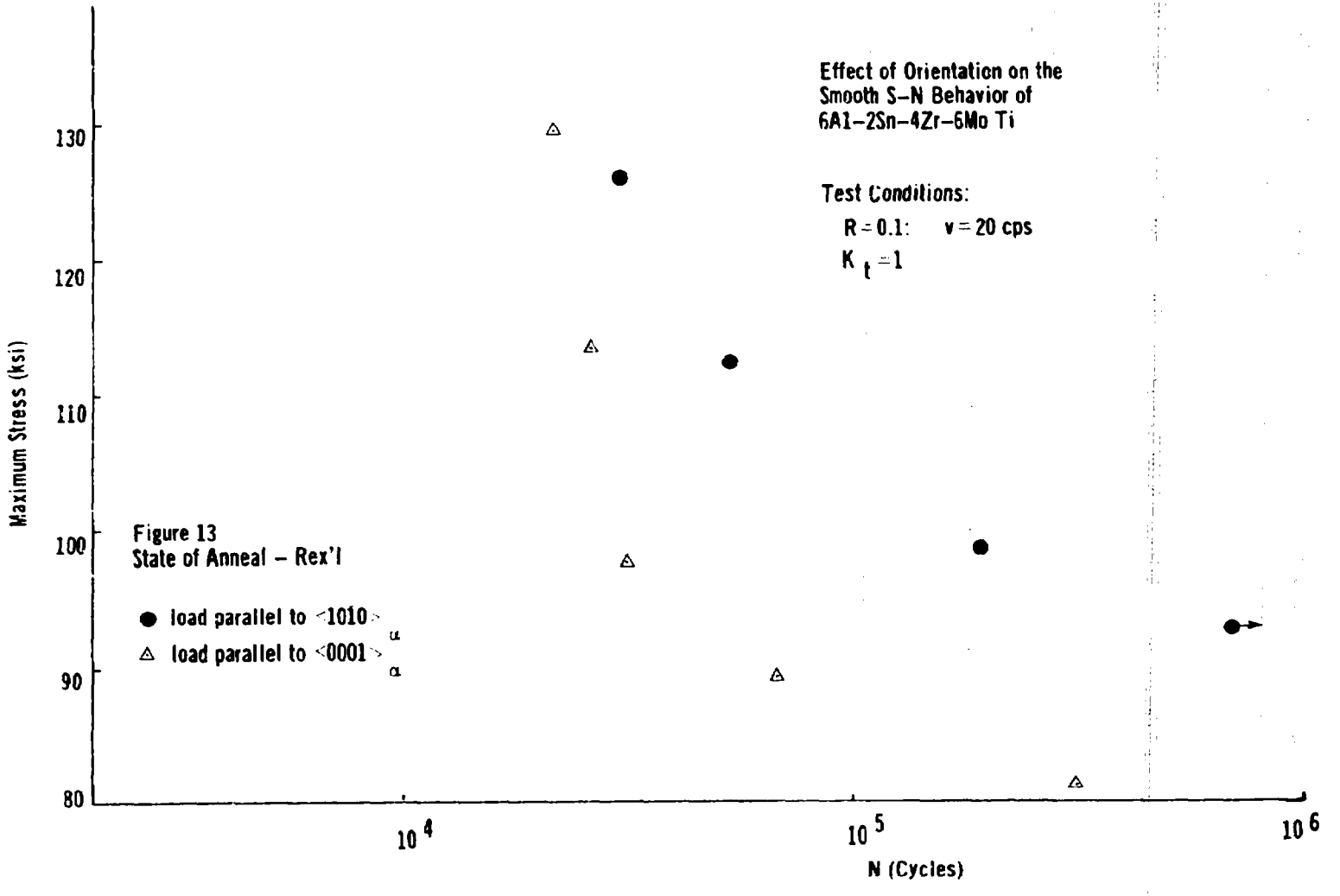

Figure 13
State of Anneal – Rex'l

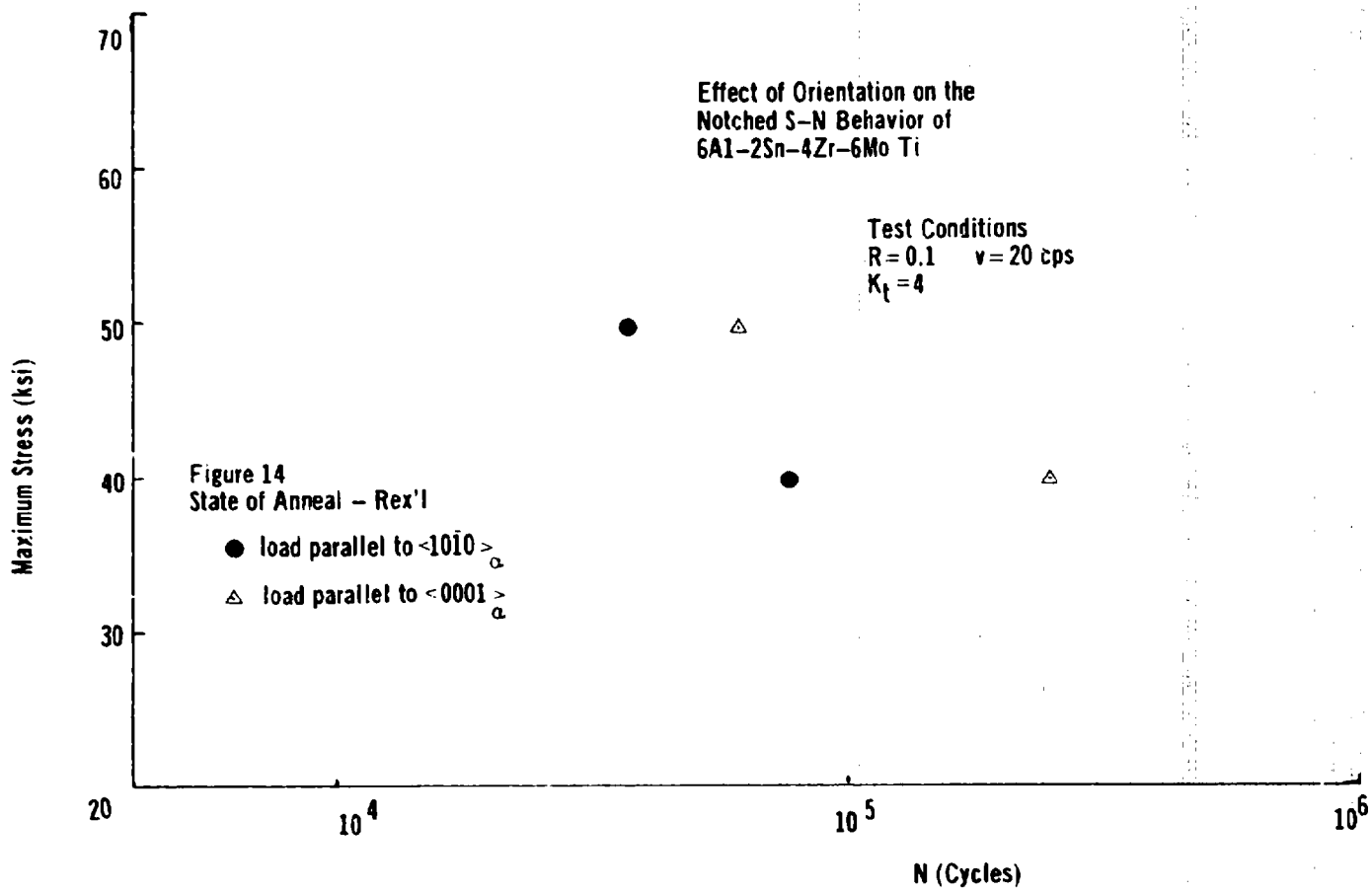

Figure 14
State of Anneal – Rex'l

in the case of 6Al-4V Ti ELI Grade, one expects on the basis of the monotonic and cyclic stress:strain data for 6Al-2Sn-4Zr-6Mo Ti posted in Table V that low cycle fatigue performance of samples oriented in the $<0001>_\alpha$ direction should be superior to those oriented in the $<10\bar{1}0>_\alpha$ direction. Indeed if one extrapolates the data presented in Figure 13 to stress levels above 130 Ksi this does appear to be true. Below 130 Ksi, the "smooth" fatigue life of $<0001>_\alpha$ oriented samples of this alloy composition in the specific heat treatment condition defined for it in Table II is significantly inferior to its $<10\bar{1}0>_\alpha$ counterpart. Just as was the case in 6Al-4V Ti, limited data is presented in Figure 14 which verifies our expectation that th orientation dependence witnessed for the "smooth" fatigue performance of this material is eliminated when notched fatigue life performance is evaluated.

Creep parallel to both $<0001>_\alpha$ and $<10\bar{1}0>_\alpha$ has also been monitored for highly textured 6Al-4V Ti ELI Grade in both air and vacuum over the temperature range 700°F to 1000°F. At 700°F in vacuum no appreciable creep was observed after 40 hours of loading in either direction ($<10\bar{1}0>_\alpha$ or $<0001>_\alpha$) until one applied greater than 90% of the direction's monotonic yield strength. In Tables VI and VII we present minimum creep rates observed in vacuum and air respectively as a function of temperature, applied stress and orientation.

TABLE VI

VARIATION OF MINIMUM CREEP RATE OF

TEXTURED 6Al-4V Ti ELI GRADE TESTED IN VACUUM

(a) $\langle 10\bar{1}0 \rangle_\alpha$

Stress, (Ksi)	Minimum Creep Rate (in/in/hr)	Temperature ($^\circ$F)	Young's Modulus (psi)
60*	4.4×10^{-6}	700	11.6×10^6
50*	8.3×10^{-6}	800	10.2×10^6
40	1.60×10^{-5}	900	10.9×10^6
45	3.15×10^{-5}	900	10.9×10^6
50	7.00×10^{-5}	900	10.9×10^6
30	5.15×10^{-5}	1000	9.3×10^6
35	1.10×10^{-4}	1000	9.3×10^6
40	3.10×10^{-4}	1000	9.3×10^6

(b) $\langle 0001 \rangle_\alpha$

85>	(No appreciable creep observed for a total of 35 hours)	700	17.9×10^6
60>	(No appreciable creep observed for a total of 45 hours)	800	16.3×10^6
65	1.3×10^{-6}	800	16.3×10^6
40	4.5×10^{-6}	900	15.8×10^6
50	7.5×10^{-6}	900	15.8×10^6
60	1.70×10^{-5}	900	15.8×10^6
25	6.5×10^{-6}	1000	13.9×10^6
35	1.45×10^{-5}	1000	13.9×10^6
50	6.70×10^{-5}	1000	13.9×10^6

*No measurable creep was observed until 90% of the yield stress was applied.

TABLE VII

VARIATION OF MINIMUM CREEP RATE OF TEXTURED 6Al-4V Ti ELI GRADE IN AIR

(a) $\langle 10\bar{1}0 \rangle_\alpha$

Stress (Ksi)	Minimum Creep Rate (in/in/hr)	Temperature ($^\circ$F)	Young's Modulus (psi)
40	3.4×10^{-6}	700	11.6×10^6
50	5.0×10^{-6}	700	11.6×10^6
55	1.10×10^{-5}	700	11.6×10^6
60	1.20×10^{-5}	700	11.6×10^6
30	3.25×10^{-5}	900	10.9×10^6
35	1.55×10^{-4}	900	10.9×10^6
45	5.86×10^{-4}	900	10.9×10^6

(b) $\langle 0001 \rangle_\alpha$

70	2.00×10^{-5}	700	17.9×10^6
80	2.21×10^{-5}	700	17.9×10^6
35	3.86×10^{-4}	1000	13.9×10^6
50	5.80×10^{-4}	1000	13.9×10^6

As one can note from Tables VI and VII, the material in both directions is markedly more creep resistant in vacuum than it is in air. The absolute value of the creep rate parallel to $\langle 0001 \rangle_\alpha$ at any given stress level and temperature was always significantly lower than its $\langle 10\bar{1}0 \rangle_\alpha$ counterpart. Additionally the stress sensitivity of the creep rate in the $\langle 10\bar{1}0 \rangle_\alpha$ direction is significantly higher than is its counterpart in the $\langle 0001 \rangle_\alpha$ direction in both environments.

Creep resistance improvement in $\langle 0001 \rangle_\alpha$ over that observed along $\langle 10\bar{1}0 \rangle_\alpha$ has also been reported at elevated temperature by Hodi (Reference 10) in the case of basal transverse textured 4Al-4V Ti tested in ai Mechanistically, the crystallography motivated improvement is relatable here again to the higher crss required for <c + a> versus <a> in the aluminum rich alpha phase (Reference 3) and the low Schmidt factor associated with <a> slip in the $\langle 0001 \rangle_\alpha$ oriented samples. The enhancemen of creep resistance associated with transferring the material from air to a vacuum environment must be relatable to an interaction between oxygen and/or nitrogen and the beta phase of the 6Al-4V Ti ELI Grade since the amount of dissolved oxygen in the alpha phase is not expected to play any significant role in the mechanical behavior of this phase above 500°F (Reference 11). Just what the nature of this interaction is will require further investigation.

CONCLUSIONS

1. The uniaxial unnotched mechanical properties of basal transverse textured 6Al-4V Ti and 6Al-2Sn-4Zr-6Mo Ti are highly anisotropic.
2. Young's Modulus of basal transverse textured 6Al-4V Ti at 70°F is 20% greater parallel to $<0001>_\alpha$ than it is parallel to $<10\bar{1}0>_\alpha$.
3. Monotonic tensile strength enhancements of 25% have been found at 70°F on comparing the tensile properties of samples aligned along $<0001>_\alpha$ versus $<10\bar{1}0>_\alpha$ in 6Al-4V Ti after Rex'l I processing.
4. The 70°F cyclic compression yield strength of the 6Al-4V Ti ELI Grade composition in the $<0001>_\alpha$ direction was 188 Ksi vs. 94 Ksi in the $<10\bar{1}0>_\alpha$ direction.
5. At 700°F, Young's Modulus parallel to $<0001>_\alpha$ in basal transverse textured 6Al-4V Ti exceeds that parallel to $<10\bar{1}0>_\alpha$ by 54% and the monotonic yield strength parallel to $<0001>_\alpha$ is 60% higher than its $<1010>_\alpha$ counterpart.
6. Examination of the cyclic stress:strain behavior of basal transverse textured 6Al-4V Ti at 70°F and 700°F demonstrates that the monotonic mechanical property improvements just summarized are not diminished by cyclic softening.

7. Similar results in terms of mechanical property anisotropy have been obtained for basal transverse textured 6Al-2Sn-4Zr-6Mo Ti as are described above for basal transverse textured 6Al-4V Ti.

8. Smooth fatigue lives of $<0001>_\alpha$ oriented samples in basal transverse textured 6Al-4V Ti exceeded their $<10\bar{1}0>_\alpha$ counterparts at 70°F by a factor of 10 when fatigue performance at a given stress level was compared.

9. The notched fatigue life ($K_t = 4$) of both orientations ($<0001>_\alpha$ and $<10\bar{1}0>_\alpha$) was the same at any stress level in 6Al-4V Ti and 6Al-2Sn-4Zr-6Mo Ti.

10. In contrast to the enhanced smooth fatigue performance of $<0001>_\alpha$ over $<10\bar{1}0>_\alpha$ in basal transverse textured 6Al-4V Ti, $K_t = 1$ $<10\bar{1}0>_\alpha$ samples of basal transverse 6Al-2Sn-4Zr-6Mo Ti exhibited fatigue lives approximately a factor of 5-10 times better than their $<0001>_\alpha$ counterparts depending on maximum stress level.

11. The elevated temperature creep resistance of basal transverse textured 6Al-4V Ti depends on both environment and alpha phase crystallography. Creep rates in the temperature range 700°F to 1000°F can be reduced by a factor of ten in either orientation by running the test in vacuum rather than lab air. Additionally, creep rates parallel to $<0001>_\alpha$ are always

a factor of 10 lower than those observed parallel to $\langle 10\bar{1}0\rangle_\alpha$ when similar stress levels and tempers are compared.

12. Microstructural mechanisms are offered to rationalize the several mechanical property improvements noted in this work.

REFERENCES

1. J. M. Fitzpatrick and F. A. Crossley, "Development of Improved Biaxial Strength in Titanium Alloy Rocket Motor Cases Through Texture Hardening"; Phase I AFRPL-TR-67-302; December, 1967.

2. S. Fredericks, "Manu. Methods for Production Processing of Ti Sheet With Controlled Texture" AFML-TR-73-265; November, 1973.

3. N. E. Paton, R. G. Baggerly and J. C. Williams, "Deformation and Solid Solution Strenthening of Titanium:Aluminum Single Crystals"; Final Report on AFOSR Contract F44620-72-C-0043; January, 1976.

4. M. J. Harrigan, A. W. Sommer, P. A. Reimers, and G. A. Alers, "The Effect of Textures on the Mechanical Properties of Titanium Alloys"; Rockwell Int'l Report No. NA-69-909; December, 1969.

5. M. S. Harrigan, A. W. Sommer, P. A. Reimers and G. A. Alers, "The Effect of Rolling Texture on the Fracture Mechanics Properties of Ti-6Al-2Sn-4Zr-6Mo Alloy"; 2nd International Conference on Titanium, May, 1972, Plenum Press; N.Y. N.Y.; J. Jaffee and H. M. Burte - Editors.

6. A. Zarkades and F. Larson, MCIC Review of Metal Technology, "Ti and Ti Alloy Structures"; February, 1973.

7. M. Lowden and W. Hutchinson, Met. Trans. 6A, 441, March, 1975.

8. R. E. Peterson, "Stress Concentration Design Factors"; John Wiley and Sons, N. Y. N. Y.; 1953.

9. B. M. Wundt, ASTM STP 490, Chap. C and I; 1972.

10. F. Hodi, " Effect of Textures on the Creep and Stress Properties of 4Al-4V Ti"; AMMRC-TR-73-49; November, 1973.

11. J. C. Williams, A. W. Sommer and P. Tung, Met. Trans. 1972, Vol.3, pp. 2979-84.

PART III

ON THE GROWTH OF CRACKS IN BASAL TRANSVERSE TEXTURED α + β TITANIUM ALLOYS AS A FUNCTION OF CHEMICAL ENVIRONMENT

The spreading application of fracture mechanics as a design analysis tool in the aerospace industry of the '70s has made it mandatory that the crack growth resistance properties of engineering materials be not only measured but also controlled. Property control during metal manufacturing procedures requires a knowledge of the manner in which alloy chemistry and processes such as thermomechanical metal working influence the matrix of properties obtained in the final product. Experience has shown, moreover, that the crack growth resistance properties of α + β Ti alloys will vary markedly when compared on a lot-to-lot basis. The purpose of the present work is then twofold. Firstly, we shall report results on crack growth resistance in lab air and saline water for three commercial α + β Ti alloy compositions where the TMT working procedures have been carefully controlled and monitored. The three alloy compositions are 6Al-4V Ti (0.09 wt% oxygen), 6Al-4V Ti (0.162 wt% oxygen) and 6Al-2Sn-4Zr-6Mo Ti. Secondly, we shall endeavor to provide fundamental insight into the relationship between the microstructural/crystallographic origins of crack growth resistance in these commercial alloy compositions and production controllable

material/process parameters (i.e., alloy chemistry and thermomechanical processing).

Attainment of the second objective will be greatly enhanced because all the metal employed in this study was processed in a manner which left the various alloys both well annealed and with very strong basal transverse textures.* Since the recrystallized microstructure of all three Ti alloy compositions employed in this work are preponderantly hexagonal at room temperature, one can conceptually think of these materials as pseudo α single crystals possessing one of three alloy chemistries (see Figure 1).

While numerous investigators have reported results on the relation of crack growth resistance (in terms of either fracture toughness, stress corrosion or fatigue crack growth rates) to overall microstructure/fractographic morphology (e.g., Widmannstatten vs. equiaxed, etc., References 1 - 5), only three prior investigations have made any systematic attempt to correlate crack growth resistance to alpha phase crystallography (References 6 - 8). Probably the first crack growth "resistance": crystallography correlation is the now classic result of Blackburn and Williams (Reference 6) in which they showed the primary fracture path associated with static load induced saline stress

*A detailed description of the thermomechanical processing required to generate these textures can be found in Part I.

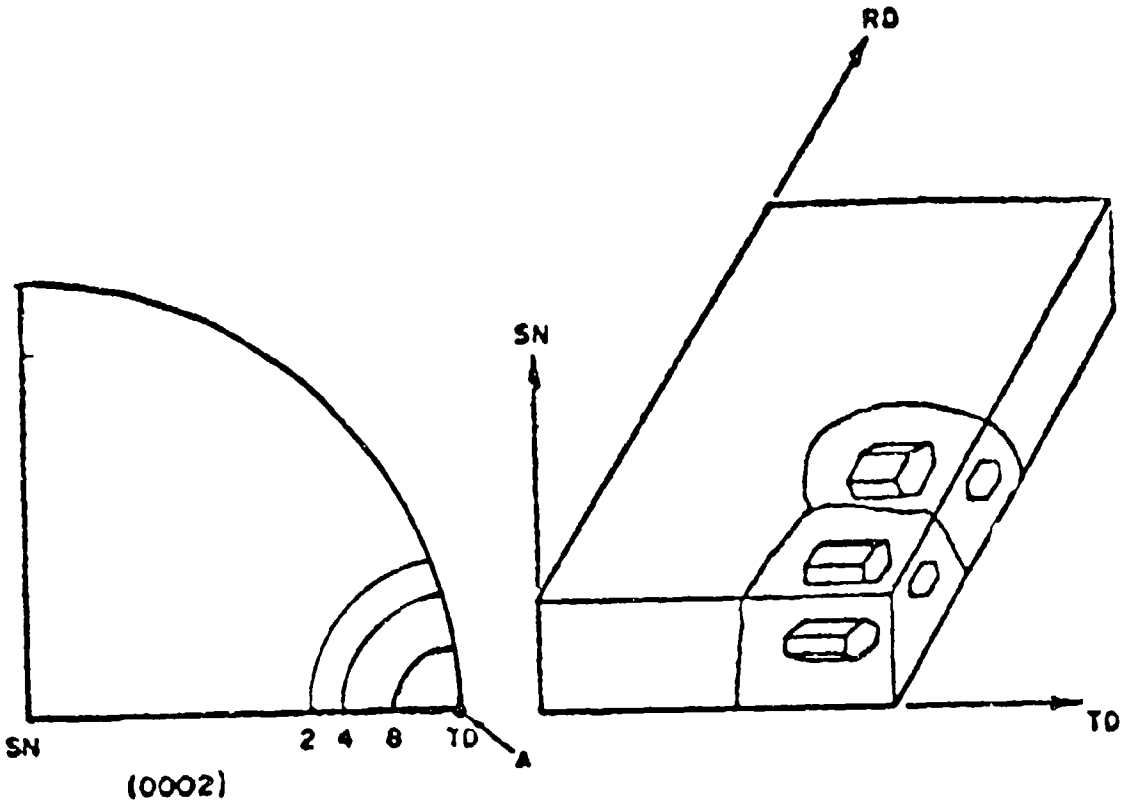

FIGURE 1 - BASAL POLE SCHEMATIC FOR A BASAL TRANSVERSE TEXTURED α TI MATERIAL

NOTE: POINT A REPRESENTS THE CASE OF PERFECT ALIGNMENT OF ALL CRYSTALLITES.

(REF. LARSON AND ZARKADES, MCIC-74-20)

corrosion of the α phase (i.e., low values of K_{ISCC}) is "near basal" cleavage [i.e., on $(10\bar{1}7)$ or $(10\bar{1}8)$]. In addition, there have been two fatigue crack growth rate studies in this area. Both of the earlier crystallography related fatigue crack growth studies were conducted only in lab air. The first of these two studies was performed by Harrigan, Sommer, Reimers and Alers on basal transverse textured 6Al-2Sn-4Zr-6Mo Ti which was recrystallized prior to crack growth observations (Reference 7). These authors showed the metal to be anisotropic with respect to both its plane strain fracture toughness and fatigue crack growth rate. They reported K_{IC} to vary by a factor of two with orientation. The tougher orientation was that wherein the load was applied parallel to the direction of most intense basal pole or $\vec{c}$ axis concentration. In terms of lab air fatigue crack growth rate anisotropy, they observed da/dn at low ΔK (< 18 Ksi$\sqrt{in.}$) to be nearly an order of magnitude faster when loads were applied parallel to the direction of major $\vec{c}$ axis concentration as opposed to directions orthogonal to this product direction. At higher ΔK (>18 Ksi$\sqrt{in.}$), the orientation dependence of the growth rate reversed and cracks propagating in Mode I parallel to the basal plane moved more slowly at any ΔK than cracks propagated normal to this crystallographic plane.

A far more complete investigation of the relation between crystallography and Stage II fatigue crack growth in basal

transverse textured and annealed 6Al-4V Ti (0.13 wt% oxygen) was performed by Bowen (Reference 8). He observed fatigue crack growth rate differences with test orientation similar to that reported earlier by Harrigan et al (Reference 6) in their more highly beta stabilized alloy. He demonstrated that the growth rate differences observed as a function of test piece orientation are associated with changes in crystallographic deformation mode required by the various loading directions and crack plane orientations employed. Specifically he showed that da/dn above ΔK = 20 Ksi $\sqrt{in.}$ was not a strong function of ΔK (in terms of a low value of the Paris exponent,"m")when a crystallographic deformation mode satisfied the shear stresses set up in the continuum flow field at the crack tip (i.e., slip or twinning happens symmetrically, about the crack plane tip and crack advance occurs on a linear front which is normal to the applied load). By contrast, da/dn in the high ΔK region (i.e., >20 Ksi $\sqrt{in.}$) was a much stronger function of ΔK (in terms of higher Paris "m" values) for those crack plane:loading direction orientations where large differences existed between the orientation of the available crystallographic deformation modes and the shear stresses of the continuum flow field. For example, in a basal transverse textured product, the ΔK insensitive test orientations were shown to be LS, SL and TS. Significantly higher ΔK sensitivity was found for growth rates measured in TL, ST and LT orientations. In these latter three

orientations, fractographic evidence taken from regions cracking macroscopically at rates greater than 1×10^{-5} inches/cycle, indicates that crack advance is quite complex. It is neither linear across the sample on any given crack plane nor planar. This complexity arises because in these orientations slip and/or twinning are forced to occur assymetrically about the crack plane tip and microscopic regions of ductile tear are found connecting regions of striation formation. Bowen rationalizes the higher ΔK da/dn rate sensitivities of the TL, ST and LT about $\Delta K = 20$ Ksi $\sqrt{in}$. in terms of his monotonic or ductile tear fracture observations since this fracture mode isn't a function of ΔK but only K_{max}.

Based on Bowen's association of monotonic fracture with increasing ΔK sensitivity at high ΔK, one would expect those orientations with the higher rate sensitivity (TL, ST and LT)when K_{max} is high enough to promote ductile tear to also exhibit higher ΔK threshold values than the linear crack advance group (TS, LS, SL). At low ΔK the microscopic regions which can tear at high values of K_{max} should become very effective barriers to further growth when K_{max} is too low to permit ductile tear within the plastic zone at the crack tip. Unfortunately, Bowen made very few crack growth rate measurements below $\Delta K = 20$ Ksi$\sqrt{in}$. In the two orientations where he did make a consistant series of measurements in the 10^{-6} inches/cycle region (i.e., LS and LT), his results

show the LS orientation [measured Paris "m" value = 2.7 (at high ΔK] tending to a ΔK threshold at least 2 Ksi$\sqrt{in.}$ lower than the LT orientation [measured Paris "m" values = 4.1 (at high ΔK)]. It will be interesting to see if this proposed relationship between propensity to ductile tear at high ΔK and ΔK threshold extends to a comparison between crack growth rates in the TL orientation (measured Paris "m" = 3.1) and the LT orientation (measured Paris "m" = 4.1) in basal transverse textured Ti alloy products. Confirmation of this prediction will also be sought during the current effort since these two crack orientations are often the most important from an engineering structural analysis viewpoint. In fact, such ΔK threshold shifts can significantly impact predictive analyses where fatigue crack retardation effects are considered. Da/dn rates under spectrum loading conditions are determined by combining the appropriate constant load amplitude da/dn vs ΔK relation with a knowledge of the instantaneous value of $K_{effective}$. $\Delta K_{effective}$ in turn is obtained after reducing the applied ΔK by instantaneous value of $K_{closure}$. Thus, one required knowledge of the da/dn vs ΔK relation at ΔK values well below those actually applied to the hardware being analyzed.

Another subject of great interest in titanium alloy metallurgy are the origins of crack growth acceleration in adverse environments. Such acceleration has been observed under both static load (References 2 and 6) as well as during fatigue load cycling (References 1 and 3) when results are compared for cracking in lab air versus in aqueous salt solutions of various levels of salinity. Specifically, Pettit et al (Reference 2) reported very low values of K_{ISCC} in the TL orientation of intensely basal transverse textured and recrystallized 6Al-4V Ti plate which had been fabricated by the RMI Company to Rockwell International's High Fracture Toughness B-1 specification. They also reported that the fatigue crack growth rate of this orientation was markedly accelerated when one compared results obtained in lab air and salt water. The growth rate acceleration they reported in salt water, moreover, was a complex function of load cycle frequency and applied ΔK in a manner similar to that reported by Dawson and Pelloux for 6Al-4V Ti plate of undetermined basal texture pedigree. For example, at low ΔK ($<10 Ksi\sqrt{in.}$ @ R = 0.1), low load cycling frequencies in salt water ($\nu<1$ cps) generated da/dn results very similar to those measured in dry air at the same ΔK. By contrast high load cycling rates in salt water at low ΔK caused an appreciable da/dn acceleration. The reverse was true above ΔK's in the range 13 $Ksi\sqrt{in.}$ to 15 $Ksi\sqrt{in.}$

Dawson and Pelloux explain the complex frequency behavior in terms of the rate of formation of a passivating film on the crack tip which forms quickly enough at low frequency to effectively separate the cracking metal from its environment if the ΔK is low enough. In this case, high frequency loading is really defined in terms of wave shape and rise time with the important characteristic that the load rise time be significantly shorter than the time required for repassivation of a surface whose protective film has just been ruptured. The term " high ΔK" here becomes synonomous with that stress intensity level where conventional time dependent static stress corrosion cracking is a major component of the corrosion fatigue process.

By contrast with the above reports of strong acceleration of crack growth in salt water (versus lab air) for the ELI grade of 6Al-4V Ti sheet (Reference 9) and plate (Reference 2) products, Chesnutt et al have reported the crack growth characteristics (K_{ISCC} and da/dn) of several separated processed 6Al-4V Ti ELI Grade pancake forgings to be only mildly accelerated (and in some cases, not at all) when the metal was immersed in salt water (versus lab air). They thermomechanically processed their pancakes to produce seven distinct phase/grain morphologies which spanned the range from equiaxed particle shapes to

to Widmannstatten structure. The basal pole textures of all seven microstructural conditions were relatively weak. Moreover, these textures were such that the compact tension samples they extracted from these samples for stress corrosion and corrosion fatigue testing exhibited few basal poles parallel to the direction of applied load. This observation is apparent from both the X-Ray basal pole figures they present for each microstructural condition as well as their report of $\approx 16 \times 10^6$ psi for Young's modulus in this product direction. Having thus precluded "near basal" cleavage (Reference 6) geometrically, their study emphasizes again the association of "near basal" cleavage and crack growth acceleration in an aqueous saline solution. Having once precluded the existence of a continuous "near basal" cleavage path normal to a principal stress direction in the compact sample, no further significant corrosion induced crack growth acceleration was found for any of the several microstructural conditions studied.

One, thus, could conclude from the above that corrosion induced crack growth acceleration in $\alpha + \beta$ Ti alloys results solely from the propensity of the alpha Ti phase to cleave in a near basal orientation when exposed to a saline environment under load (static or cyclic). There are three significant questions that still remain to be answered. One, what is the microstructural origin

of this "near basal" cleavage process and how is it influenced by alloy chemistry. Two, is it possible for an $\alpha + \beta$ Ti alloy sample to exhibit virtually 100% near basal cleavage as a fracture mode and still not show significantly accelerated crack growth in salt water? Three, what is the relationship between microstructural grain/phase morphology and corrosion induced crack growth acceleration in an $\alpha + \beta$ Ti alloy material where a significant quantity of basal poles adopts a strongly preferred direction? In our current effort, we shall attempt to provide answers to the first two of the questions. The third question although of great interest is beyond the scope of the present research.

EXPERIMENTAL PROCEDURE

Three distinct α + β Ti alloy chemistries were employed in this work. Two of these were of the basic 6Al-4V Ti composition differing only in their oxygen contents. The ELI version of this alloy contained 0.095 wt% oxygen. The Standard Grade 6Al-4V Ti composition contained 0.162 wt% oxygen. The wt% of all other alloy constituents in both heats were identical. The third alloy composition employed was 6Al-2Sn-4Zr-6Mo Ti. All materials used in this work were derived from production melting stock. They were thermomechanically processed to one quarter inch thick, six and one half inch wide plate stock. The metal process schemes employed were all designed to produce a plate product which exhibited an intense basal transverse crystallographic texture. X-Ray diffraction basal pole figures for each of the three alloy compositions are given in Figures 2-4. Another method for expressing basal pole preferred orientation is elastic constant anisotropy. Young's moduli for all three alloy products are given in Table I. Detailed accounts of the individual alloy chemistries thermomechanical process schemes employed and experimental procedures to obtain the X-Ray pole figures and Young's moduli can be found in Part I. Conventional mechanical properties for these materials are enumerated in Part II.

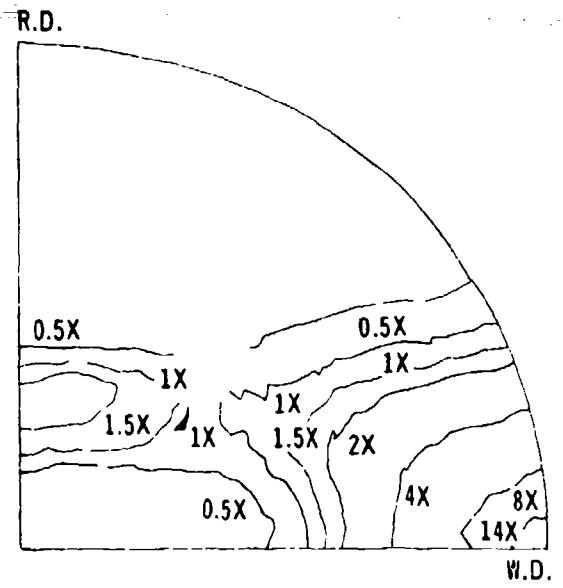

Figure 2: Material–6Al–4V Ti ELI Grade
TMT Process Method:7

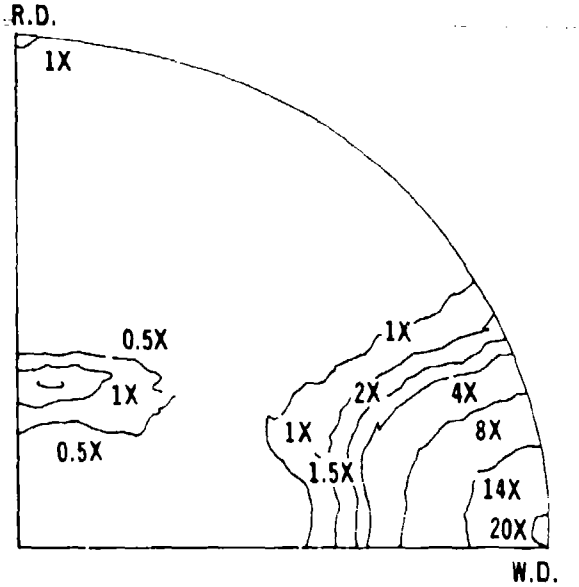

Figure 3: Material–6Al–4V Ti
Standard Grade
TMT Method 11

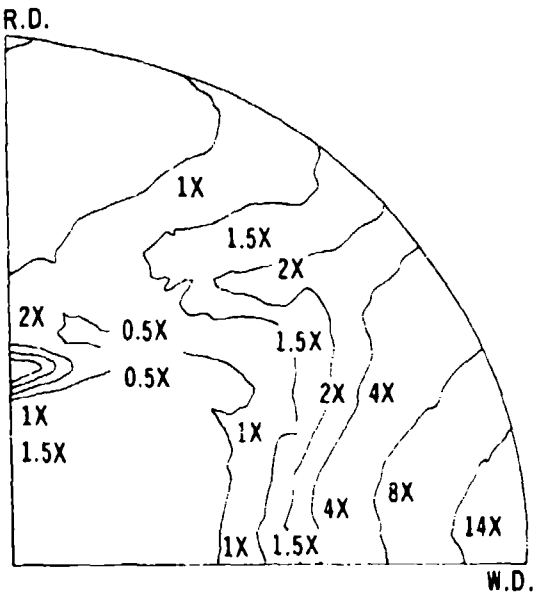

Figure 4: Material–6Al–2Sn–4Zr–6Mo Ti
TMT Method – 16

TABLE I

BASAL TRANSVERSE TEXTURE DETERMINATIONS

VIA YOUNG'S MODULUS ANISOTROPY

Alloy Composition	Heat Treatment*	E_{Width} ($\times 10^6$ psi)	$E_{Rolling}$ ($\times 10^6$ psi)	E_{W-R} ($\times 10^6$ psi)
6Al-4V Ti: ELI Grade	Rex'l I	20.18	15.75	4.43
	Rex'l II	19.65	15.55	4.10
	Duplex	20.25	15.45	4.80
6Al-4V Ti: Standard Grade	Rex'l	21.20	16.00	5.20
6Al-2Sn-4Zr-6Mo Ti	Rex'l	19.04	15.81	3.23
αTi Single Crystal	Annealed	21.00 ($\vec{c}$ axis)	14.50 ($\vec{a}$ axis)	6.50

*For details of these treatments, please see Table II

Table II details the heat treatments our various alloy compositions were subjected to prior to test. As one can note, the ELI or low oxygen grade of 6Al-4V Ti was examined in three conditions and the other compositions in only one each. The elastic moduli of the variously heat treated alloys are given in Table I. The mechanical behavior of the three alloy products after these various heat treatments is given in Part II.

TABLE II

POST ROLLING THERMAL PROCESS SCHEDULES

Alloy Chemistry	Heat Treat Designation	Heat Treatment*
6Al-4V Ti:ELI Grade	Rex'l I	1710°F/4 hrs. + furnace cool at less than 100°F/ hour to 70°F.
	Rex'l II	1710°F/4 hrs. + air cool to 70°F
	Duplex	1710°F/4 hrs. + furnace cool at less than 100°F/ hour to 1400°F/1 hr. + air cool to 70°F.
6Al-4V Ti: Standard Grade	Rex"L	1780°F/4 hrs. + furnace cool at less than 100°F/ hour to 70°F
6Al-2Sn-4Zr-6Mo To	Rex'l	1700°F/8 hrs. + furnace cool to 1200°F/1 hr. + air cool to 70°F

*Microstructurally, all three materials have $\sim$ 10 μ grain size and are fully recrystallized and equiaxed.

The crack growth resistance of compact tension samples fashioned from all three alloy products were assessed as a function of orientation within the products. In all cases, the compact tension sample's dimensions were B = ½" and W = 2½". The two product orientations employed here were LT and TL. Employing the pseudo single crystal hypothesis mentioned earlier (see Figure 1), LT oriented samples can be regarded as being so configured that loads are applied parallel to a $<10\bar{1}0>$ direction in our α phase "single crystal" and the crack advances along <0001>. Conversely TL oriented samples apply a load parallel to <0001> and cracks propagate parallel to $<10\bar{1}0>$.

Three measures of crack growth resistance were employed in this work. All measurments were made at 70°F. These were:

- fracture toughness in lab air
- K_{ISCC} in lab air and 3.5% NaCl in H_2O
- da/dn vs ΔK in lab air and 3.5% NaCl in H_2O

Fracture toughness measurements were obtained in the form of R-curves since our one quarter inch plate thickness procluded measurement of K_{IC}. Our experimental technique was modelled after that described in ASTM Part 31 (1975) for "Proposed Recommended Practice for R-Curve Determination". An MTS closed

loop electro-hydraulic facility was employed for both fatigue precracking and final loading during the R-curve test itself. The approach taken here was to obtain the instantaneous crack length at any given load along the load:displacement raw data plot from experimental knowledge of the COD associated with that particular load. Instantaneous COD was obtained by first taking a cracked sample to a given load and then measuring the slope of the load:displacement curve associated with unloading that sample to approximately 80% of its prior load. By iterating this load:unload sequence to higher and higher loads, the raw data for entire R-curve was generated. In order to convert load vs. COD to K vs crack length, we assumed that the standard K:COD relation derived for the CT sample fabricated from isotropic material is valid here as well so long as the proper choice of elastic modulus is inserted into the equation. It was necessary to make this assumption since no satisfactory K:COD relation for a CT sample fabricated from an anisotropic solid exists at this time. Since the stress field in a CT sample is quite complex, it would only be fortuitous if the appropriate elastic modulus for either orientation could be found among the uniaxially determined moduli listed in Table I. For this reason we selected the appropriate "modulus" value to be used in this relation from a knowledge of the initial fatigue precrack length

and the linear portion of the load:deflection curve obtained during the first loading after precracking. In general, the "moduli" determined in this fashion represented an averaging of the uniaxial moduli given in Table I for the L and T directions of any given alloy composition.

K_{ISCC} measurements employed fatigue precracked compact tension samples which were exposed to either lab air or 3.5% NaCl in distilled water. Fatigue precracking was always accomplished in lab air to an a/w value of at least 0.3. The final maximum precrack stress intensity applied to the specimen during the fatigue precrack process itself was always less than one half of the initial K applied during the K_{ISCC} determination. Sample loading for the test itself was accomplished in an MTS electro-hydraulic facility. An autographic record of load:COD was obtained for each sample. The test was run at constant deflection and the sample was fixtured such that the load originally applied by the MTS machine could be isolated in the constant deflection fixture:sample assembly. For those tests run in artificial sea water (3.5% NaCl in H_2O), the environmental exposure was such that fresh sea water continuously flowed past the crack tip during the 500 hours the test was in progress. In some cases, the initial loading after fatigue precracking was accomplished in the presence of salt water. The crack length of each sample was monitored visually using a low power microscope (60X). After 500 hours had elapsed, the fixtured surviving samples were placed once again in the MTS machine

with a COD gauge attached across the loading plane. The residual displacement on the fixtured sample was released and autographically recorded. The sample was then loaded in the test machine until the "released" deflection was obtained. The load at this point corresponded to the residual load on the constantly displaced specimen. It was particularly important in this Program that we record both residual load and final crack length for our K_{ISCC} calculation since we are dealing with an acknowledged anisotropic material. Here again, the load:COD relations in the literature for the CT sample assume the crack to exist in an isotropic solid, essentially the same problem we faced in interpreting our R-Curve raw data. Here, however, our "residual load" measurement at the termination of the test removed the necessity of making assumptions about effective elastic moduli, etc.

In two instances, K_{ISCC} tests were conducted using a constant load technique. In these situations, precracking was performed to very low ΔK (e.g., 5-6 Ksi$\sqrt{in.}$) in salt water. The samples were then loaded in our MTS facility to a static K value 2 Ksi$\sqrt{in.}$ higher than the precrack K_{max} in the salt water and held for 1 hour or until the crack began to grow under static load. If no growth occurred, the load was raised such that $K_{applied}$ was not 4 Ksi$\sqrt{in.}$ higher than the former precrack maximum. This load was again held for one hour and assuming no growth here, the load was raised again and held for observation of crack growth. Here again, fresh salt water was continually fed to the crack tip from a

reservoir during the test. The applied K was designated as K_{ISCC} when one observed first motion of the crack. Since our microscopic observation tool allowed us to detect crack advances as small as 0.001 inches, holding for one hour assured us of being able to identify stress corrosion crack advance rates as low as 5×10^{-7} inches/second in determining a K_{ISCC} value with this test technique.

Fatigue crack growth rate measurements were performed on compact tension samples between a/w ratios of 0.3 and 0.75 at constant load amplitude in MTS electro-hydraulic facility. Crack growth rates were monitored optically using a 20X travelling microscope and electronically by means of COD measurements. Each sample was precracked in air for a distance of at least ¼" (a full sample thickness) at a series of declining load amplitudes with the final 0.050" to 0.100" of precrack advance occurring at the same load amplitude as was planned for use during the data collection portion of the experiment. Once the precrack phase was completed, no further changes in load amplitude were made during the test until it was complete. Tests were run at 70°F in both lab air (average humidity - 20%) and 3.5% NaCl in H_2O. During salt water tests, fresh salt water was continuously pumped into the crack tip from a reservoir in order to maintain a constant crack tip chemistry situation. In lab air, all tests

RESULTS

Results obtained in this effort for all three Ti alloy chemistries will be reported in subsections entitled

- Fracture Toughness
- Static Displacement/Load Crack Growth
- da/dn vs ΔK in lab air
- da/dn vs ΔK in 3.5% NaCl in H_2O as a Function of Final Thermal Practice.

Fracture Toughness

Crack growth resistance measurements (i.e., "R-Curves") were employed to assess the fracture toughness of all three alloy compositions as tion of product orientation (see Figures 5 - 7). In order to provide additional perspective on these dat we have also catalogued the highest K level for which no evidence of crack growth could be detected during the rising load test (Table III). Additionally, the highest values of K associated with slow stable tear in a given product orientation (i.e., the asymptotic K value found for a given "R-Curve") are recounted in Table IV.

Figure 5 Effect of Orientation on
Crack Growth Resistance

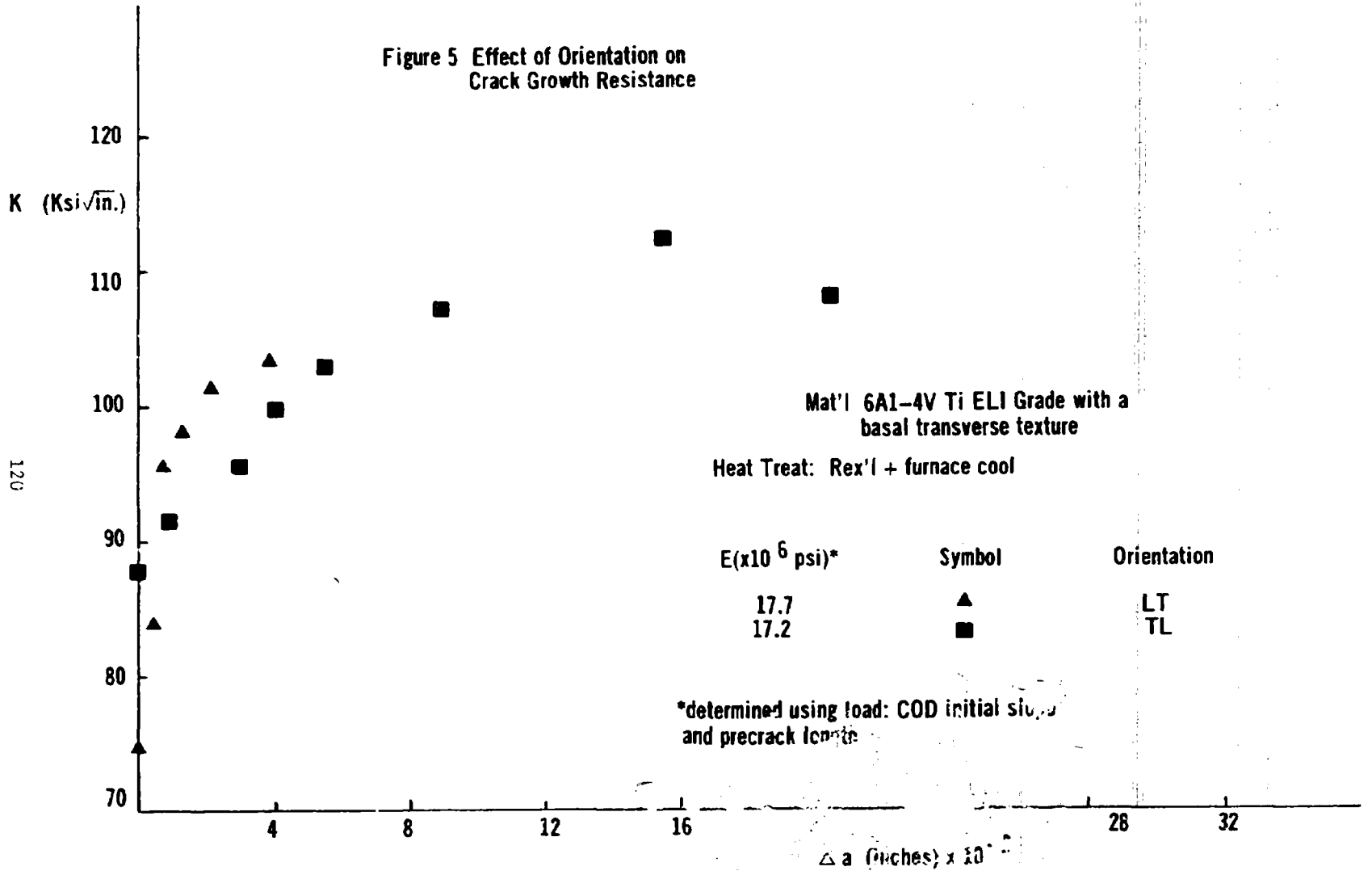

Figure 6 Effect Of Orientation on Crack Growth Resistance

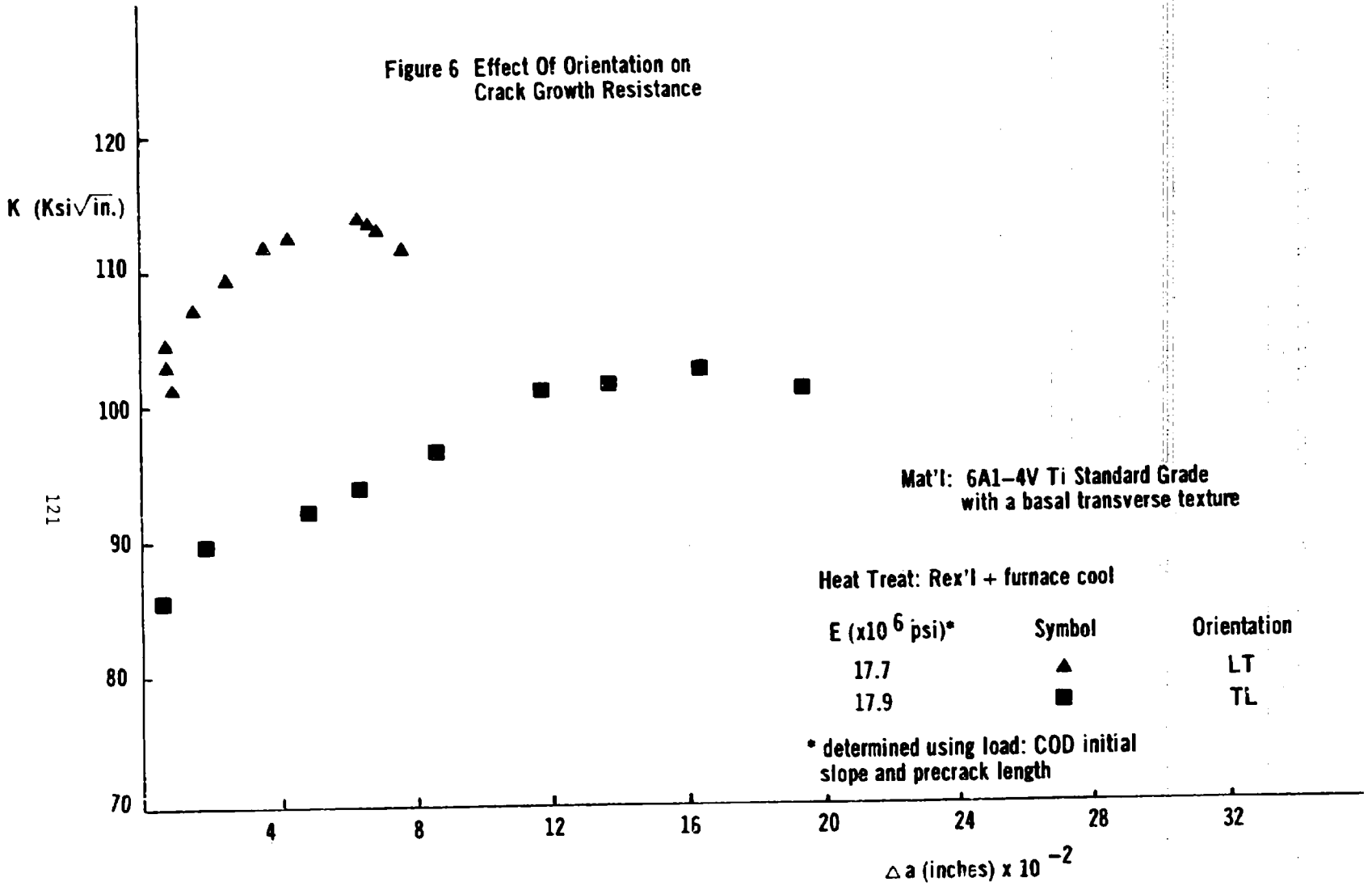

Figure 7 Effect of Orientation on
Crack Growth Resistance

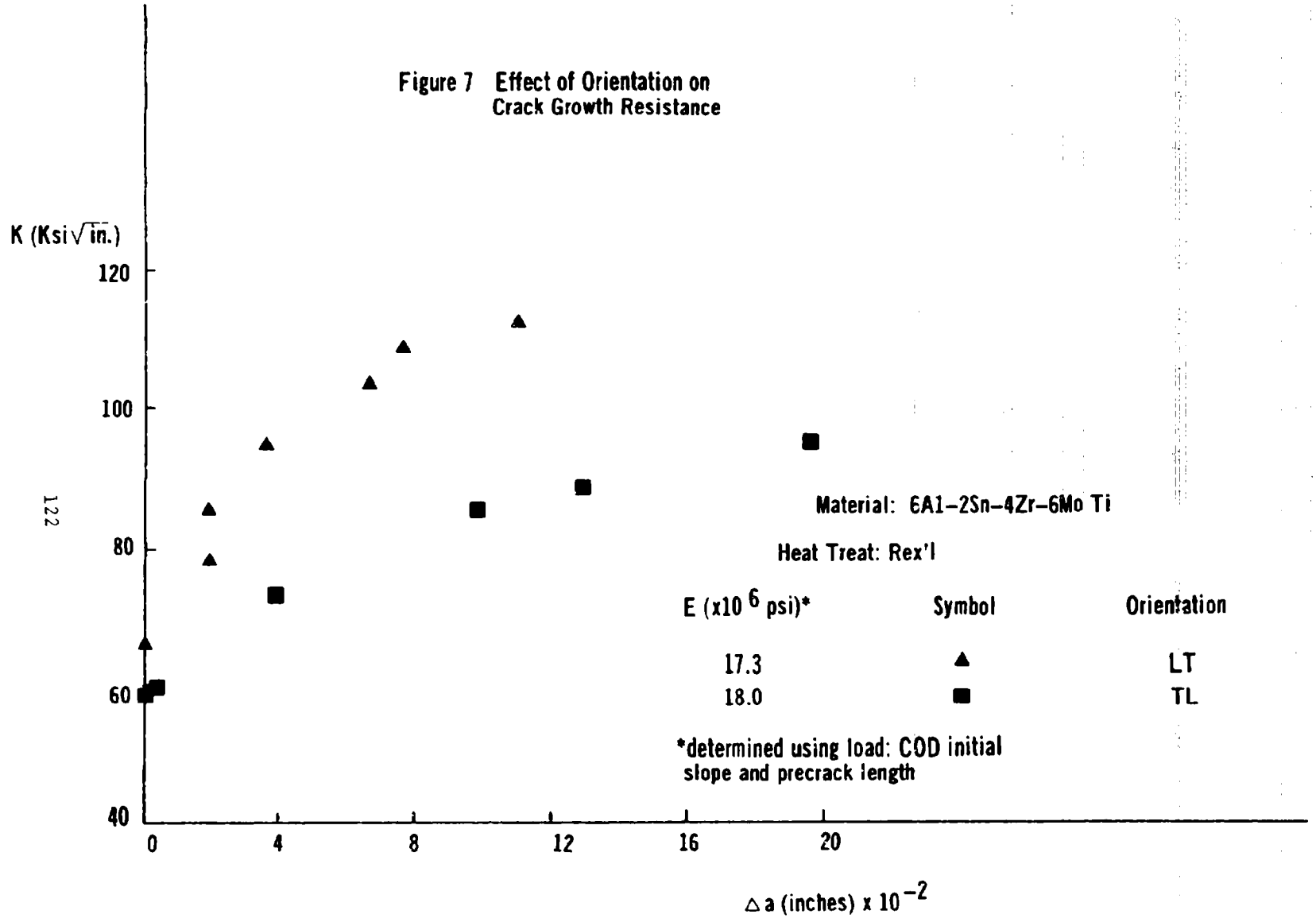

TABLE III

RESISTANCE TO THE INITIATION OF SLOW STABLE TEAR AS A FUNCTION OF ALLOY CHEMISTRY AND PRODUCT ORIENTATION

Alloy Chemistry	$K_R^{Initiation}$ (Ksi $\sqrt{in.}$)	
	TL Orientation	LT Orientation
6Al-4V Ti ELI Grade	88	80
6Al-4V Ti Standard Grade	84	98
6Al-2Sn-4Zr-6Mo Ti	60	66

TABLE IV

MAXIMUM STRESS INTENSITY FOR SLOW STABLE TEAR AS A FUNCTION OF ALLOY CHEMISTRY AND PRODUCT ORIENTATION

Alloy Chemistry	$K_R^{Maximum}$ (Ksi $\sqrt{in.}$)	
	TL Orientation	LT Orientation
6Al-4V Ti ELI Grade	112	103
6Al-4V Ti Standard Grade	103	113
6Al-2Sn-4Zr-6Mo Ti	96	113

Referring to Table III, load application parallel to $<0001>_\alpha$ with the crack expanding along $<10\bar{1}0>_\alpha$ in a mixed mode situation provides an unexpected result in that $K_R^{Initiation}$ in the TL orientation is essentially independent of interstitial content level. By contrast, it is now well accepted that plane strain fracture toughness, K_{IC}, of 6Al-4V Ti products decreases sharply with increasing oxygen level over the same chemistry range defined by the ELI and Standard Grades employed here. The maximum stress intensity associated with slow stable tear (Table IV) in a mixed mode for the TL orientation does depend on the oxygen content of the 6Al-4V Ti alloy in question but here again the dependence is not very strong. The mixed mode crack growth resistance observed in the LT orientation of the two 6Al-4V Ti alloy chemistries (i.e., the $<10\bar{1}0>_\alpha$: $(0001)_\alpha$ opening mode system) is even more unexpected, based on the established dependence of K_{IC} on interstitial chemistry in this alloy system. Here, in both Tables III and IV, we observe that the crack growth resistance of the standard grade metal is superior to its ELI Grade counterpart.

In Table III, one notes that the resistance of the 6Al-2Sn-4Zr-6Mo Ti alloy to the initiation of slow stable tear in the rising load or R-Curve test is significantly poorer than either of the 6Al-4V Ti alloy chemistries. Moreover, this observation is independent of

product orientation. By contrast, the maximum K associated with slow stable tear in the 6-2-4-6 Ti alloy depends on product orientation with an opening load applied parallel to $<0001>_\alpha$ (TL orientation) yielding a significantly lower K value than its $<1010>_\alpha$ counterpart (LT orientation). Surprisingly, the maximum K for slow stable tear in the $<1010>_\alpha : <0001>_\alpha$ opening mode system in 6-2-4-6 Ti is equivalent to its 6Al-4V Ti counterparts (Table IV).

Static Displacement/Load Crack Growth

The effects of alloy chemistry, thermal practice, product orientation and chemical environment on statically displaced or loaded cracks in basal transverse textured Ti alloys are given in Table V. As one can note in this Table, the vast majority of these tests were conducted under conditions of constant displacement amplitude. In two cases where the measured K_{ISCC} values were quite low compared to our lab air R-curve test data (Table III) we confirmed our 500 hour salt water results by running constant load or K tests as well. $K_{Initial}$ values in Table V were selected initially based on the results of Table III to assure that our precracked samples did not exhibit additional crack growth during their initial loading sequence.

TABLE V

STATIC DISPLACEMENT/LOAD CRACK GROWTH RESISTANCE IN LAB AIR AND 3.5% NaCl IN H_2O AT 70°F

Material Chemistry

Al wt%	V wt%	O wt%	H ppm
6.0	3.8	0.095	30

Material Orientation	Post Rolling Thermal Practice as Defined in Table I	Environment	$K_{Initial}$ (Ksi$\sqrt{in.}$)	K_{ISCC} (Ksi$\sqrt{in.}$)	Remarks
LT	Rex'l I	lab air	72	>72*	No growth in 500 hours
TL	Rex'l I	lab air	70	>70*	No growth in 500 hours
LT	Rex'l I	3.5% NaCl in H_2O	70	>70*	Loaded initially in air; no growth in 500 hours
TL	Rex'l I	3.5% NaCl in H_2O	70	<< 70*	Loaded initially in air; crack grew 1.36" in 120 minutes and severed CT sample
1L	Rex'l I	3.5% NaCl in H_2O	35	30*	Loaded in salt water; crack propagated a small distance in the first few hours and then ceased to grow during the next 500 hours.
TL	Rex'l I	3.5% NaCl in H_2O	-	20**	Rising K test which was begun at K = 10 Ksi$\sqrt{in.}$ with 30 minute hold times at each K level.

TABLE V (Cont.)

Material Orientation	Post Rolling Thermal Practice as Defined in Table I	Environment	$K_{Initial}$ (Ksi$\sqrt{in.}$)	K_{ISCC} (Ksi$\sqrt{in.}$)	Remarks
LT	Duplex	3.5% NaCl in H_2O	80	>80*	Loaded in salt water; no growth in 500 hours
TL	Duplex	3.5% NaCl in H_2O	60	>60*	Loaded in salt water; no growth in 500 hours
TI	Duplex	3.5% NaCl in H_2O	70	>70*	Loaded in salt water; no growth in 500 hours
TL	Duplex	3.5% NaCl in H_2O	80	>80*	Loaded in salt water; no growth in 500 hours

Material Chemistry

Al wt%	V wt%	O wt%	H wt%
5.94	3.83	0.16	50

LT	Rex'l	3.5% NaCl in H_2O	80	See Remarks*	Loaded in salt water; crack would not grow in T direction but rather turned 90° and grew in L direction.
TL	Rex'l	3.5% NaCl	35	<< 35*	Loaded in salt water; rapid crack propagation severed sample in several hours

TABLE V (Cont.)

Material Chemistry

Al wt%	Sn wt%	Zr wt%	Mo wt%	O wt%	H ppm
5.75	2.07	4.16	6.2	0.127	68

Material Orientation	Post Rolling Thermal Practice as Defined in Table I	Environment	$K_{Initial}$ (Ksi$\sqrt{in.}$)	K_{ISCC} (Ksi$\sqrt{in.}$)	Remarks
LT	Rex'l + 1200°F/1 hr. + air cool	lab air	50	>50*	No growth in 500 hours
LT	Rex'l + 1200°/1 hr. + air cool	3.5% NaCl in H_2O	35	>35*	No growth in 500 hours
LT	Rex'l + 1200°/1 hr. + air cool	3.5% NaCl in H_2O	50	*	Crack turns 90° to propagate along L direction
TL	Rex'l + 1200°/1 hr. + air cool	lab air	44	<<44*	Crack growth in L direction and breaks sample within hours of loading.
TL	Rex'l + 1200°/1 hr. + air cool	3.5% NaCl in H_2O	25	<<25*	Crack grows in L direction and breaks sample within hours of loading.
TL	Rex'l + 1200°F/1 hr. + air cool	3.5% NaCl in H_2O	-	13.5**	Rising K test which was begun at K = 6 Ksi$\sqrt{in.}$ with 30 minute hold times at each K level.

* Constant displacement test
**Constant load test

Reviewing the data presented in Table V for crack growth in lab air under static crack opening displacement, one notes that neither the LT orientation ($<10\bar{1}0>_\alpha$: $<0001>_\alpha$)nor the TL orientation ($<0001>_\alpha$: $<10\bar{1}0>_\alpha$) of 6Al-4V Ti ELI Grade (i.e., 0.095 25% O, 20 ppm H_2 exhibits any crack growth in 500 hours at a stress intensity of 70 Ksi$\sqrt{in}$. This result validates our R-Curve results given in Table III and as well is in keeping with Meyn's findings that such low interstitial contents in 6Al-4V Ti only give rise to slow crack growth under static load in lab air at 80 Ksi$\sqrt{in}$. or above (Reference 10). By contract opening mode cracks in the 6Al-2Sn-4Zr-6Mo Ti alloy chemistry metal were not stable on $(0001)_\alpha$ in lab air at static K levels well below those given in Table III for the initiation of crack growth under rising load. As one can note, the TL orientation exhibited extensive crack growth under this relatively chemically benign condition at $K_{Initial}$ = 44 Ksi$\sqrt{in}$. The LT orientation of this alloy composition by comparison exhibited no crack growth in 500 hours at a somewhat higher $K_{Initial}$ level (i.e., 50 Ksi$\sqrt{in}$.) thus demonstrating the important role played by α phase crystallography in this cracking process.

Turning to the salt water environment results enumerated in Table V, we observe that cracks could never be made to grow

parallel to $\langle 0001 \rangle_\alpha$ when loads were applied parallel to $\langle 10\bar{1}0 \rangle_\alpha$ (i.e., the LT orientation) at $K_{Initial}$ levels as high as 80 Ksi $\sqrt{in.}$ in the case of 6Al-4V Ti and 50 Ksi $\sqrt{in.}$ in the case of 6Al-2Sn-4Zr-6Mo Ti. The corresponding tests in the TL orientation provided results wherein substantial crack growth was observed down to very low K levels in some cases. As one also observes here, K_{ISCC} in the TL orientation of 6Al-4V Ti ELI Grade is quite sensitive to final thermal practice. For example, application of the "Rex'l I" process to 6Al-4V Ti results in a K_{ISCC} between 20-30 Ksi $\sqrt{in.}$ whereas the "Duplex" anneal eliminates all sensitivity to salt water crack growth parallel to $\langle 0001 \rangle_\alpha$. Refering to Table II, we note that the "Rex'l I" thermal treatment differs from its "Duplex" counterpart only in that the latter treatment returns the recrystallized microstructure to 1400°F for 1 hour and cools the one quarter inch thick metal in air.

K_{ISCC} in salt water in the TL orientation of 6Al-4V Ti also appears to depend on oxygen chemistry. One notes in Table V that increasing the oxygen content of the basic alloy in its furnace cooled condition significantly lowers its K_{ISCC} level.

The recrystallization practice applied to the 6Al-2Sn-4Zr-6Mo Ti metal chemistry was also duplex in nature. However, as one can

note in Table V, it was not effective in preventing "near basal" cleavage in either lab air or salt water at low values of K (see Figure 8) although the extent of such cleavage was considerably less in lab air.

da/dn vs. ΔK in Lab Air

In Figures 9 - 11 we present fatigue crack growth rate data obtained in lab air for all three alloy compositions. The basal pole X-ray textures and elastic modulus anisotropy associated with Figures 9 and 10 are essentially the same (see Figures 2 - 3 and Table I). The basal transverse texture emplaced in the 6Al-2Sn-4Zr-6Mo Ti was not as intense (see Figure 4 and Taule I).

At first glance, one might be tempted to conclude that the lab air fatigue crack growth rate behavior of the lower oxygen grade of 6Al-4V Ti is essentially the same in the two diverse sample orientations, (see Figure 9). However, the results in Figure 9 have been verified by repeated testing and the results shown here of the da/dn data for the two orientations crossing one another at about ΔK of 16 Ksi $\sqrt{in}$. are real. As one can note in this Figure, it appears that the threshhold value of ΔK in the LT orientation is going to be significantly higher than its TL counterpart. Corroboration evidence to the existence of the difference in crack growth

Lab Air Environment

←<10$\bar{1}$0>$_\alpha$→

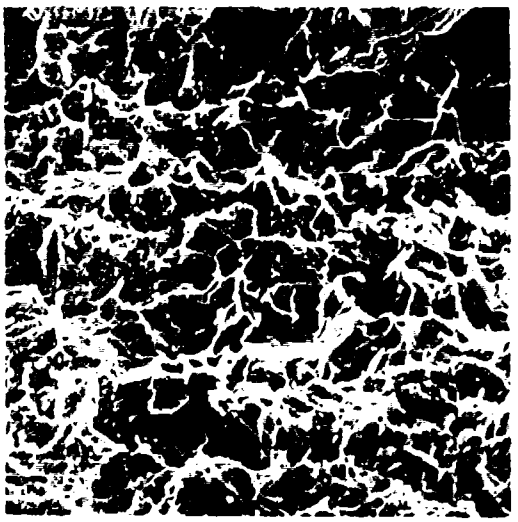

(a) 1000X in SEM

Sample Orientation: TL

Loading Direction: <0001>$_\alpha$

Nominal Crack Growth Direction: <10$\bar{1}$0>$_\alpha$

$K_{applied}$ = 44 Ksi $\sqrt{in.}$

←<10$\bar{1}$0>$_\alpha$→

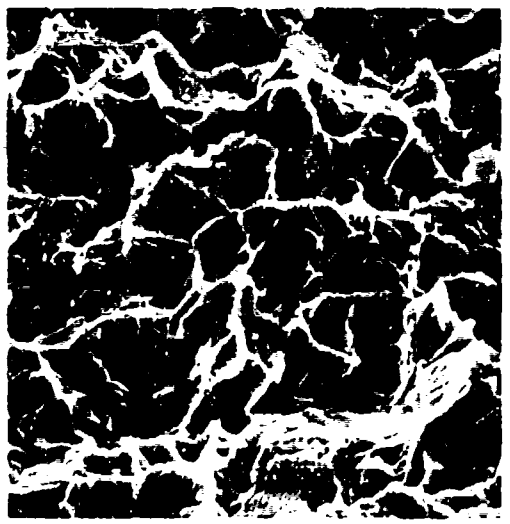

(b) 2000X in SEM

Sample Orientation: TL

Loading Direction: <0001>$_\alpha$

Nominal Crack Growth Direction <10$\bar{1}$0>$_\alpha$

$K_{applied}$ = 44 Ksi $\sqrt{in.}$

Figure 8 - Fractographic Observations of Static Displacement Induced Crack Growth in Basal Transverse 6Al-2Sn-4Zr-6Mo Ti

3.5% NaCl in H_2O Environment

←<$10\bar{1}0$>$_\alpha$→

(c) 1000X
in SEM

Sample Orientation: TL

Loading Direction <0001>$_\alpha$

Nominal Crack Growth
Direction <$10\bar{1}0$>$_\alpha$

$K_{applied}$ = 25 Ksi $\sqrt{in.}$

←<$10\bar{1}0$>$_\alpha$→

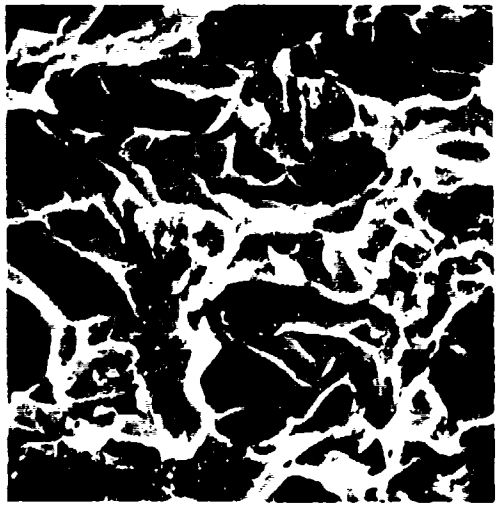

(d) 2000X
in SEM

Sample Orientation TL

Loading Direction <0001>$_\alpha$

Nominal Crack growth
Direction <$10\bar{1}0$>$_\alpha$

$K_{applied}$ = 25 Ksi $\sqrt{in.}$

Figure 8-Cont.

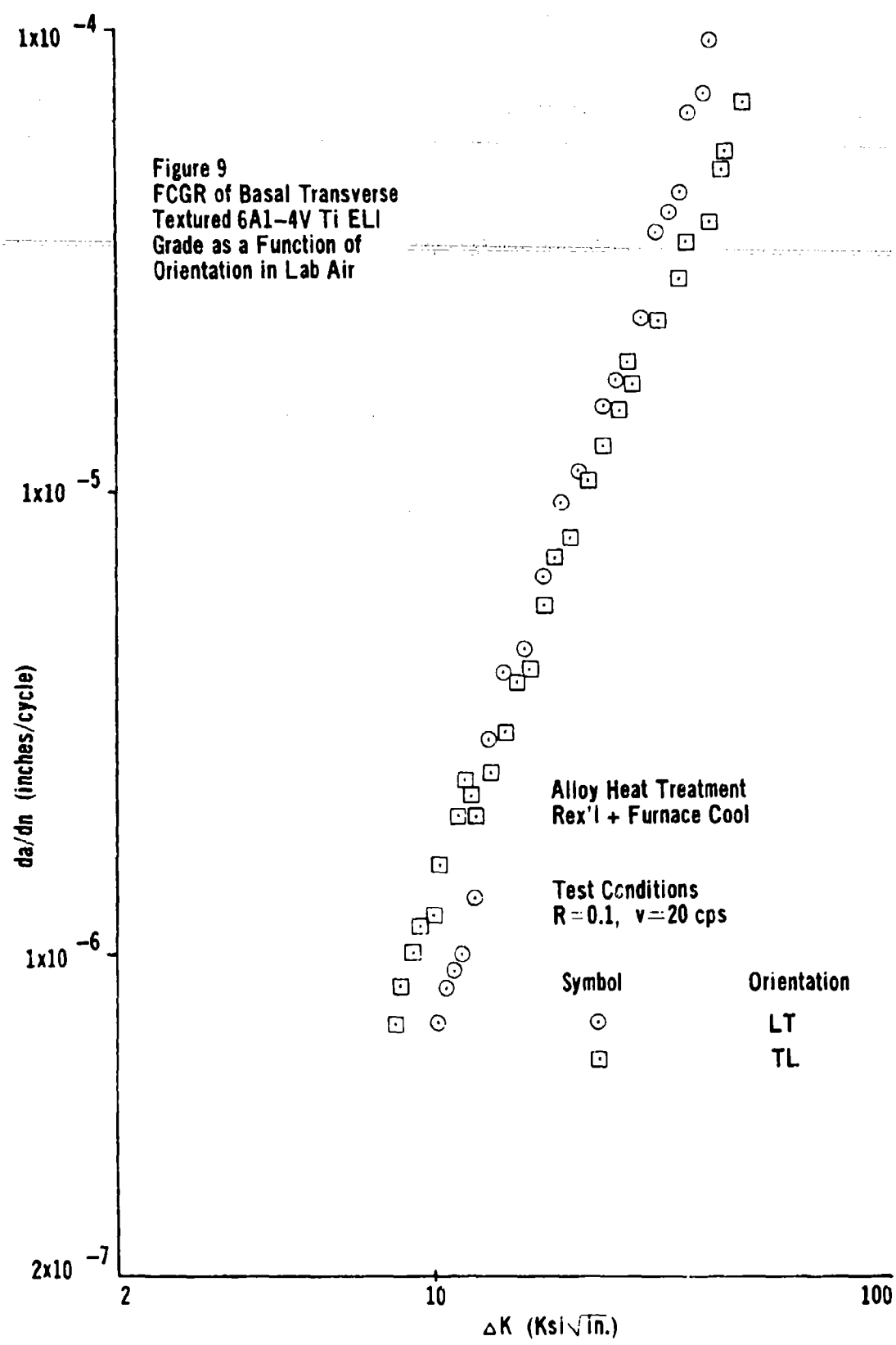

Figure 9
FCGR of Basal Transverse Textured 6A1–4V Ti ELI Grade as a Function of Orientation in Lab Air

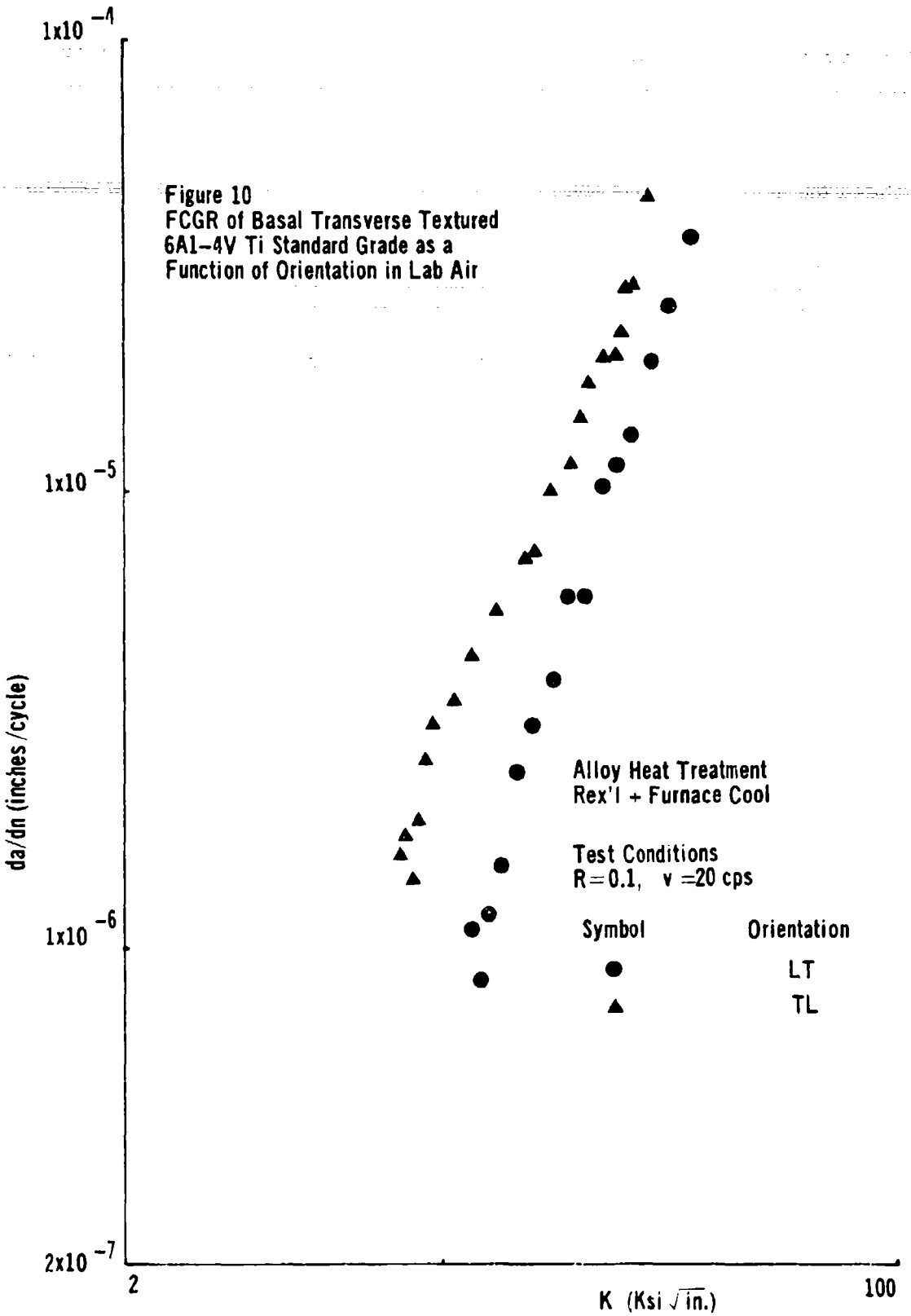

Figure 10
FCGR of Basal Transverse Textured 6Al–4V Ti Standard Grade as a Function of Orientation in Lab Air

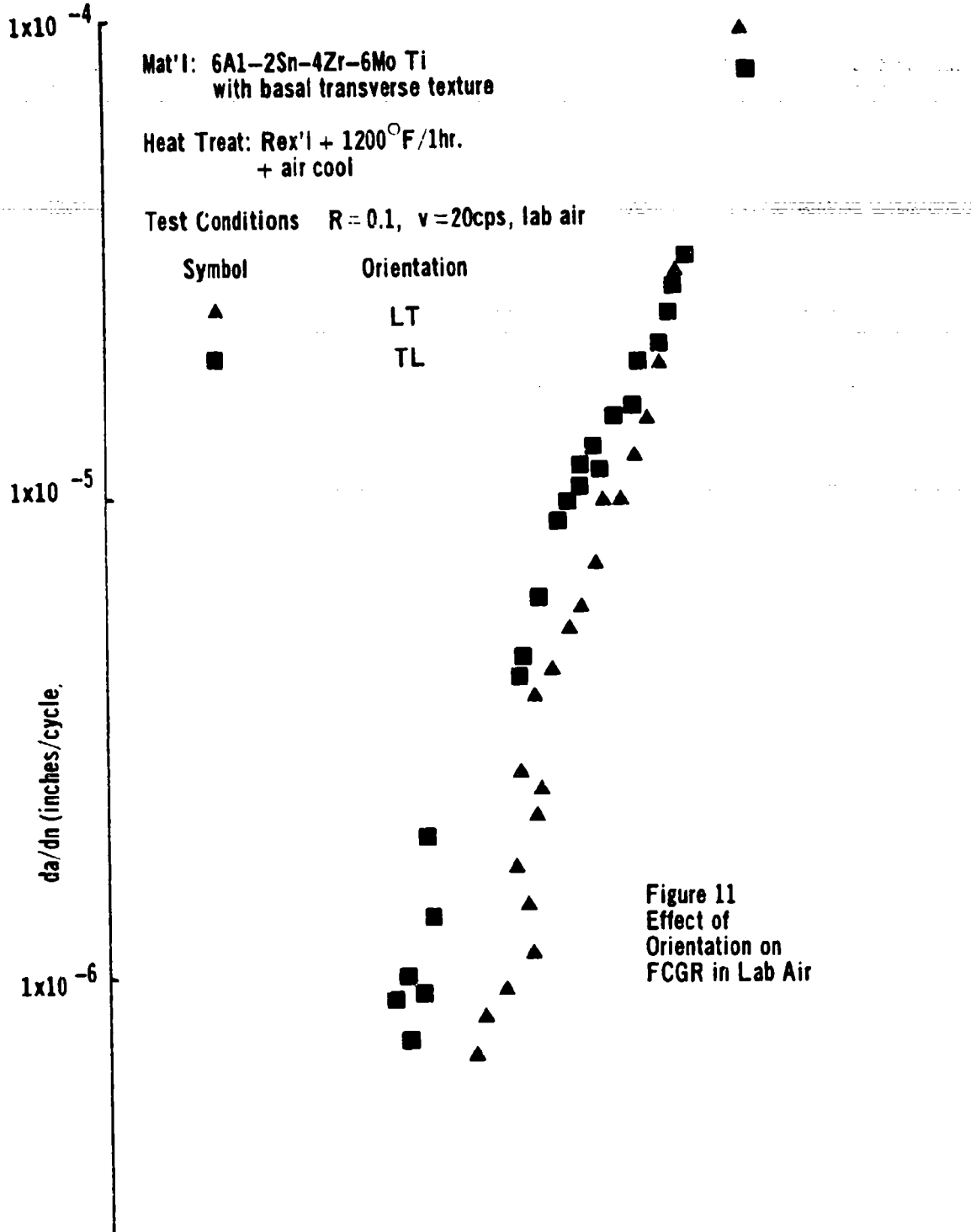

Figure 11
Effect of
Orientation on
FCGR in Lab Air

behavior at low K between the two orientations can be seen fractographically in Figure 12 employing an SEM. In Figures 12(a) and 12(b), we compare fractographic features for both orientations at a common value of da/dn (7×10^{-7} inches/cycle). In Figure 12(a), the crack grows predominately in a "near basal" cleavage mode along $<10\bar{1}0>_\alpha$ in contrast to the complex path it pursues in the LT orientation (Figure 12(b)). In the LT orientation in Figure 12, there is substantial evidence of secondary shear cracking at large angles with respect to $<0001>_\alpha$ that in some cases even approaches $<10\bar{1}0>_\alpha$ as well as scattered observations of ductile tearing. An attempt was made to determine what fraction if any of the fractographic topography shown in Figure 12(b) was formed in a striated fashion. No evidence of fatigue striations could be found at 10,000X in that region of the LT sample where da/dn = 7×10^{-7} inches/cycle employing the SEM technique. Switching to a carbon:chromium replica technique in an electron transmission mode exploration of this same area revealed several grains which manifested very fine fatigue striations at a magnification of 6,970X (e.g., see Figure 12(c))*

In Table VI, we present da/dn data evaluations employing both a macroscopic optical crack growth technique (i.e., that used to generate Figures 9 - 11) as well as determinations made via striation counting for the LT orientation of the 6Al-4V Ti ELI sample.

---

*TEM fractographic results in Figure 12(c) and Table VI were supplied by Mr. Austin Phillips of S.E.A.L., Los Angeles, Ca 90066.

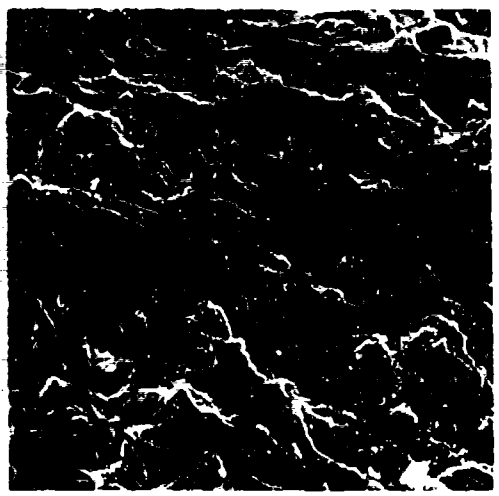

(a) 2000X in SEM

Sample Orientation: TL

Loading Direction: $<0001>_\alpha$

Nominal Crack Growth Direction: $<10\bar{1}0>_\alpha$

$da/dn = 7.0 \times 10^{-7}$ inches/cycle

$\Delta K = 8.30$ Ksi$\sqrt{in}$.

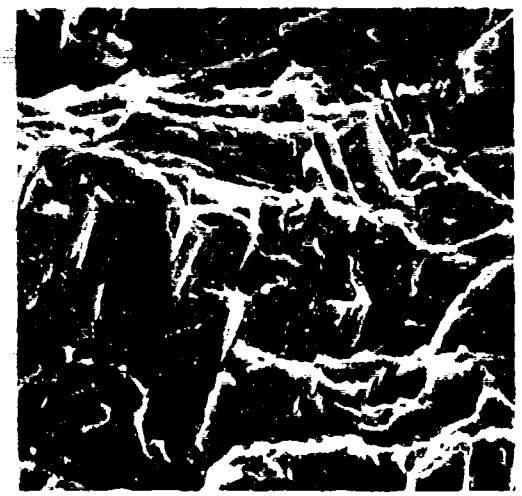

(b) 2000X in SEM

Sample Orientation: LT

Loading Direction: $<10\bar{1}0>_\alpha$

Nominal Crack Growth Direction: $<0001>_\alpha$

$da/dn = 7.0 \times 10^{-7}$ inches/cycle

$\Delta K = 10$ Ksi$\sqrt{in}$.

(c) TEM Technique ibid (b)

6970X

Figure 12: Effect of Orientation on the FCGR Characteristic of 6Al-4V Ti ELI Grade at Low ΔK in Lab Air

TABLE VI

A COMPARISON OF MACROSCOPIC CRACK GROWTH
AND ELECTRON MICROSCOPIC STRIATION
COUNTS FOR THE LT ORIENTATION
OF 6A1-4V TI ELI GRADE

ΔK ($Ksi\sqrt{in.}$)	da/dn (inches/cycle)*		
	Macroscopic	TEM	SEM
10.0	7.0×10^{-7}	1.9×10^{-6}	n.f.
12.5	2.0×10^{-6}	2.0×10^{-6}	n.f.
15.1	4.15×10^{-6}	4.0×10^{-6}	n.f.
20.0	1.0×10^{-5}	9.0×10^{-6}	n.s.
29.7	3×10^{-5}	n.s.	4.4×10^{-5}

*n.f. - not found at 10,000X; n.s. - not sought

As one observes in the above Table, the agreement between crack growth rates measured macroscopically and by striation counting agree quite well at all ΔK levels but the lowest measured here. In the case of $\Delta K = 10Ksi\sqrt{in.}$, striation counting overestimates the macroscopic rate by a factor of three.

Fractographs taken at higher ΔK from both the TL and LT orientations of the 6A1-4V Ti ELI grade metal are shown in Figure 13. In both orientations, crack progression is predominately by striation formation although scattered

evidence of ductile tear regions can also be seen in Figures 13(a) and (b).

In Figure 10, we present lab air da/dn data for the same basal transverse 6Al-4V Ti alloy except in this case the metal contains a higher interstitial content (i.e., 70% more oxygen and 150% more hydrogen, see Table V). Here one sees that interstitial content plays a strong role in determining the crack growth rate of the TL orientation at all levels of ΔK. Note that the da/dn vs. ΔK characteristic associated with the LT orientation of both 6Al-4V Ti alloy chemistries are identical (compare Figures 9 and 10). The fractographic appearance of the TL oriented sample whose data are presented in Figure 10 were similar to its ELI Grade counterparts in Figures 12(a) and 13(a).

In Figure 11, we present similar lab air da/dn vs. ΔK for basal transverse textured 6Al-2Sn-4Zr-6Mo Ti. Interestingly enough, one finds on comparing the crack growth rates of the LT orientation in Figure 11 at various ΔK levels with its counterparts in Figures 9 - 10 that the da/dn vs. ΔK relation is very similar to those we reported earlier for the other two alloy chemistries. It then appears at least over this small range of alloy compositions, that da/dn variability with alloy chemistry at constant

←<$10\bar{1}0>_\alpha$→

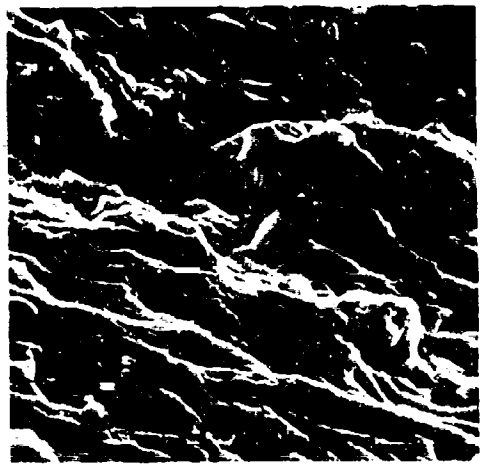

(a) 2000X in SEM

Sample Orientation: TL

Loading Direction: $<0001>_\alpha$

Nominal Crack Growth Direction: $<10\bar{1}0>_\alpha$

$da/dn = 6.6 \times 10^{-6}$ inches/cycle

$\Delta k = 17.9$ Ksi $\sqrt{in.}$

←<$0001>_\alpha$→

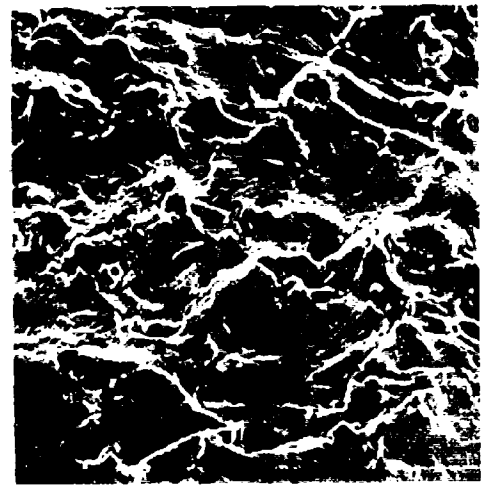

(b) 3000X in SEM

Sample Orientation: LT

Loading Direction $<10\bar{1}0>_\alpha$

Nominal Crack Growth Direction $<0001>_\alpha$

$da/dn = 3.0 \times 10^{-5}$ inches/cycle

$\Delta K = 29.7$ Ksi $\sqrt{in.}$

Figure 13: Effect of Orientation on the FCGR Characteristics of 6Al-4V Ti ELI Grade at High ΔK.

microstructure may well be associated with cracking in the $<10\bar{1}0>$ direction due to loads applied along <0001>. Fractographs corresponding to those in Figure 12 at low ΔK for 6Al-4V Ti ELI Grade are shown for 6Al-2Sn-4Zr-6Mo Ti in Figure 14. Although the differences in fractographic topography generated by cracks propagating on $(0001)_\alpha$ [Figure 14(a) and (b)] and $(10\bar{1}0)_\alpha$ [Figure 14(c) and (d)] are not as pronounced as they are for the case of similar cracks growing in 6Al-4V Ti [See Figure 12(a) and 12(b)] , one can still fairly state that crack growth on $(0001)_\alpha : <10\bar{1}0>_\alpha$ is more planar and contains significantly less evidence of ductile tear than does its $(10\bar{1}0)_\alpha : <0001>_\alpha$ counterpart in 6Al-2Sn-4Zr-6Mo Ti. It should be noted, however, that in Figure 14 (c) and (d), we observe distinct evidence of flat areas with cleavage-like river markings on them. These areas must be oriented parallel to the prism plane of the 6Al-2Sn-4Zr-6Mo Ti alloy. Thus, cleavage must also occur on or near $<10\bar{1}0>_\alpha$ under certain conditions in $\alpha + \beta$ Ti alloys.

$\leftarrow\langle 10\bar{1}0\rangle_\alpha\rightarrow$

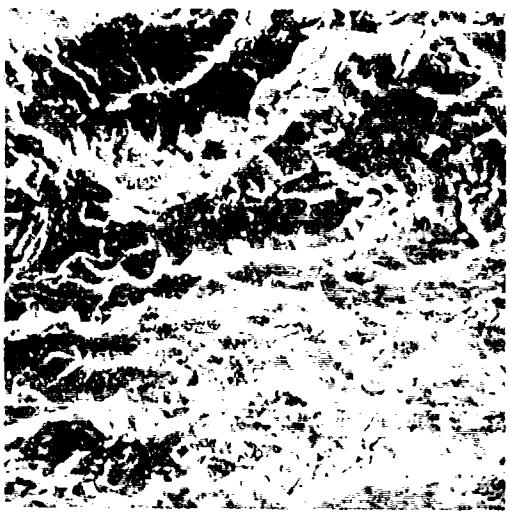

(a) 1000X in SEM

Sample Orientation: TL

Loading Direction: $\langle 0001\rangle_\alpha$

Nominal Crack Growth Direction: $\langle 10\bar{1}0\rangle_\alpha$

$da/dn = 7.5 \times 10^{-7}$ inches/cycle

$\Delta K = 8.4$ Ksi$\sqrt{in.}$

$\leftarrow\langle 10\bar{1}0\rangle_\alpha\rightarrow$

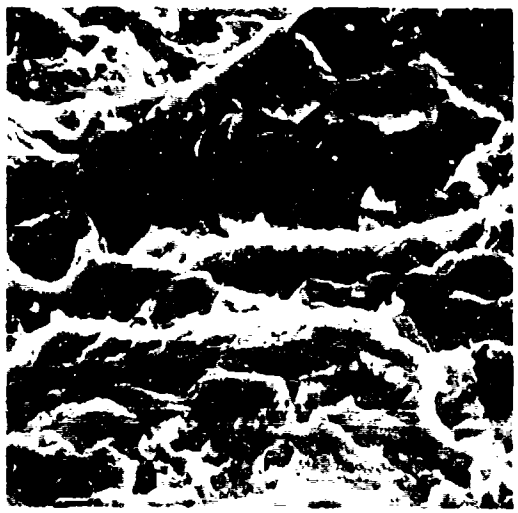

(b) 2000X in SEM

Sample Orientation: TL

Loading Direction: $\langle 0001\rangle_\alpha$

Nominal Crack Growth Direction: $\langle 10\bar{1}0\rangle_\alpha$

$da/dn = 7.5 \times 10^{-7}$ inches/cycle

$\Delta K = 8.4$ Ksi$\sqrt{in.}$

Figure 14 - Effect of Orientation on the FCGR Characteristic of 6Al-2Sn-4Zr-6Mo Ti at low ΔK in lab air.

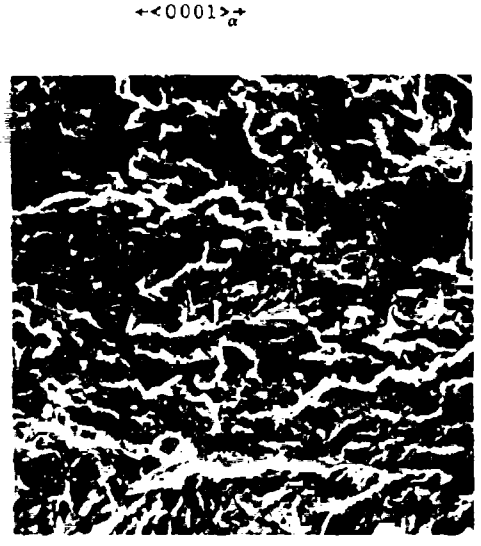

(c) 1000X in SEM

Sample Orientation: LT

Loading Direction: $<10\bar{1}0>_\alpha$

Nominal Crack Growth Direction: $<0001>_\alpha$

$da/dn = 7.0 \times 10^{-7}$ inches/cycle

$\Delta K = 11.5$ Ksi$\sqrt{in.}$

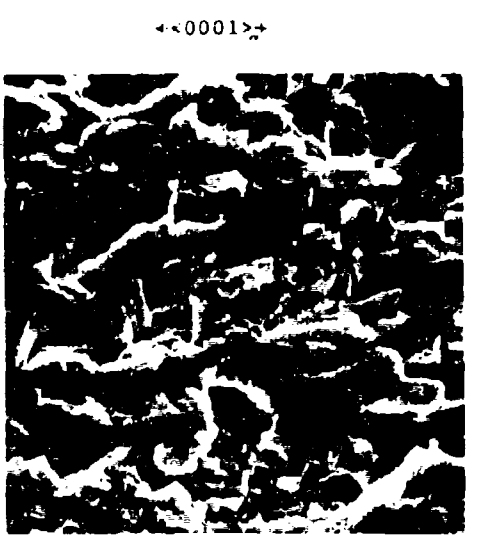

(d) 2000X in SEM

Sample Orientation: LT

Loading Direction: $<10\bar{1}0>_\alpha$

Nominal Crack Growth Direction: $<0001>_\alpha$

$da/dn = 7.0 \times 10^{-7}$ inches/cycle

$\Delta K = 11.5$ Ksi$\sqrt{in.}$

Figure 14 (Cont.)

da/dn vs. ΔK in 3.5% NaCl in H_2O: 6Al-4V Ti

In Figure 15 we present fatigue crack growth rate data for 6Al-4V Ti ELI Grade obtained when the crack propagated parallel to $(0001)_\alpha$ (loading direction $\langle 0001 \rangle_\alpha$) in 3.5% NaCl in H_2O. Two load cycling frequencies were employed during our salt water tests in order to estimate the magnitude of the expected frequency shift (References 2 and 3) in this adverse environment. The material employed here was recrystallized after rolling and furnace cooled (Rex'l I, see Table II). Also replotted in Figure 15 for reference purposes is the corresponding lab air TL data initially presented in Figure 9. As one can note in Figure 15, if one compares the salt water data obtained at 20 cps with its dry air counterpart, he observes a 5:1 crack growth rate acceleration at low ΔK (8-10 Ksi $\sqrt{in.}$) in the aggressive environment. As the ΔK rises, the salt water acceleration at 20 cps decreases until at 25 Ksi $\sqrt{in.}$ it is less than 2:1. At very low ΔK (5 Ksi $\sqrt{in.}$ - 6 Ksi $\sqrt{in.}$), the da/dn data observed at 20 cps and 2 cps are identical. As ΔK increases, da/dn rates at the two test frequencies diverge with the 2 cps data rising in a step-like fashion at about 7 Ksi $\sqrt{in.}$ and then deccelerating with further increase in ΔK. Although it is not as obvious in Figure 15 as it will be in subsequent Figures, the 20 cps salt water crack growth data exhibits this same step-like rise in da/dn at a similarly low ΔK level as that associated with the 2 cps data.

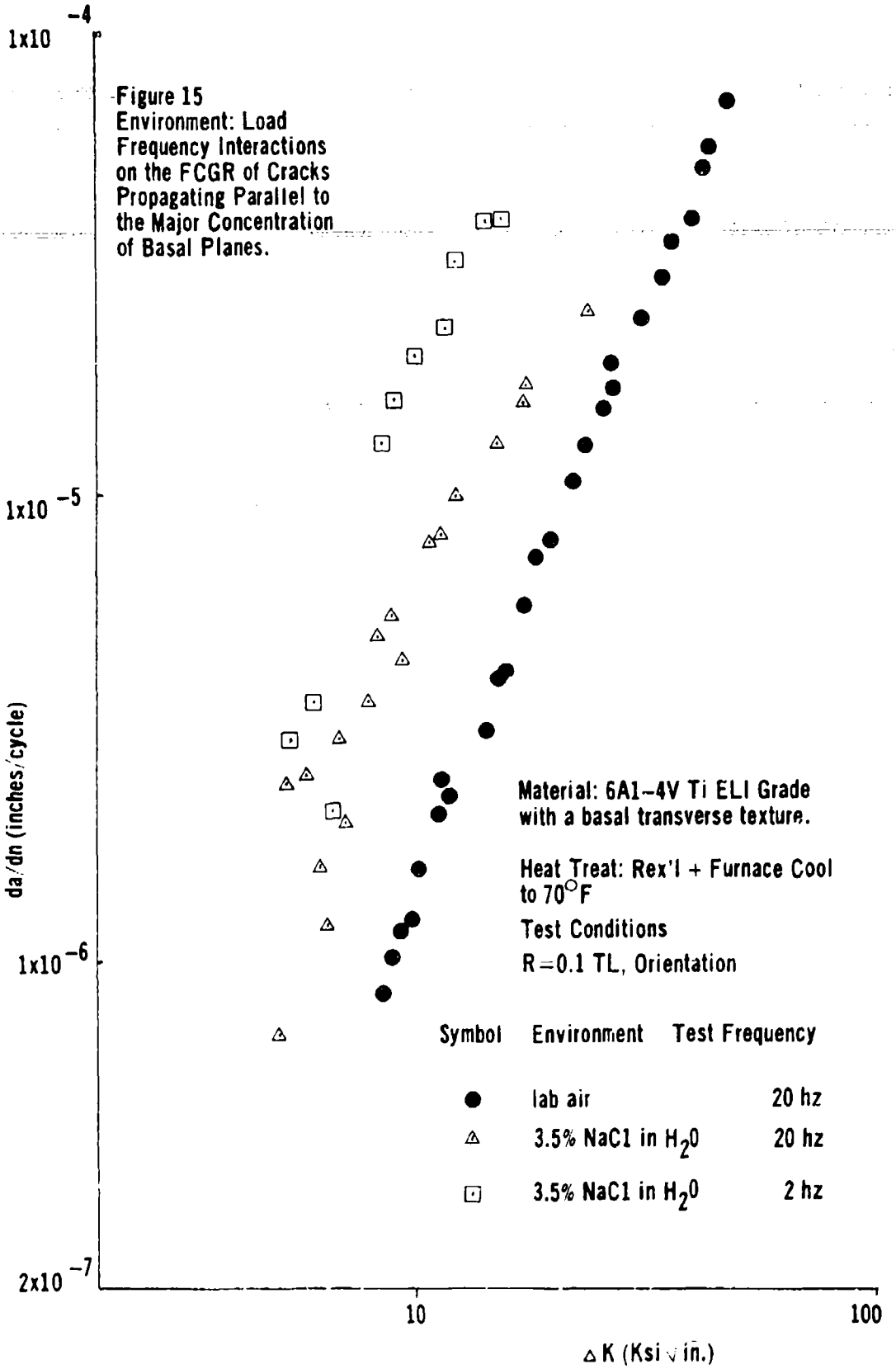

Figure 15
Environment: Load Frequency Interactions on the FCGR of Cracks Propagating Parallel to the Major Concentration of Basal Planes.

In Figure 16, we present a data set for 6Al-4V Ti Standard Grade representing a study similar to that shown in Figure 15 for the ELI Grade version of this alloy. Here again, these crack rate results in air and salt water were obtained after the metal was recrystallized and furnace cooled (see Table II for details). The gross pattern of acceleration in salt water as function of test frequency is similar here to that shown for the lower interstitial content alloy in Figure 15. In Figure 16, it appears like the step-like change in crack growth rate with frequency occurs at a lower ΔK value in the 20 cps data (~ 5 Ksi $\sqrt{\text{in.}}$) than it does in the 2 cps data (~ 8 Ksi$\sqrt{\text{in.}}$). Another comparison of these data can be found in Figure 17. Here we find replots of our 20 cps salt water da/dn data obtained with both grades of 6Al-4V Ti employed in this work. As was earlier the case in the lab air da/dn and K_{ISCC} results, the higher the interstitial content of the 6Al-4V Ti alloy, the faster is the opening mode fatigue crack growth rate on $(0001)_\alpha$ in salt water. For simplicity of presentation, we did not replot our 2 cps data in Figure 17. Inspection of these data in Figures 15 and 16, however, does indicate the same trend with interstitial level as is seen in Figure 17.

Let us now attempt to identify microstructural corrosion fatigue crack paths by simultaneously viewing the fracture faces of tested corrosion fatigue CT samples and the metal's microstructure on a plane at 90° to

Figure 16
EFFECT OF ENVIRONMENT ON
THE FCGR CRACKS PROPAGATING
PARALLEL TO THE MAJOR CONCENTRATION
BASAL PLANES

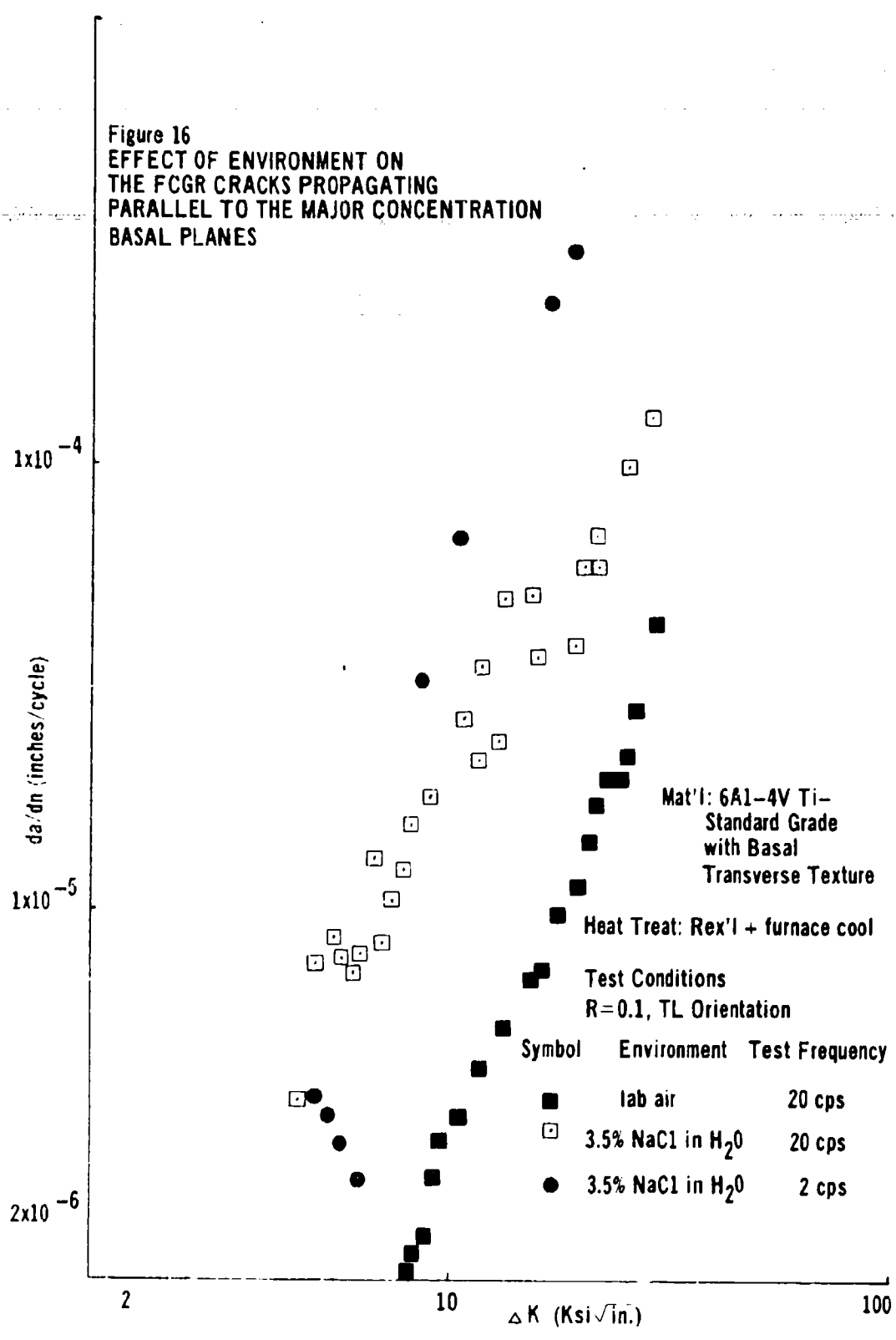

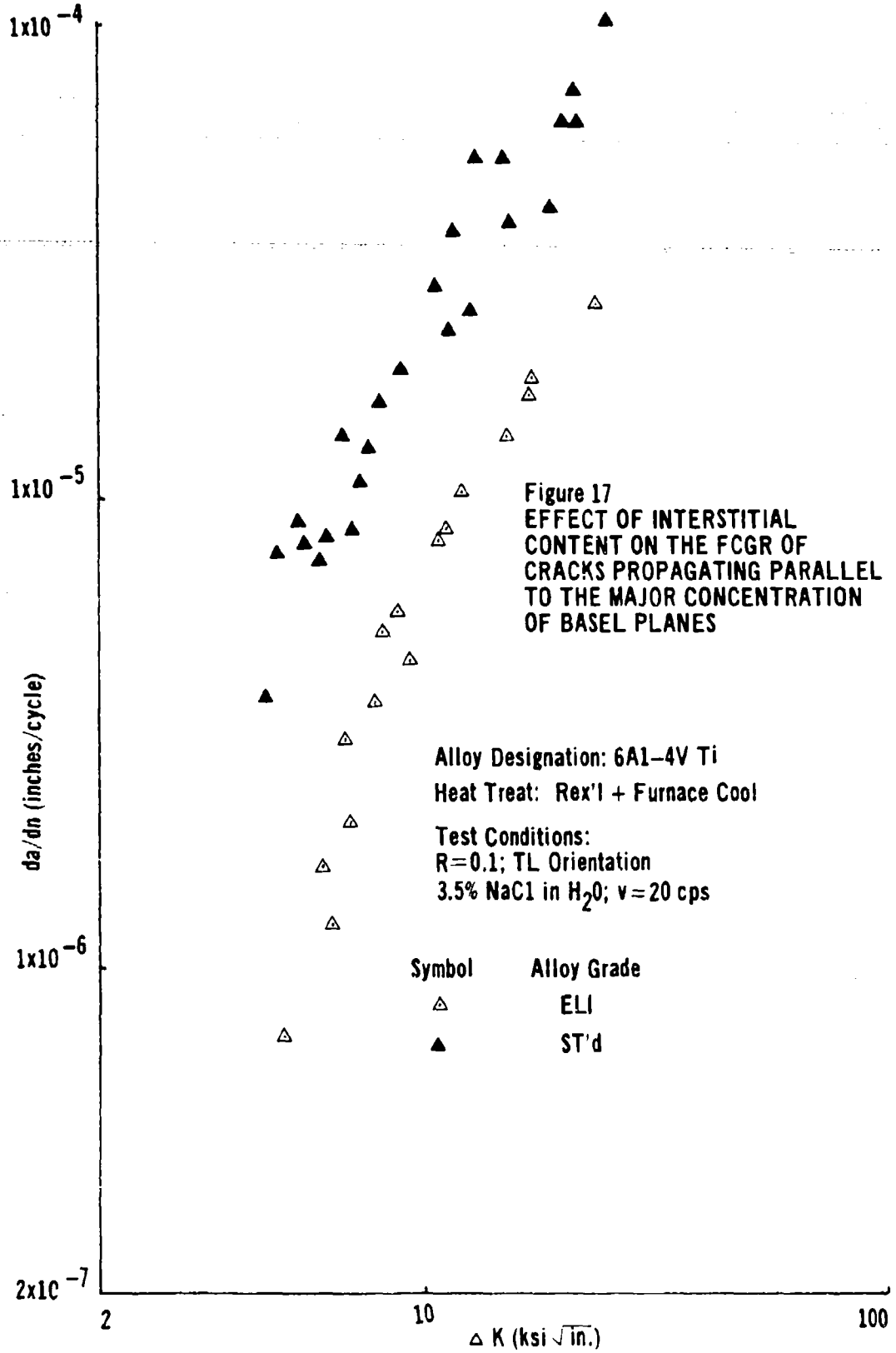

Figure 17
EFFECT OF INTERSTITIAL CONTENT ON THE FCGR OF CRACKS PROPAGATING PARALLEL TO THE MAJOR CONCENTRATION OF BASEL PLANES

the fracture plane in a Scanning Electron Microscope In order to perform this task, the fracture face of the tested CT sample was protected by Bakelite while the side of the sample was metallographically polished and etched (Kroll's Etch). The Bakelite was then removed mechanically from the fracture surface and the entire sample was cleaned in ultrasonically agitated acetone.

A typical result obtained employing the above described technique is shown in Figure 18. In this case, we are viewing a TL oriented CT sample fatigue tested in salt water. The fracture location shown in Figure 18 corresponds to a ΔK in the range 10 Ksi$\sqrt{in}$. to 12 Ksi$\sqrt{in}$. The basal transverse material employed in producing Figure 18 was 6Al-4V Ti ELI Grade which had been furnace cooled after recrystallization. In this orientation it exhibited a 500 hour salt water K_{ISCC} of 30 Ksi$\sqrt{in}$ compared to a value in excess of 70 Ksi$\sqrt{in}$. obtained when the same material was tested in the LT orientation. In Figure 18 one observes the fracture surface to consist entirely of transgranular cleavage. The orientation of this sample is such that we are applying our external load normal to the major concentration of basal planes in the product. Thus, it is not surprising, based on the work of Blackburn and Williams (Reference 6), that one finds "near basal" cleavage as the sole primary alpha phase fracture mode. One should note here that the crack is

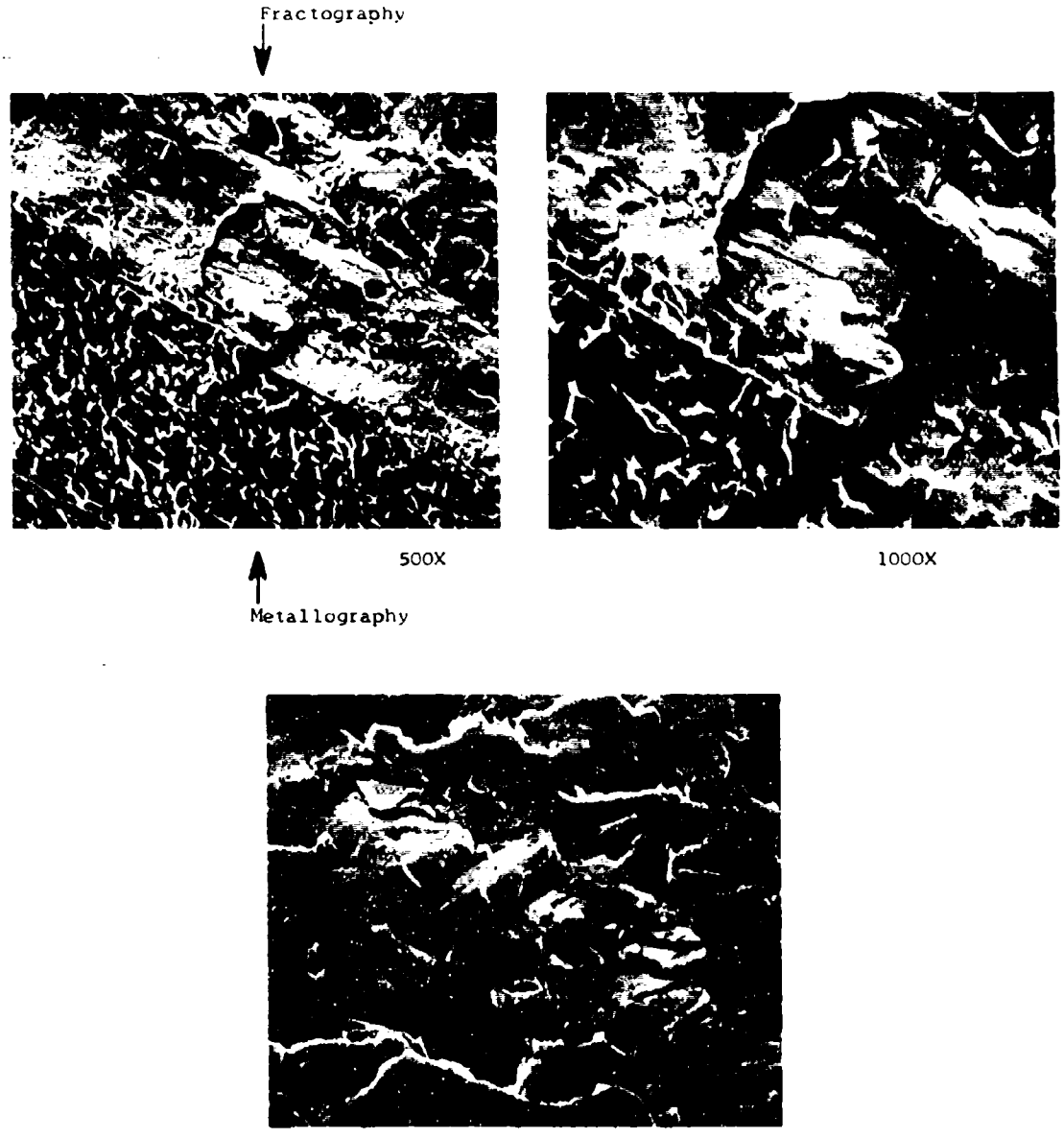

Figure 18 - Fractography/Metallography of Basal Transverse Textured 6Al-4V Ti ELI Grade; Condition - Rex'1 at 1700°F + Furnace Cool; da/dn Test in 3.5% NaCl in H_2O at 20 cps; Orientation - TL; 10 Ksi$\sqrt{in}$ < ΔK < 12 Ksi$\sqrt{in}$; da/dn ~3 x 10^{-5} inches/cycle.

growing in a strictly transgranular mode in this equiaxed microstructure and does not appear to be either impeded or accelerated as it crosses $\alpha:\beta:\alpha$ grain boundary regions. Although the crack growth rate in Figure 18 was high enough for the SEM technique to resolve fatigue striations (see Table VI), none are observed when $(0001)_\alpha$ cracking occurs in such an environmentally accelerated situation.

In addition to examining the fatigue crack growth rate parallel to $(0001)_\alpha$ in salt water after the 6Al-4V Ti ELI Grade metal was recrystallized and cooled slowly from $\beta_T - 50^\circ F$ (i.e., $<100^\circ F$/hour), these same measurements were made after the metal was placed in three additional conditions. The first of these additional conditions involved reheating the recrystallized and slowly cooled metal to $1400^\circ F$ holding for 1 hour and then air cooling the product to room temperature (Duplex anneal as described in Table II). Following recrystallization at $\beta_T - 50^\circ F$, a portion of the basal transverse textured metal was air cooled directly to room temperature and tested with no further heat treatment (Rex'l II as detailed in Table II). Finally a third condition resulted when a portion of Rex'l I metal was vacuum annealed at $1550^\circ F$ to remove hydrogen. This metal was slowly cooled (at $<100^\circ F$/hour) to $1400^\circ F$ in vacuum. At this point furnace power was disconnected and the vacuum was removed by flooding the belljar chamber with cold He gas.

In Table VII, we present elastic modulus data as a function of product direction for all three air atmosphere recrystallization heat treatments.

just described.

TABLE VII

EFFECT OF THERMAL PRACTICE ON THE TEXTURE OF 6Al-4V Ti ELI GRADE

Thermal Practice	$E_{Rolling\ Direction}$ (m.s.i.)	$E_{Width\ Direction}$ (m.s.i.)	E_{W-R} (m.s.i.)
(1) Recrystallization + furnace cool at <100°F/hour (Rex'l I)	15.65	20.25	4.60
(2) (1) + Reheat to 1400°F & air cool at >2000°F/hour (Duplex)	15.45	20.25	4.80
(3) (1) + Reheat to 1700°F & air cool at >2000°F/hour (Rex'l II)	14.85	18.95	4.10

As one can note from the above Table, the addition of a reheat to 1400°F and air cool does not alter the basal transverse textural intensity of the simply recrystallized and slowly cooled product. It has been shown elsewhere (see Part II) that the static strength of the two products are also identical (i.e., Rex'l I and Duplex annealed metals). By contrast, the Rex'l II practice results in a small but measurable loss in basal transverse textural intensity. Fatigue crack growth rate tests in lab air were also conducted for the Duplex Annealed metal in both the LT

and TL orientations over the growth rate range 1×10^{-6} - 1×10^{-4} inches/cycle. The fractographic appearance of those samples was also examined. The results obtained here were indistinguishable from the Rex'1 I results obtained in the same environment. Recall that the relevant Rex'1 I results are presented in Figures 9, 12, and 13.

Figure 19 reports on da/dn vs ΔK results obtained at test frequencies of 2 cps and 20 cps in salt water with the opening mode crack expanding parallel to $(0001)_\alpha$ in the Duplex Annealed metal. Also plotted in this Figure is the relevant lab air data for this orientation (i.e., TL). Inspection of Figure 19 reveals that below a ΔK of 7 Ksi $\sqrt{in.}$ the lab air data and the 20 cps salt water results appear to be convergent. As the ΔK rises, to a level between 8 - 9 Ksi $\sqrt{in.}$ the da/dn at 20 cps in salt water is mildly accelerated in a steplike fashion on the order of a factor of two (considering extremal scatter values). Above a ΔK of 10 Ksi $\sqrt{in.}$, the slope of the da/dn vs. ΔK relation at 20 cps in salt water decreases with respect to its lab air counterpart and the two curves (air and salt water at 20 cps) become a single valued relationship above 20 Ksi$\sqrt{in.}$ By contrast, the 2 cps salt water appears to follow its lab air counterpart below a ΔK of 12 Ksi$\sqrt{in.}$ In the ΔK range 13 Ksi $\sqrt{in.}$ to 15 Ksi$\sqrt{in.}$, the 2 cps sea water data rises steeply ($\sim$by a factor of 6-7 in rate) with respect to the lab air

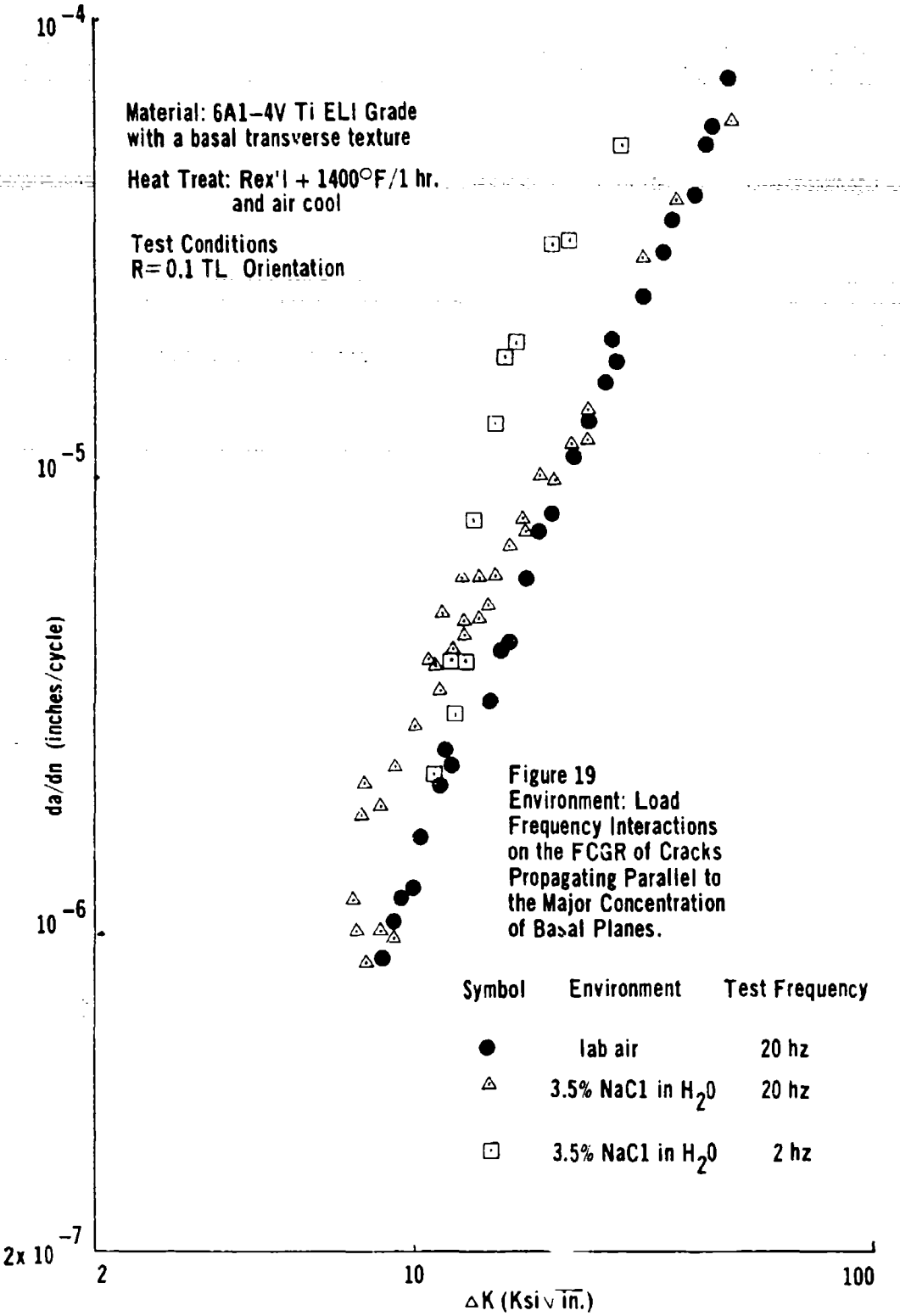

Figure 19
Environment: Load Frequency Interactions on the FCGR of Cracks Propagating Parallel to the Major Concentration of Basal Planes.

data shown here. Above 15 Ksi $\sqrt{in.}$ it begins to slow down again until at a ΔK of 28 Ksi$\sqrt{in.}$, the 2 cps salt water data exceeds its lab air counterpart by only a factor of 2 1/2.

The effect of final thermal practice (Rex'l I and Duplex) on the sea water fatigue crack growth rate of the 6Al-4V Ti ELI Grade parallel to $(0001)_\alpha$ are compared in Figure 20. In this Figure, we crossplot the salt water da/dn data taken at 2 and 20 cps parallel to $(0001)_\alpha$ for both heat treatment conditions. Also presented here for reference purposes is the TL lab air data drawn as a solid line. Just as was the case earlier in our sea water K_{ISCC} measurements (see Table V), air cooling the recrystallized product after stabilization at 1400°F has a profound effect on the metals corrosion fatigue crack growth propensity parallel to $(0001)_\alpha$. In Table VIII, we summarize this point by comparing the ΔK level associated with a steplike rise in da/dn as a function of test frequency and heat treatment condition. Also listed in this Table is the associated magnitude of the steplike rise in da/dn rate.

TABLE VIII

EFFECT OF THERMAL PRACTICE ON THE CORROSION FATIGUE OF 6Al-4V Ti ELI GRADE

Thermal Practice	Test Frequency	K_{step}	da/dn Step Factor*
Rex'l	20	5 → 7	>4 1/2
	2	7 → 8	>6
Duplex	20	7 → 9	∿2 1/4
	2	13 → 15	∿4

*ratio of da/dn at the highest ΔK in the step to the da/dn at the lowest ΔK in the step.

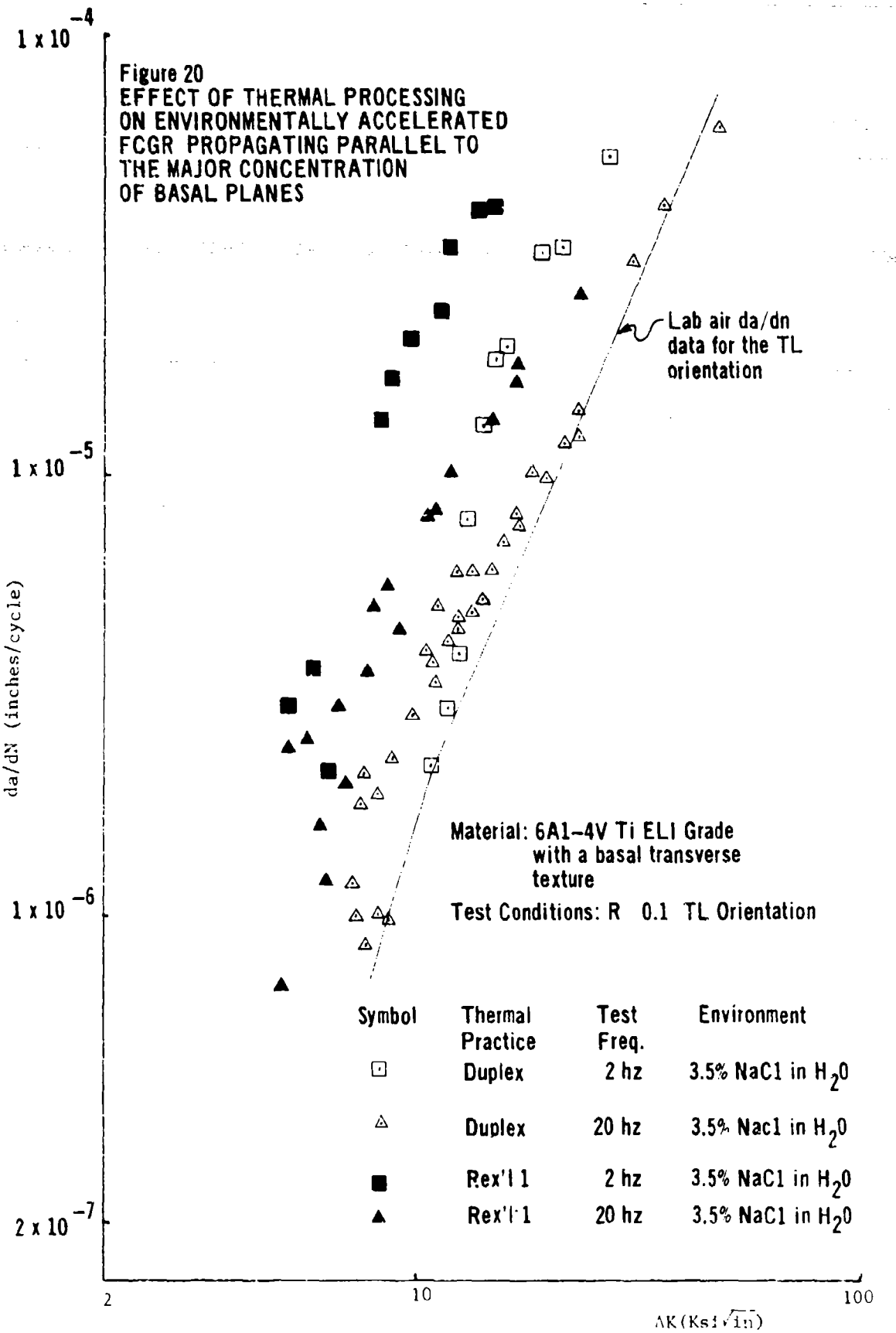
Figure 20
EFFECT OF THERMAL PROCESSING ON ENVIRONMENTALLY ACCELERATED FCGR PROPAGATING PARALLEL TO THE MAJOR CONCENTRATION OF BASAL PLANES
1 x 10 -4
1 x 10 -5
1 x 10 -6
2 x 10 -7
da/dN (inches/cycle)
Lab air da/dn data for the TL orientation
Material: 6A1-4V Ti ELI Grade with a basal transverse texture
Test Conditions: R 0.1 TL Orientation
Symbol
Thermal Practice
Test Freq.
Environment
Duplex
2 hz
3.5% NaCl in H2O
Duplex
20 hz
3.5% Nacl in H2O
Rex'l 1
2 hz
3.5% NaCl in H2O
Rex'l 1
20 hz
3.5% NaCl in H2O
2
10
100
ΔK(Ksi√in)

As one can note in Table VIII, the steplike rise in da/dn rate on $(0001)_\alpha$ in sea water occurs at a lower ΔK level the higher the test frequency. This is the case in both heat treatment states. Moreover, the Duplex treatment causes the magnitude of the da/dn rise during the step to be significantly smaller and the step to occur at a higher ΔK level when it is compared to its Rex'l I counterpart at either test frequency. The da/dn step factors in the case of Rex'l metal are quoted in terms of "greater than" a given number since our da/dn versus ΔK measurements did not extend to a low enough value of ΔK to insure that we have observed the full extent of the steplike rise.

In order to ascertain whether air cooling from temperatures higher than 1400°F would further improve sea water fatigue growth resistance on $(0001)_\alpha$, samples were air cooled directly from their recrystallization temperature (Rex'l II). In this situation da/dn observations were restricted to 20 cps in 3.5% NaCl in H_2O. Results obtained here were similar to those shown in Figure 19 for the Duplex annealed metal. Thus stabilization at temperatures in excess of 1400°F but less than the alloy's beta transus provided no additional improvement in stress corrosion resistance.

A final attempt was made to lower the residual salt water acceleration associated with crack propagation on $(0001)_\alpha$ in the 6Al-4V Ti ELI Grade. In this case the metal was vacuum annealed at 1550°F and its internal hydrogen content was reduced from 20 ppm to 8 ppm. As noted above, it was slowly cooled to 1400°F following which it was cooled by flooding the baffled vacuum chamber/furnace arrangement with cold He gas. In Figure 21, we present the results of a fatigue crack growth rate experiment in salt water wherein the opening mode crack was expanding on $(0001)_\alpha$ in the 8ppm hydrogen containing material. As one can note here, removal of hydrogen at first glance appears to have a deleterious effect on the metal's resistance to fatigue crack growth in 3.5% NaCl in H_2O. However, we know from Figure 20 that corrosion fatigue crack growth on $(0001)_\alpha$ is a strong function of the rate at which the metal cools from 1400°F. Captured as it was within the baffled vacuum chamber/furnace arrangement, the helium cooled specimen probably chilled at lesser rate than its air cooled counterparts. Thus, the difference in rates noted in Figure 21 for the two hydrogen content samples probably relate to the experimental difficulty of chilling the semi-encapsulated sample rather than to any inate difference between the two samples shown in Figure 21.

Let us now turn our attention to the interrelation between the fractographic appearance of the duplex annealed da/dn samples run in sea water at 20 cps (with an opening mode crack expanding on

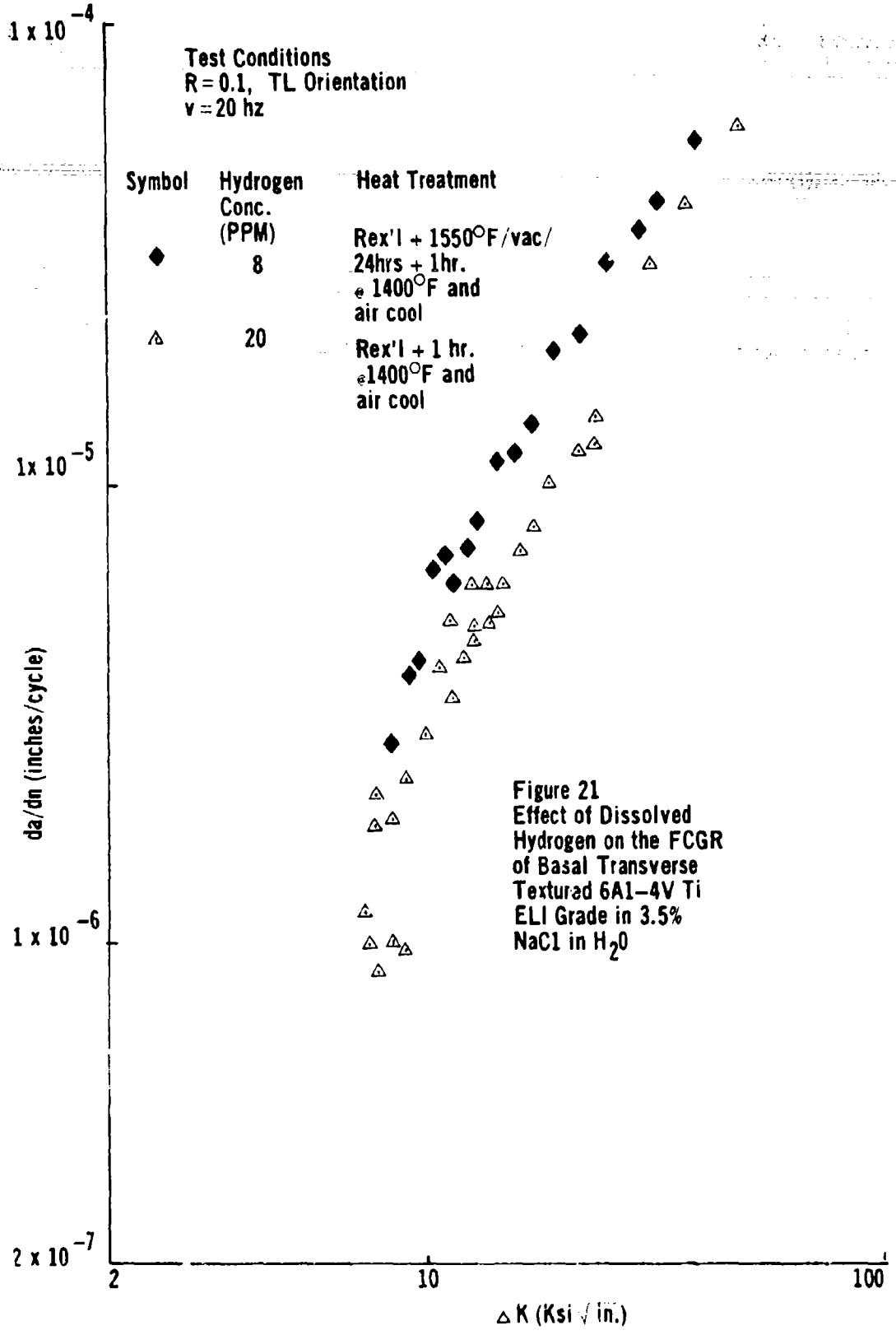

Figure 21
Effect of Dissolved Hydrogen on the FCGR of Basal Transverse Textured 6Al–4V Ti ELI Grade in 3.5% NaCl in H_2O

$(0001)_\alpha$) and their underlying microstructure as a function of ΔK (see Figure 22). Fractographically, the results shown in Figure 22 are indistinguishable from those shown in Figure 18 for the much faster growth rate, Rex'l I material. In other words, corrosion fatigue crack growth in both mateiral conditions occurs $(0001)_\alpha$ via transgranular cleavage and there is no evidence on the fracture faces themselves of the $\alpha:\beta:\alpha$ grain boundary region cracking by some other mode or acting in some manner to accelerate crack growth rates in the Rex'l I metal or retard it in the duplex annealed material. Moreover, no evidence of fatigue crack growth via striation formation can be seen even when the growth rate intervals were on the order of 1.5×10^{-5} inches/cycle in Figure 22. Metallographically one difference that can be seen between the Rex'l I and duplex annealed TL samples relates to the relative etching rates of the primary alpha vs prior beta grain regions. In Figure 18 the prior beta grains etched at a slower rate than the primary alpha grains whereas these phase related etching rates were reversed in the Figure 22 duplex annealed samples. Both samples were etched identically employing Kroll's etch. Thus the different phasal etch rates may relate to real chemical composition differences caused by the different heat treatments applied to the two samples.

In addition to examining the propagation of opening mode fatigue cracks on $(0001)_\alpha$ in both grades of 6Al-4V Ti in salt water, similar tests were also conducted when the nominal opening mode fatigue growth

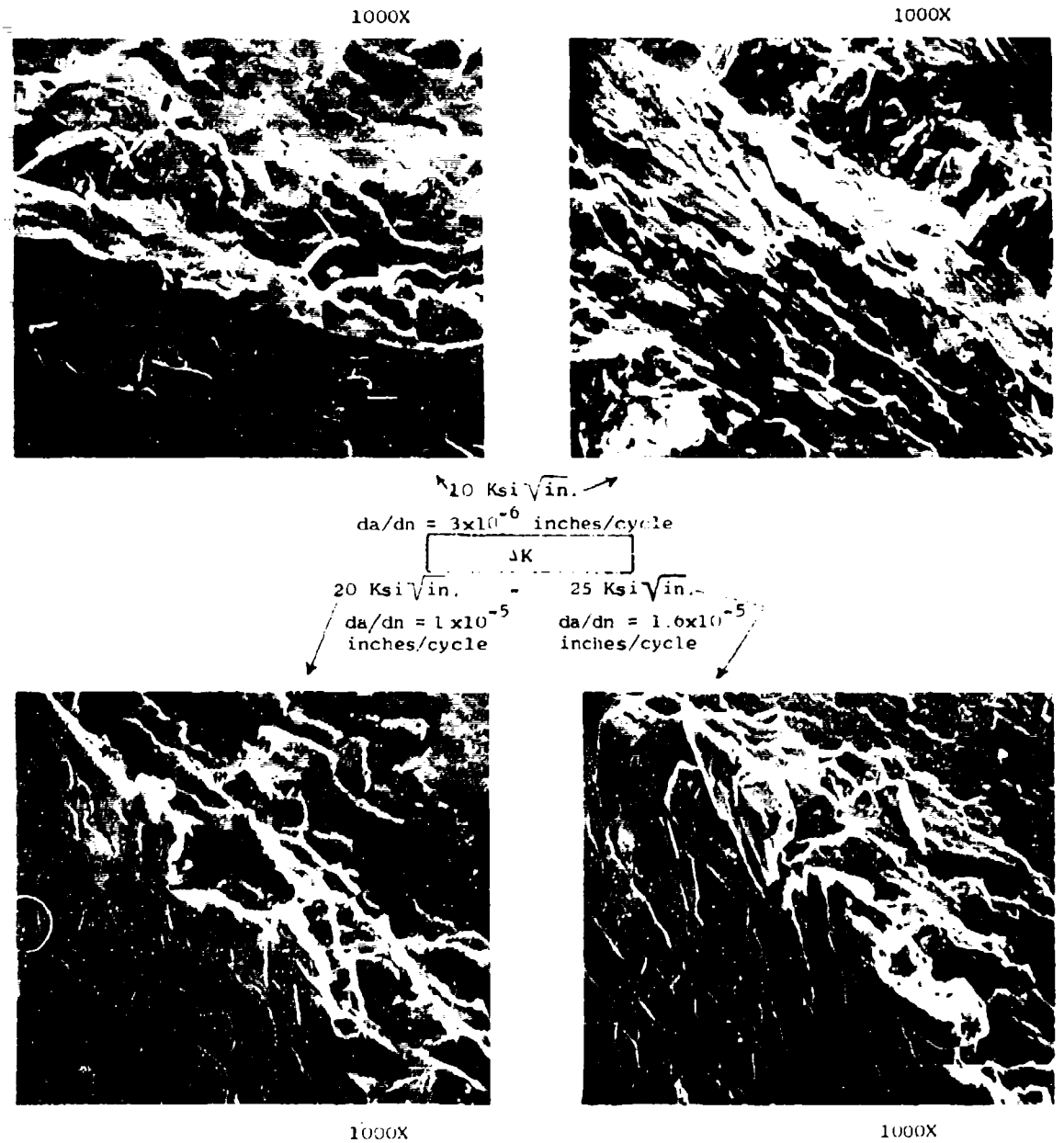

Figure 22 - Ibid Figure 18, Except Material Condition Here is Rex'l at 1700°F + Furnace Cool + 1400°F/1 hr. + Air Cool To Orientation; 20 cps

plane was $(10\bar{1}0)_\alpha$ (i.e., the LT orientation). Here again information was sought as a function of material condition in the case of the ELI Grade. The conditions examined were Rex'l I, Duplex and Rex'l I + vacuum anneal + helium cool in the case of ELI Grade and Rex'l in the case of the Standard Grade metal.

In the Rex'l condition, it was virtually not possible to observe fatigue crack advance on the $(10\bar{1}0)_\alpha$ plane in the 6Al-4V Ti ELI Grade metal even when the applied ΔK on such an opening mode crack was as low as 6.8 Ksi $\sqrt{in}$. At ΔK values above this level on two occasions in 3.5% NaCl in H_2O the crack in the compact tension sample turned ninety degrees and propagated parallel to the load line on $(0001)_\alpha$. One valid measurement crack growth rate measurement was made on each occasion prior to the crack deviating from $(10\bar{1}0)_\alpha$. At a ΔK = 6.5 Ksi $\sqrt{in}$., the da/dn rate in 3.5% NaCl in H_2O was 2.0×10^{-7} inches/cycle (R = 0.1, ν = 20 cps). Not surprisingly, the same problem of severe crack path deviation arose immediately on immersion in salt water when an attempt was made to propagate an opening mode fatigue crack along $(10\bar{1}0)_\alpha$ in the Standard Grade 6Al-4V Ti metal. In this case no measurements at all were possible along $(10\bar{1}0)_\alpha$ even at a ΔK = 5 Ksi$\sqrt{in}$.

Once the ELI Grade 6Al-4V Ti material was duplex annealed fatigue crack growth measurements in salt water along $(10\bar{1}0)_\alpha$ were possible

(see Figure 23). The results shown in Figure 23 represent a compilation of results from several samples. Moreover, the severe crack path deviation problem in salt water experienced with the Rex'l I metal was never encountered with the LT orientation of the duplex annealed metal. The relationship between fatigue crack growth rate and ΔK on $(10\bar{1}0)_\alpha$ in salt water differs in several respects from that observed on $(0001)_\alpha$ in salt water after duplex annealing (compare Figures 19 and 23). For example, there is no marked steplike change in da/dn vs ΔK on $(10\bar{1}0)_\alpha$ at 20 cps in salt water. Over the da/dn range investigated, the 20 cps salt water crack growth data appear to be simply displaced from their lab air counterparts by $\sim$ 2 Ksi$\sqrt{\text{in.}}$ over the entire ΔK range. On the other hand, the 2 cps salt water growth data on $(10\bar{1}0)_\alpha$ at low ΔK behaves in a fashion similar to that observed for low cyclic frequency growth data on $(0001)_\alpha$. Below a ΔK of 16 Ksi$\sqrt{\text{in.}}$ at 2 cps, the salt water growth data and lab air data on $(10\bar{1}0)_\alpha$ are coincident. Above this value, da/dn in 3.5% NaCl in H_2O increases more rapidly than does its lab air counterpart. On an absolute comparison basis of any ΔK above 16 Ksi$\sqrt{\text{in.}}$ salt water fatigue crack growth proceeds at a much less accelerated rate on $(10\bar{1}0)_\alpha$ at 2cps than it does on $(0001)_\alpha$ (at 20 Ksi$\sqrt{\text{in.}}$, crack growth on $(10\bar{1}0)_\alpha$ is 2.5 x faster in salt water than lab air as compared to a 4 x faster rate experienced on $(0001)_\alpha$ in a similar situation in the duplex annealed material). Finally there is some preliminary evidence that the low ΔK salt water acceleration experienced at 20 cps

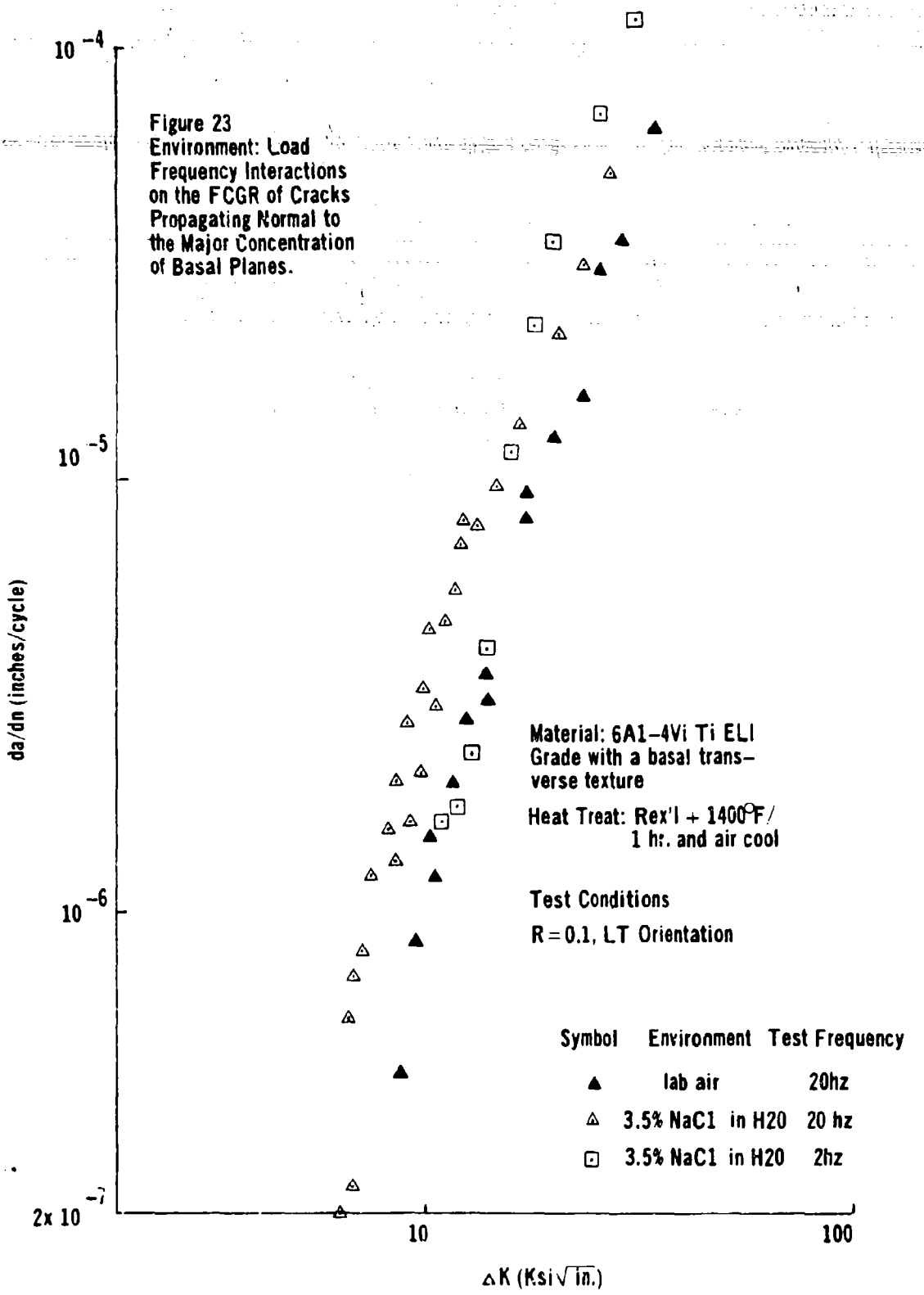

Figure 23
Environment: Load Frequency Interactions on the FCGR of Cracks Propagating Normal to the Major Concentration of Basal Planes.

on $(10\bar{1}0)_\alpha$ is independent of whether the metal is in the Rex'l I condition or duplex annealed state. Recall, we obtained one valid crack growth rate data point of 2×10^{-7} inches/cycle at 6.5 Ksi$\sqrt{\text{in.}}$ in the Rex'l I metal prior to the crack deviating badly from $(10\bar{1}0)_\alpha$. Plotting this point on Figure 23 shows that its value is right in line with the low ΔK 20 cps salt water data we observed after duplex annealing. By comparison the low da/dn 20 cps salt water growth data for the Rex'l I metal on $(0001)_\alpha$ are 3-4 Ksi$\sqrt{\text{in.}}$ lower at a da/dn level of 8×10^{-7} inches/cycle than their duplex annealed counterparts.

An effort was also made to assess the alteration in sea water induced crack growth rate acceleration on $(10\bar{1}0)_\alpha$ associated with a diminution in the internal hydrogen content of the 6Al-4V Ti ELI Grade metal. The dehydriding procedure here was the same as that described earlier for our $(0001)_\alpha$ opening mode crack growth samples. The results of this effort are presented in Figure 24. Here again, reducing the hydrogen content of the metal from 20 ppm hydrogen to 8 ppm hydrogen had no effect on our salt water da/dn results on $(10\bar{1}0)_\alpha$ over the entire range of ΔK employed in this work.

Recognizing that the presence of 3.5% NaCl in H_2O had produced a relatively small but distinct acceleration of fatigue crack growth rate on $(10\bar{1}0)_\alpha$, a metallographic/fractographic investigation was

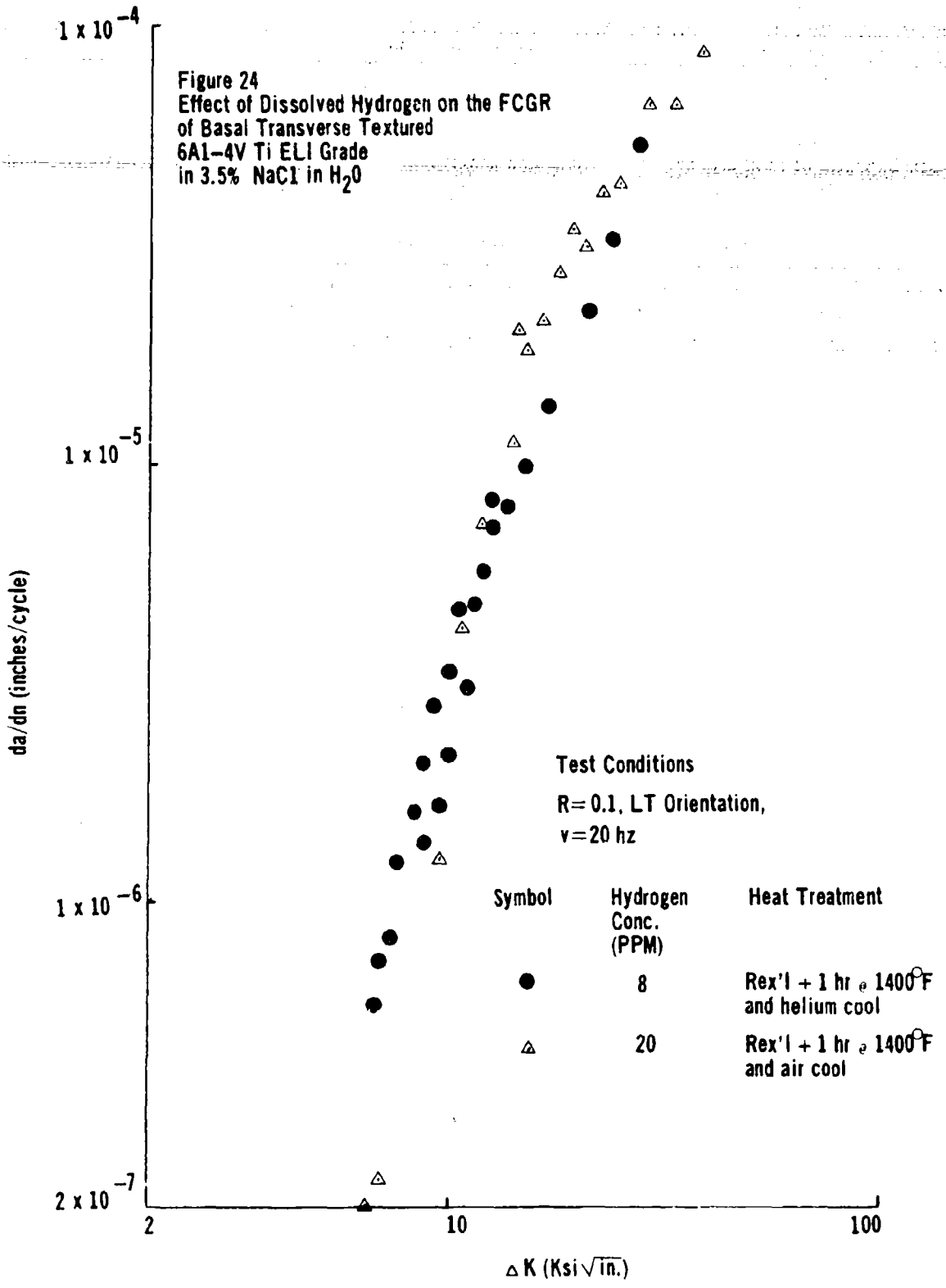
Figure 24
Effect of Dissolved Hydrogen on the FCGR
of Basal Transverse Textured
6Al-4V Ti ELI Grade
in 3.5% NaCl in H_2O
1×10^{-4}
1×10^{-5}
1×10^{-6}
2×10^{-7}
da/dn (inches/cycle)
Test Conditions
R=0.1, LT Orientation,
v=20 hz
Symbol
Hydrogen Conc. (PPM)
Heat Treatment
8
Rex'l + 1 hr @ 1400°F and helium cool
20
Rex'l + 1 hr @ 1400°F and air cool
2
10
100
ΔK (Ksi$\sqrt{in.}$)

performed to identify whether or not a distinct change in fracture mode could be associated with this sea water acceleration. As one can note by comparing Figure 25 and Figure 12, the fractographic appearance of opening mode fatigue crack growth on $(10\bar{1}0)_\alpha$ in salt water and lab air are distinctly different at low ΔK. In lab air, the fracture surface associated with propagation on $(10\bar{1}0)_\alpha$ was a complex mixture of striations, secondary shear cracking and ductile tear. The presence of salt water during fatigue cracking on $(10\bar{1}0)_\alpha$ eliminated all evidence of ductile tear and secondary shear. The fracture face in Figure 25 appears as a series of cleavage-like tire tracks on $(10\bar{1}0)_\alpha$. These are infrequently interrupted by cleavage-like cracking on $(0001)_\alpha$ as in Figure 25(a) and (b). The depth of the $(0001)_\alpha$ cleavage cracks are quite small compared to their length normal to $\langle 0001 \rangle_\alpha$. Interestingly enough, although these shallow depth $(0001)_\alpha$ cracks occur from time to time, they do not appear to limit the length of a $(10\bar{1}0)_\alpha$ cleavage crack or tire track in that the same track appears on both sides of the $(0001)_\alpha$ crack normal to $(10\bar{1}0)_\alpha$. In some instances, the $(0001)_\alpha$ cleavage side cracking was associated with the primary α:Widmanstutten α + β interface, in others, this cracking occurred in the center of a primary α grain (see Figure 25(b)). The length of the tire track-like $(10\bar{1}0)_\alpha$ cleavage cracks is considerably greater than the comparable primary α grain dimension (see Figure 25(a)). Based on the metallography shown in Figures 22 and 25, one can conclude that the 6Al-4V Ti ELI Grade metal possesses an equiaxed primary α grain

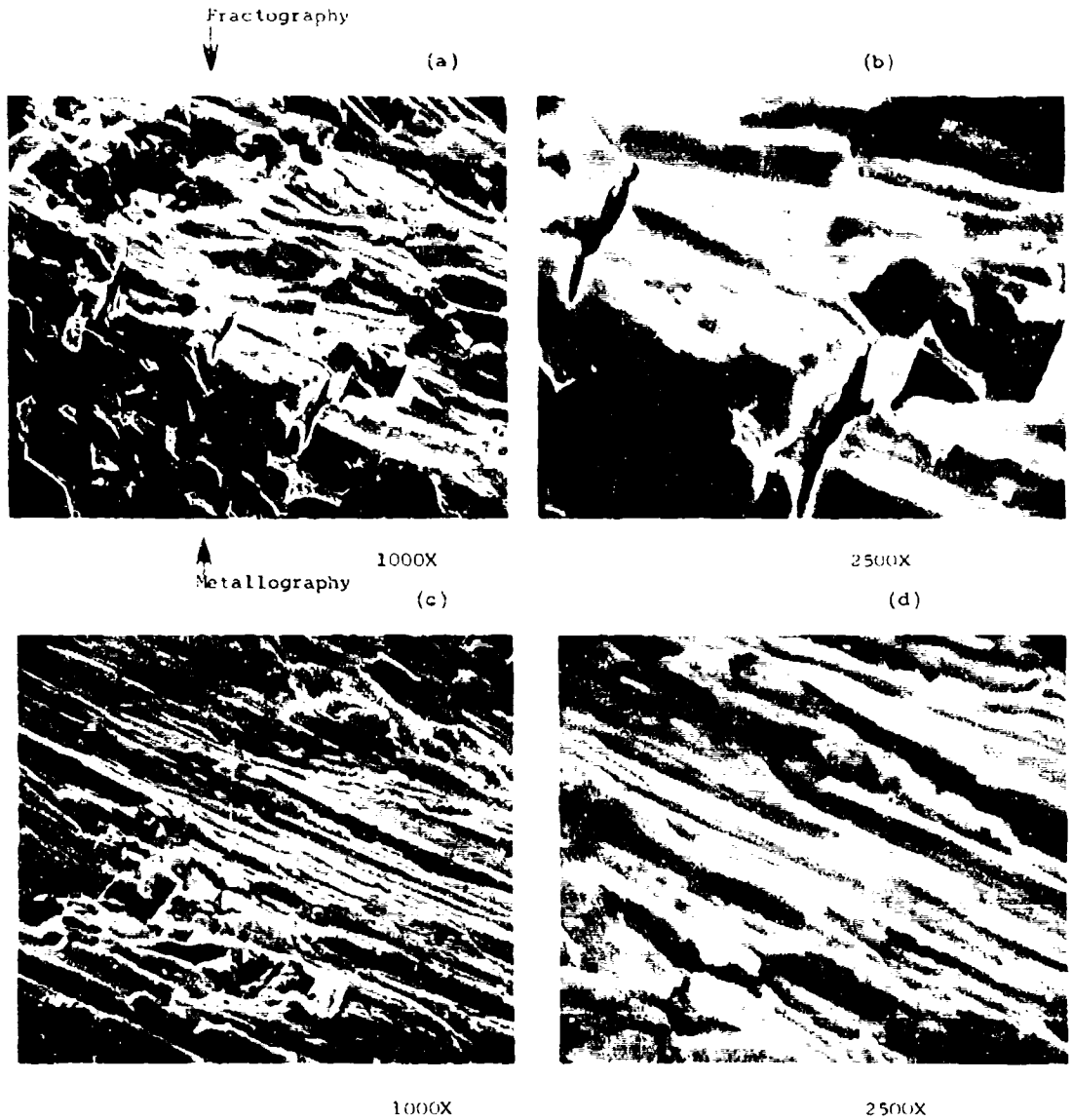

Figure 25 - Fractography/Metallography of Basal Transverse Textured 6Al-4V Ti ELI Grade; Condition - Duplex Annealed; da/dn Test in 3.5%NaCl in H_2O at 20 cps; Orientation - LT; $\Delta K = 9$ Ksi $\sqrt{in}$; da/dn $\sim 2 \times 10^{-6}$ inches/cycle.

size of μ12 . Thus the width of these tire tracks are considerably smaller than the relevant primary α dimension as well.

Above a ΔK of 20 Ksi$\sqrt{\text{in.}}$, the salt water crack growth data on $(10\bar{1}0)_\alpha$ closely approaches its lab air counterpart in Figure 23. Under such conditions of high ΔK in salt water, one finds striated growth on $(10\bar{1}0)_\alpha$ (see Figure 26) that is indistinguishable from that shown in Figure 13(b) for similar crack growth in lab air. Striation spacing in Figure 26 is on the order of 5×10^{-5} inches which agrees well with our Figure 23 20 cps salt water result of 4.2×10^{-5} inches/cycle at 25 Ksi $\sqrt{\text{in.}}$

In Figure 27, we present salt water fatigue crack growth rate results for an opening mode crack propagating on $(0001)_\alpha$ in 6Al-2Sn-4Zr-6Mo Ti (Condition - Rex'1, see Table II for details) as a function of cyclic loading frequency. The test frequency dependence of the results we obtained here is similar to that reported earlier for cracks propagating on $(0001)_\alpha$ in 6Al-4V Ti. Here again, a steplike rise in salt water growth rate with ΔK occurs between 6 - 7 Ksi$\sqrt{\text{in.}}$ in the case of the 20 cps test data. In the case of the 2 cps salt water data, this same step occurs at a somewhat higher ΔK level (7 - 8 Ksi$\sqrt{\text{in.}}$). Once more the absolute magnitude of this steplike change in terms of da/dn alteration is greater in the case of the 2 cps data. As before, salt water test data taken at both

(a)

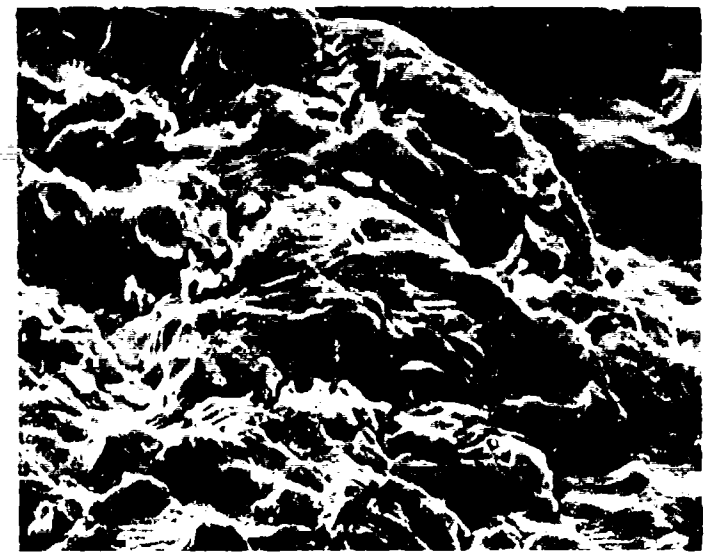

1000X

(b)

2500X

Figure 26 - Fractography of Basal Transverse Textured 6Al-4V Ti; Condition - Duplex Annealed; da/dn Test in 3.5% NaCl in H_2O at 20 cps; Orientation - LT; ΔK = 25 Ksi $\sqrt{in.}$; da/dn = 4.2 x 10^{-5} inches/cycle.

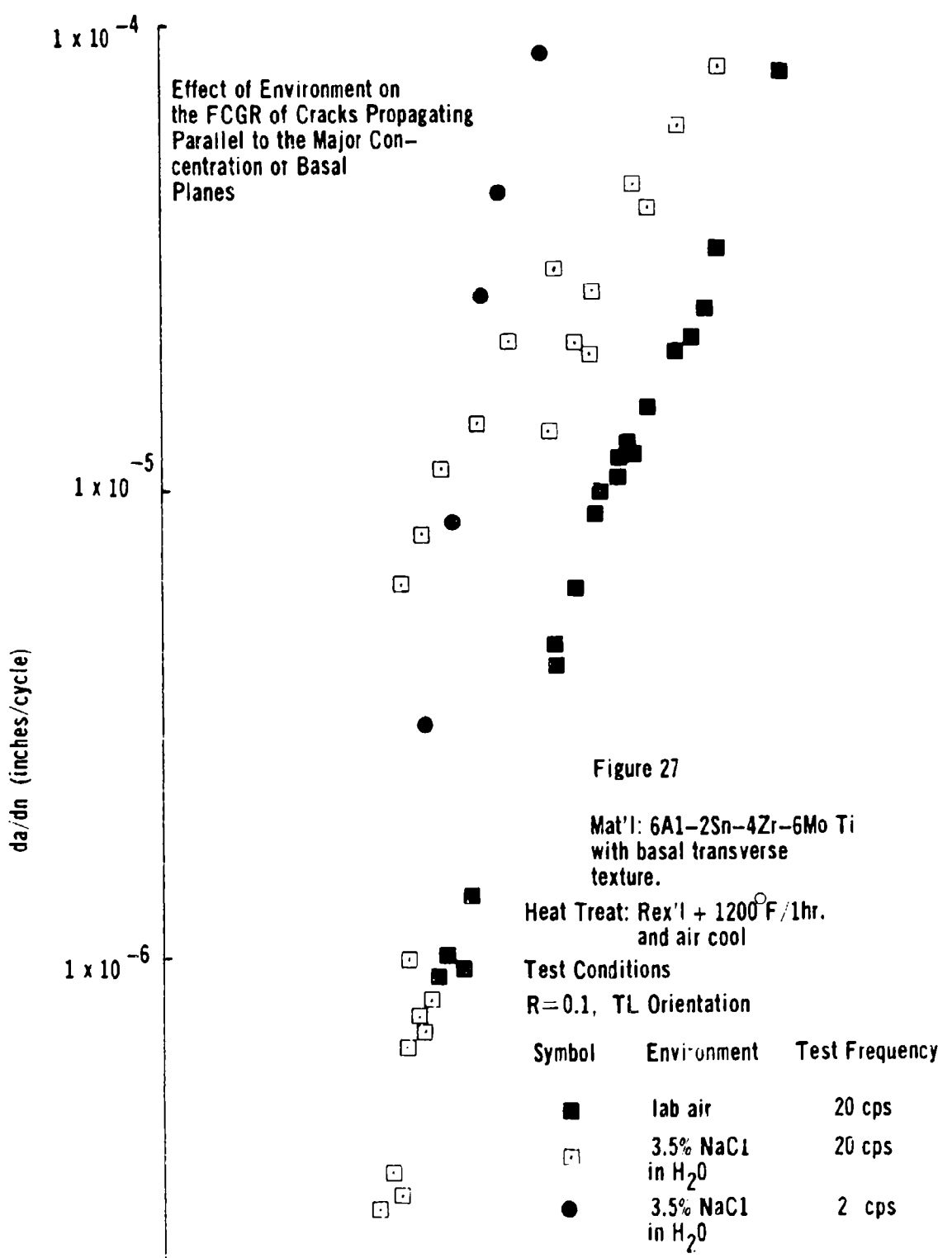
Effect of Environment on the FCGR of Cracks Propagating Parallel to the Major Concentration or Basal Planes
1 x 10 -4
1 x 10 -5
1 x 10 -6
2 x 10 -7
da/dn (inches/cycle)
2
10
100
ΔK (Ksi√in.)
Figure 27
Mat'l: 6Al-2Sn-4Zr-6Mo Ti with basal transverse texture.
Heat Treat: Rex'l + 1200°F/1hr. and air cool
Test Conditions
R=0.1, TL Orientation
Symbol
Environment
Test Frequency
lab air
20 cps
3.5% NaCl in H2O
20 cps
3.5% NaCl in H2O
2 cps

test frequencies approaches that observed in lab air at low ΔK. Finally the magnitude of the sea water acceleration in f.c.g.r. experienced by 6Al-2Sn-4Zr-6Mo Ti on $(0001)_\alpha$ at both test frequencies is very similar to that given in Figure 15 (Material: 6Al-4V Ti ELI Grade in Rex'l I condition).

An attempt was also made to measure the f.c.g.r. associated with opening mode crack propagation on $(10\bar{1}0)_\alpha$ in salt water for 6Al-2Sn-4Zr-6Mo Ti in Rex'l condition. Once again, as was the case earlier with the Rex'l I condition of 6Al-4V Ti, it was not possible to attain a very high value of ΔK without the crack path deviating ninety degrees to grow along $(0001)_\alpha$ in salt water. Those results we obtained prior to any significant crack path deviation from $(10\bar{1}0)_\alpha$ are shown in Figure 28. At low ΔK, the tread noted earlier for $(10\bar{1}0)_\alpha$ salt water crack propagation in Rex'l I 6Al-4V Ti ELI Grade is affirmed here in that da/dn in lab air and salt water appear to merge in the 8 - 10 Ksi $\sqrt{in}$. ΔK range.

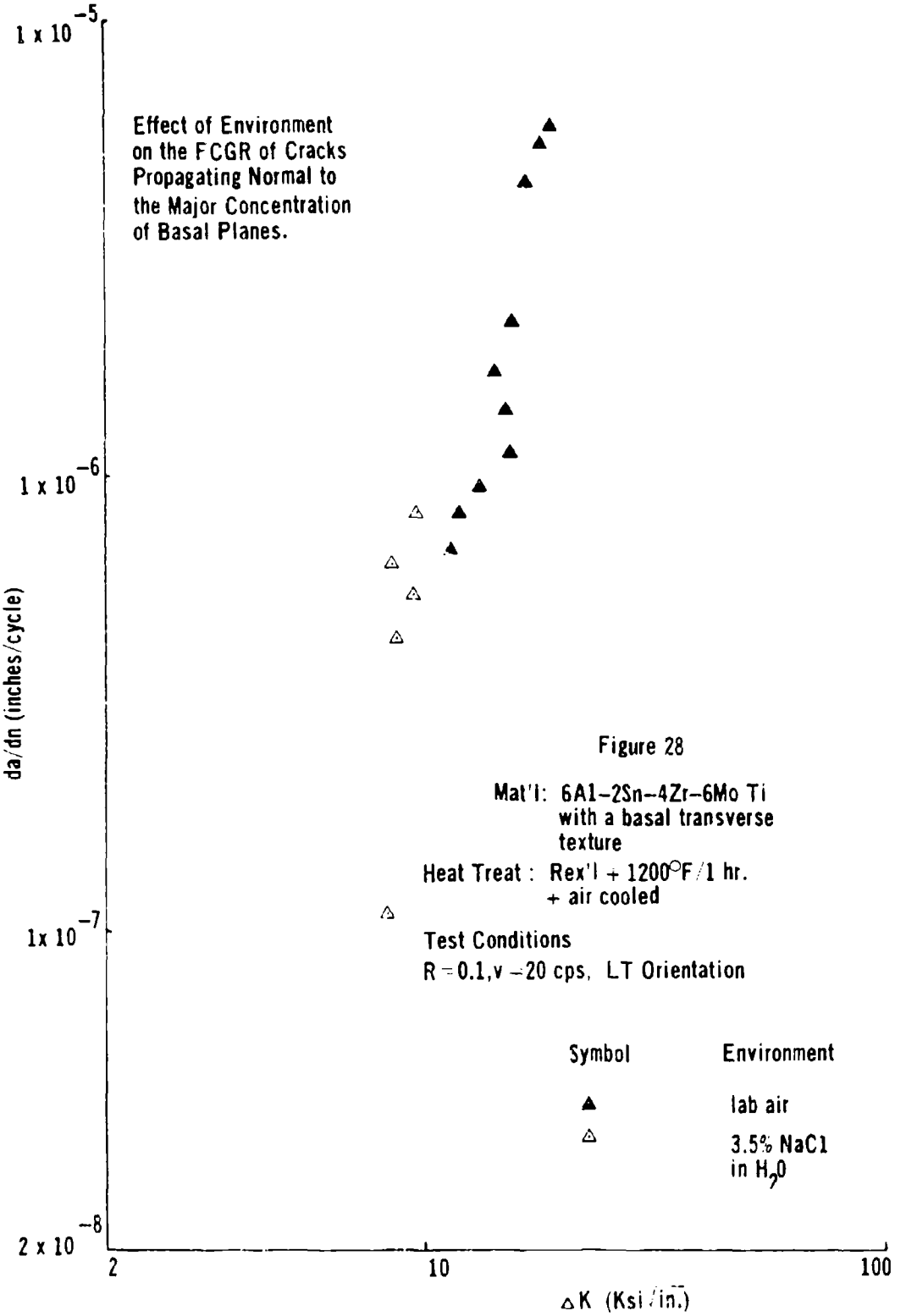
Effect of Environment on the FCGR of Cracks Propagating Normal to the Major Concentration of Basal Planes.
1 x 10^-5
1 x 10^-6
1x 10^-7
2 x 10^-8
da/dn (inches/cycle)
2
10
100
ΔK (Ksi √in.)
Figure 28
Mat'l: 6Al–2Sn–4Zr–6Mo Ti with a basal transverse texture
Heat Treat : Rex'l + 1200°F/1 hr. + air cooled
Test Conditions
R = 0.1, v – 20 cps, LT Orientation
Symbol
Environment
lab air
3.5% NaCl in H2O

DISCUSSION OF RESULTS

Several matters elucidated through our results require further discussion. These are:

- the relationship, if any between plane strain and mixed mode fracture toughness properties of titanium alloys as they are altered by metallurgical changes (alloy content, crystallographic orientation, etc.)
- the crystallographic dependence of fatigue crack growth rates in lab air and its interrelation to alloy chemistry.
- the strong interaction between opening mode crack growth on $(0001)_\alpha$ in salt water and final thermal practice in 6Al-4V Ti ELI Grade.

It is widely accepted in titanium alloy metallurgy that if one appreciably raises the oxygen level of an alloy such as 6Al-4V Ti (e.g., from say 0.095 wt% to 0.162 wt%) under conditions of constant microstructure its plane strain fracture toughness will significantly decrease. For example, Harrigan et al (Reference 5) showed the plane strain fracture toughness of equiaxed and recrystallized rolled 6Al-4V Ti products to decrease by 50% when the oxygen level of this basic alloy was raised from 0.12 wt% to 0.16 wt% in materials whose basal pole distributions were random.

Another generally accepted idea is that the plain strain fracture toughness of the 6Al-2Sn-4Zr-6Mo Ti alloy is significantly inferior to that of the 6Al-4V Ti alloy when both are compared possessing similar microstructures. Specific documentation for this general principle can be found by comparing the results of Harrigan et al. (Reference 5) in 6Al-4V Ti with those of Hall et al (Reference 11) for 6Al-2Sn-4Zr-6Mo Ti. Our current fracture toughness results expressed in terms of R-curves for slow stable tear under a mixed mode loading condition (i.e., a mixture of plane stress and strain states due to our sample geometry) are not wholly in keeping with the plane strain fracture toughness trends just reviewed. For example, slow stable tear in 6Al-4V Ti under mixed mode loading (see Figures 5 - 6 or Tables III and IV) is not sensitive to oxygen level in either test orientation. This appears to be true for both the K to initiate slow stable tear (Table IV) and the maximum K associated with this mode of tearing If one compares the initial slow stable tear resistance of 6Al-4V Ti and 6Al-2Sn-4Zr-6Mo Ti in Table III, one finds that in accord with the plane strain fracture experience reviewed earlier $K^{initial}$ for the latter alloy composition is appreciably lower than for the former. However, this accord with plane strain fracture behavior breaks down again in Table IV when results for the two major alloy compositions

are compared in terms of the maximum value of K for slow stable tear in each material.

The primary difference in stress state between plane strain and plane stress in a purely elastic material is the absence of a hydrostatic tension component in the latter case. Recall that in the case of plane strain (assuming Hookes law)

$$\sigma_{zz} = (\sigma_{xx} + \sigma_{yy})$$

of σ_{zz} is on the order of 2/3's of σ_{xx} and σ_{yy} in plane strain. Based on our current data, it appears that increasing the interstitial content of 6Al-4V Ti does not significantly reduce the metal's fracture toughness when the hydrostatic tension component of the elastic stress field surrounding the crack tip is small. As loads are applied to a crack in a metal, a plastic zone develops about the crack tip. At the onset of slow stable tear in a mixed mode increasing K situation, the crack advances, the plastic zone size increases and metal in the wake of the crack which was formerly plastic unloads. The first two procedures subtract energy from the applied strain field while the third event returns energy to the system. The mixed mode tear resistance in terms of K increases at first and then approaches an asymptotic value or steady state based on an energy balance of contributors and users. Thus, the high level of asymptotic tear resistance noted for 6Al-2Sn-4Zr-6Mo Ti reflects an increasing proportion of the total system energy being

devoted to plastic deformation ahead of the crack as K rises. This concept is supportable based on the relatively low K values for the onset of stable tear in 6Al-2Sn-4Zr-6Mo Ti irrespective of orientation noted above (Table III). and the lab air results in Figure 8. In Figure 8(a) and (b), one notes that crack growth on $(0001)_\alpha$ appears to result from a combination of cleavage faceting and ductile tear in our lab air static K experiment (K = 44 Ksi$\sqrt{in.}$). Alpha phase crystallography also plays a role here in that no crack growth could be induced on $(10\bar{1}0)_\alpha$ in a similar test at 50 Ksi$\sqrt{in.}$ (see Table V).

The R-curve results obtained in this work may have significance well beyond their value in reporting on the orientation dependence of fracture toughness in Ti pseudo single crystal alloys. Material selection, processing, and control for aerospace hardware designs are dictated in part by our knowledge of the variation of K_{IC} with alloy content and thermomechanical processing. If the design is such that fracture can be expected to occur in a plane strain mode, then choosing materials and processes to optimize K_{IC} is quite reasonable. If, however, structural arrangements are such that fracture occurs in a mixed mode situation, it is no longer clear that this approach is reasonable. For example, many aerospace designs employing 6Al-4V Ti call out the use of ELI Grade chemistry in fracture critical areas in order to provide for maximum plane strain toughness even though this

call out requires the user to pay a penalty in static tensile properties with respect to employment of the Standard Grade of this alloy. Since loss of static tensile properties generally results in heavier components, the penalty for the use of K_{IC} in the design selection process for structures that will fail in a mixed mode becomes very real. Certainly, this is a subject that is going to require more effort and attention in the future.

Current results indicate that opening mode fatigue crack growth rates in lab air on $(10\bar{1}0)_\alpha$ in 6Al-4V Ti are independent of interstitial content in the ΔK range 10 Ksi $\sqrt{in.}$ to 50 Ksi $\sqrt{in.}$ Moreover, lab air fatigue crack growth rates on $(10\bar{1}0)_\alpha$ in 6Al-2Sn-4Zr-6Mo Ti are similar enough at any given ΔK to their counterparts in 6Al-4V Ti to suggest that such crack growth on $(10\bar{1}0)_\alpha$ may also be independent of alloy chemistry over the entire alloy range investigated here (see Figure 29). This conclusion is also in concert with the fractographic morphology shown in Figures 12 - 14 for lab air prism plane cracking in these metals.

By contrast with prism plane fatigue cracking, opening mode fatigue crack propagation in lab air on $(0001)_\alpha$ is significantly different for the three alloy compositions investigated here (see Figure 30). One notes here that increasing the interstitial content of 6Al-4V Ti

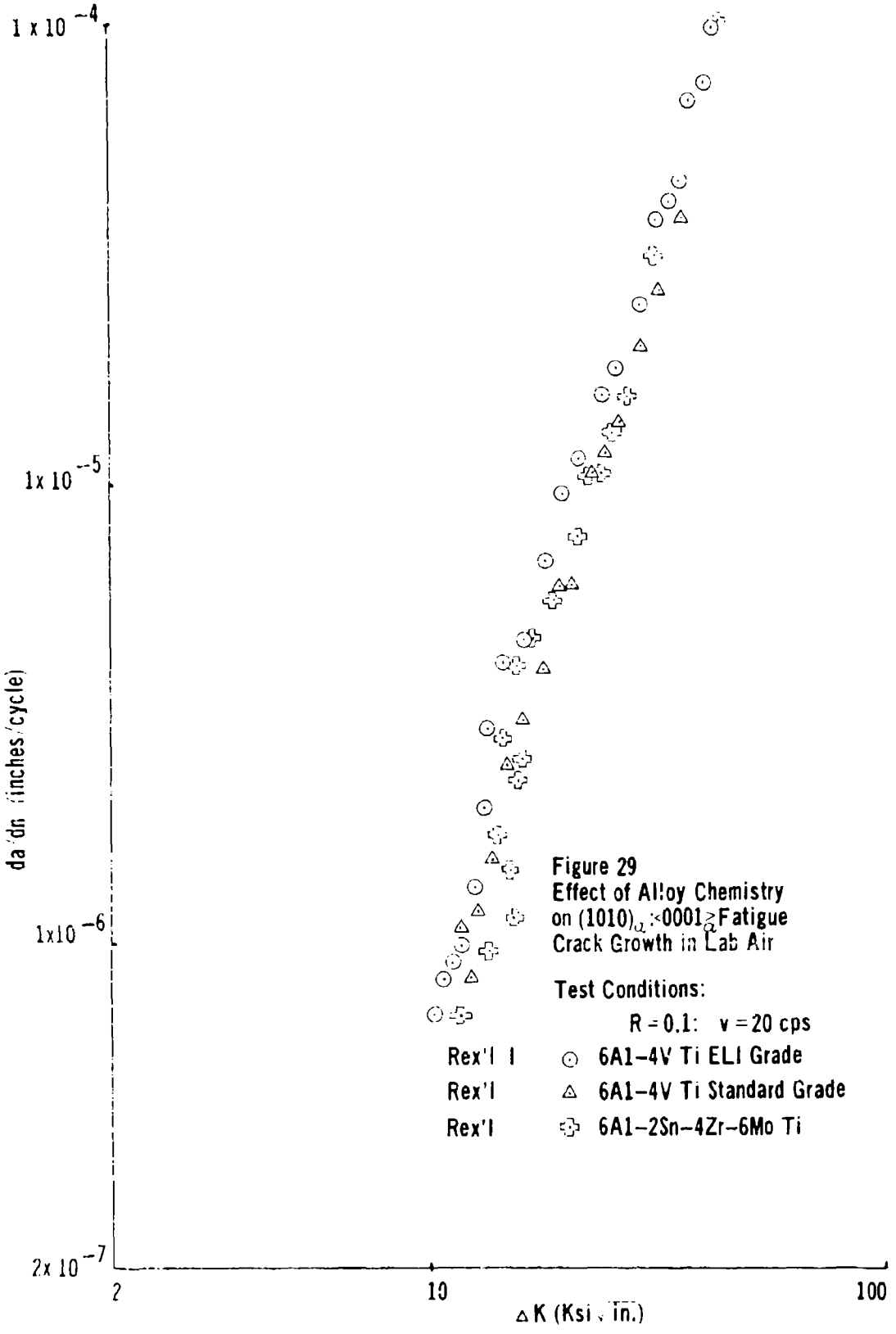

Figure 29
Effect of Alloy Chemistry on $(1010)_{\alpha}\langle 0001\rangle_{\alpha}$ Fatigue Crack Growth in Lab Air

produces a significant increase in da/dn at all values of ΔK on the basal plane. Also plotted here is the da/dn vs. ΔK relation developed in lab air for basal cracking in 6Al-2Sn-4Zr-6Mo Ti which appears to develop basal plane crack growth rates which fall in between those associated with the two grades of 6Al-4V Ti. It is tempting to assign the differences noted in Figure 30 to differences in alloy chemical composition. Support for a conclusion that the basal plane crack growth data spread in Figure 30 actually arises due to alloy chemistry differences can be found in our observations in Figures 12 and 14 wherein one notes that fractographically these diverse alloy compositions produce identical results. A common feature shared by the 6Al-4V Ti Standard Grade and the 6Al-2Sn-4Zr-6Mo Ti metals is that both materials have a higher content of alloy stabilizers dissolved in their respective alpha phases than do the ELI Grade Ti 6Al-4V alloy.

Macroscopic Alloy Chemistry	Approximate Alloy Chemistry of Alpha Phase (after a furnace cool from 1700°F)
6Al-4V Ti ELI Grade	6.6% Al + 0.10% O
6Al-4V Ti Standard Grade	6.6% Al + 0.175% O
6Al-2Sn-4Zr-6Mo Ti	7.0% Al + 2.3% Sn + 0.14% O

In this regard Lim, McMahon, Pope and Williams (Reference 12) have shown that the addition of oxygen to an 8% by wt Al-Ti binary

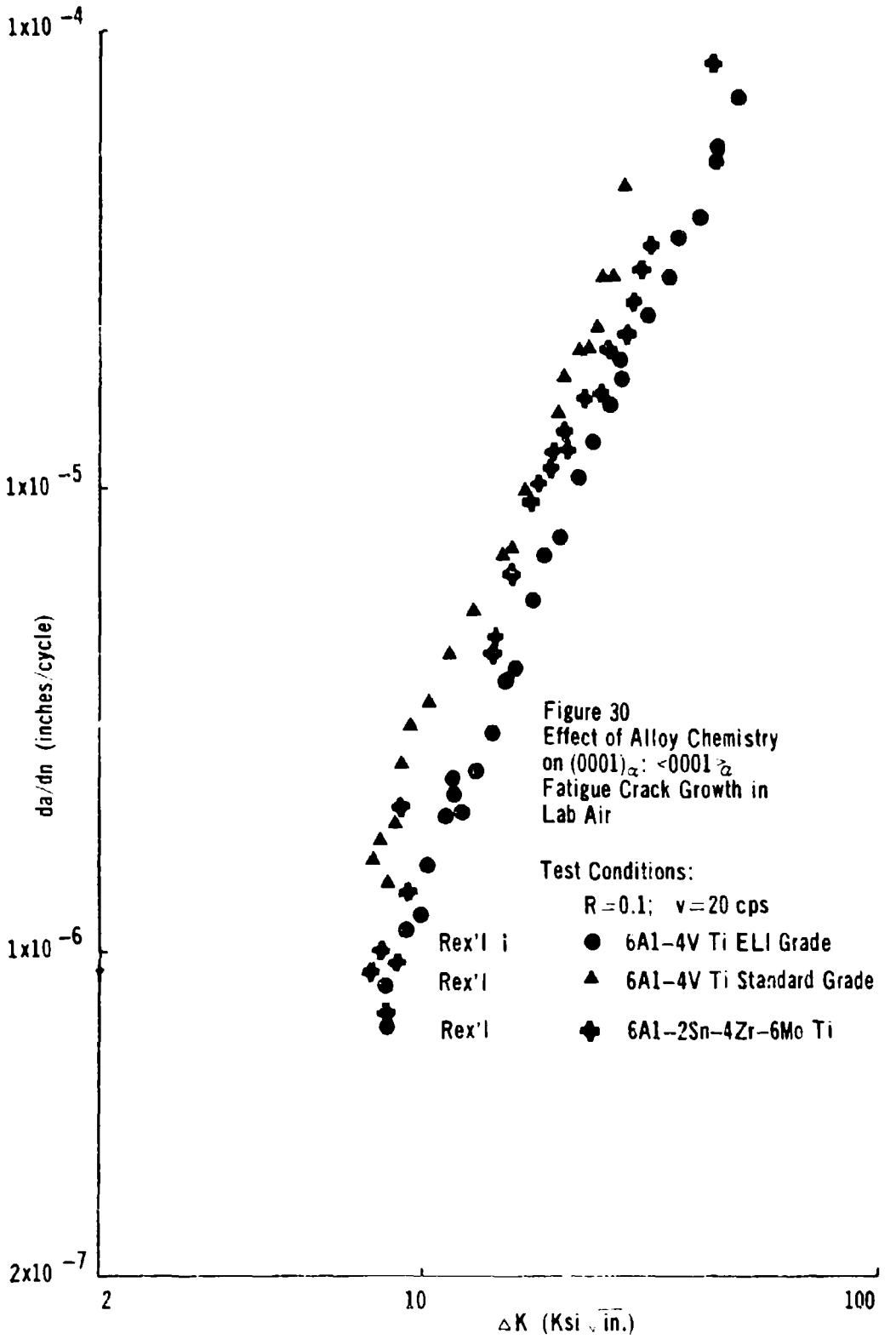

Figure 30
Effect of Alloy Chemistry on $(0001)_\alpha$: $<0001>_\alpha$ Fatigue Crack Growth in Lab Air

increases the thermal stability of the long range ordered phase, Ti_3Al. Moreover, Welsch et al (Reference 13) have observed finely dispersed α_2 (Ti_3Al) in a 6Al-4V Ti alloy containing 0.2 wt% oxygen after the metal was solution annealed at 1750°F and aged at 1025°F for several hours. Working with metal taken from the broken compact tension samples we used to generate Figure 30, S. Fujishiro (Reference 14) has examined all the three alloy materials employed in this research effort for evidence of super lattice reflections employing a standard thin film TEM technique. His work was to no avail in that he could not find any evidence of such long range ordered regions in any of the three Rex'l alloy compositions employed here. It is, however quite reasonable to assert that the more closely a given alloy phase chemistry approaches that associated with long range order, the more intense precursor short range ordering becomes (References 15 and 16). This is especially true since our metal samples have been slowly cooled (at less than 100°F/hour) through the temperature range (1400°F → 70°F) where long range order would have been introduced had our metal chemistries been slightly richer in alpha stabilizers. Invoking the concept of the short range ordering (sro) of alpha stabilizing constituents, one then can prognosticate that the degree of sro would be higher in the 6Al-4V Ti Standard Grade and 6Al-2Sn-4Zr-6Mo Ti compositions than it was in the 6Al-4V Ti ELI Grade. Since deformation occurs with less work hardening and

becomes more planar in ordered structures, one could forecast the fatigue crack growth rates to be faster at any given ΔK in the more ordered structure.

The results in Figure 30 were obtained after each of the 6Al-4V Ti alloy compositions were cooled at less than $100^{o}F$/hour to room temperature from their recrystallization temperatures (β_T-$50^{o}F$). Thus, each of these compositions should possess a substantially higher degree of sro than would say a similar material which was duplex annealed. If sro is playing a role in the growth rate stacking shown in Figure 30, one expects duplex annealing should decrease da/dn on $(0001)_\alpha$: $<10\bar{1}0>_\alpha$ during a lab air test. However, we have already reported that Rex'd and Duplex annealed versions of our 6Al-4V Ti ELI Grade metal produced the same da/dn versus ΔK relation on $(0001)_\alpha$: $<10\bar{1}0>_\alpha$ in lab air. Unfortunately, we did not duplex anneal the 6Al-4V Ti Standard Grade and repeat this critical test. There are three possible reasons why our data comparison for Duplex annealed and Rex'd processed 6Al-4V Ti ELI Grade showed no positive evidence with respect to the importance of sro. Firstly, sro is simply not an important causative factor in generating the da/dn stacking in Figure 30. Secondly, the maximum degree of sro possible in the specific composition we are dealing with in the ELI Grade alloy is small (6.0 wt% Al, 0.095 wt% O). Thirdly, sro alone is not responsible for the da/dn

acceleration noted in Figure 30 but its presence combined with another metallurgical factor are demanded in order that this acceleration occur. Some recent results of Lewis et al (Reference 17) suggest evidence that one good reason for the ELI Grade da/dn rates not showing a strong sensitivity to final thermal processing is that the degree of sro is not very large in this specific alloy composition in either heat treatment condition. Working with 6Al-4V Ti alloy plate containing 6.5 wt% aluminum and 0.2 wt% oxygen, they measured da/dn vs. ΔK relations for TL oriented samples in lab air as a function of heat treatment. These samples were recrystallized at 1775°F and then cooled at less than 100°F per hour to below 900°F. A portion of these samples were reheated to 1450°F, stabilized and air cooled. If one compares da/dn results at a ΔK of 14 Ksi $\sqrt{in.}$ for the material which was simply furnace cooled versus its duplex counterparts, he finds the furnace cooled metal cracking at a 10 times faster rate in lab air (2×10^{-5} inches/cycle versus 2×10^{-6} inches/cycle, respectively) for the test conditions R = 0.1 and ν = 20 cps. Although the basal pole texture of this material is not reported, these authors present fractographs taken from the da/dn samples in both heat treatment conditions at ΔK = 14 Ksi $\sqrt{in.}$ Both heat treatment conditions show very extensive cleavage faceting reminiscent of the current results in Figures 12 and 14 for "near basal" cleavage. It is not unreasonable, therefore, to assume that the metal in the

Lewis et al study probably was heavily basal transverse textured. Testing the TL orientation is thus equivalent to testing $(0001)_\alpha$: $\langle 10\bar{1}0\rangle_\alpha$. In the case of the Lewis et al study the extreme da/dn sensitivity to thermal processing may actually be due to the presence of α_2 in the furnace cooled metal rather than a higher degree of sro (with respect to its duplex annealed counterpart) based on the results of Welsch et al (Reference 13). Thus one could argue that the Lewis et al results support the concept that the growth rate stacking with alloy composition shown in Figure 30 for basal crack growth is caused by differing degrees of ordering.

However, sro or α_2 are three dimensional phenomena and if one alone were responsible for the alteration in growth rate with alloy composition shown in Figure 30, it would be very difficult to explain the prism plane cracking results presented in Figure 29 for the same three alloys where it is reasonable to conclude that the various materials' growth rates are not sensitive to alterations in alloy chemistry. In this regard, Powen (Reference 8) has shown that a major source of fatigue striation formation at high ΔK (>20 Ksi$\sqrt{\text{in.}}$) in both LT and TL orientations of basal transverse textured 6Al-4V Ti is $\{10\bar{1}1\}_\alpha/\{11\bar{2}2\}_\alpha$:$\langle 11\bar{2}3\rangle_\alpha$ or $\langle c+a\rangle_\alpha$ slip. Thus at high ΔK where growth rate differences exist between the various alloy compositions in Figure 30, the two sample orientations (TL & LT) even share a common slip system mechanism

which accounts for a major fraction of the crack advance we measured at any given ΔK. Thus, although sro may not be the sole cause of the differences seen in Figure 30, we shall show that it is a necessary but not sufficient condition for these differences.

In Figure 9, we note that $(0001)_\alpha : \langle 10\bar{1}0\rangle_\alpha$ or TL oriented growth for 6Al-4V Ti FLI Grade is only significantly faster than $(10\bar{1}0)_\alpha : \langle 0001\rangle_\alpha$ or LT oriented growth at a ΔK below 12 Ksi $\sqrt{in}$. A comparison of Figures 12(a) and 13(a) suggests a change in fracture mode from a major fraction of the crack advance occurring in a "near basal" cleavage mode at low ΔK where the TL growth was accelerated with respect to LT striated fatigue of the type analyzed by Bowen (Reference 8) at high ΔK. "Near basal" cleavage cracking also was the predominant mode of crack advance on $(0001)_\alpha : \langle 10\bar{1}0\rangle_\alpha$ oriented samples in 6Al-2Sn-4Zr-6Mo Ti at low ΔK (see Figure 14(a)). Thus, one of the contributors to the differences in fatigue crack growth rates noted in Figures 9-11 between TL and LT oriented samples at low ΔK is the occurrence of extensive "near basal" cleavage in the former orientation.

Having identified "near basal" cleavage as one source of lab air fatigue crack growth acceleration (with respect to $(10\bar{1}0)_\alpha : \langle 0001\rangle_\alpha$ fatigue crack growth), another chemical difference between the three major alloy compositions employed in this work takes on new significance and should be considered. The hydrogen contents of these three materials is also different.

Variation of Hydrogen Content
With Alloy Type

Alloy Type	Hydrogen Content (ppm by wt.)
6Al-4V Ti ELI Grade	20
6Al-4V Ti Standard Grade	44
6Al-2Sn-4Zr-6Mo Ti	68

In this regard, Meyn (Reference 10) has shown slow stable tear in 6Al-4V Ti plate to be a function of the hydrogen content of the metal. These observations were made in lab air under static loading. Fractographically, he reported that the major mechanism for his observed slow stable tear was "near basal" cleavage. Moreover, the aluminum, hydrogen and oxygen levels employed in his work covered the range of chemical compositions studied here. Let us assume for a moment that the "near basal" cleavage observed in Figures 12(a) and 14(a)-(b) is caused by the presence of hydrogen in the alpha phase. Incidentally the hydrogen level in the Lewis et al metal was 59 ppm by wt. Furthermore, recognizing that the hydrogen content of the 6Al-2Sn-4Zr-6Mo Ti is appreciably higher than its 6Al-4V Ti counterpart and yet the Standard Grade 6Al-4V Ti cracks more rapidly in Figure 30, then the presence of hydrogen in the overall alloy can again be assumed to be a necessary but not sufficient condition for da/dn acceleration. In this case, acceleration is defined with respect to what that growth rate would be if fatigue crack advance took place at low ΔK (Figure 12(a) and Figure 14(a) & (b)) as it does above $\Delta K = 17$ Ksi $\sqrt{in}$. (Figure 13(a)) where the dislocation slip and twinning mechanisms described by Bowen (Reference 8) apply. Schematically the da/dn versus ΔK relations hypothecated here are as follows:

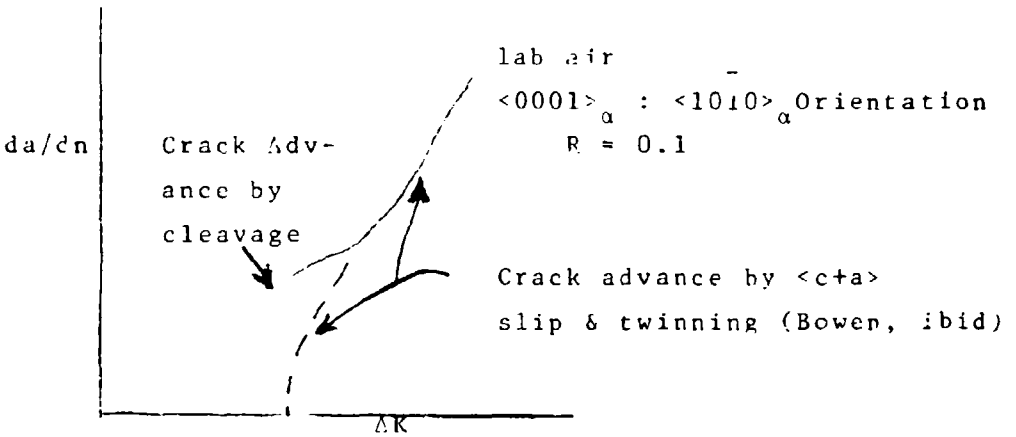

At this point in our deliberations it appears reasonable to state that there is a moderate amount of circumstantial evidence that sro and the alloy's hydrogen content are able to combine in some as yet undefined manner to cause lab air crack growth acceleration at low ΔK on $(0001)_\alpha$ in the nominal $<10\bar{1}0>_\alpha$. In order to appreciate how important these two factors are in controlling fatigue crack acceleration by "near basal" cleavage, let us review the results we obtained as a function of heat treatment in salt water with TL oriented samples. In a salt water environment, we have shown that a majority of the da/dn acceleration at low ΔK on $(0001)_\alpha$: $<10\bar{1}0>_\alpha$ present when samples of 6Al-4V Ti ELI Grade were slowly cooled from 1700°F to room

temperature (at <100°F/hour) can be removed when this same material is simply reheated to 1400°F held for one hour and cooled at a rate exceeding 2000°F/hour (see Figure 20). It should be recalled here that the additional heat treatment given the metal in the latter case did not change either its textural intensity or tensile properties (with respect to the furnace cooled metal). From the viewpoint of alpha phase chemistry, the slowly cooled metal is expected to be slightly richer in aluminum and oxygen content and slightly deficient in vanadium with respect to its duplex annealed counterparts. Considering the strong degree to which aluminum and oxygen partitions to the alpha phase and vanadium partitions to the beta phase at 1400°F, differences in the chemical consituent makeup of the α phase in the two heat treatment conditions employed here are expected to be quite small. This ascertion finds support in the fact that the tensile properties after either of the two heat treatments were identical. Based on the previously cited results associated with the stability and occurrence of long range ordering of Al and O in Ti-Al-V alloys (References 12 and 13), one factor which should have undergone a major change as a result of duplex annealing a previously furnace cooled metal is the degree to which Al and O are short range ordered. In the case of the duplex annealed metal, one expects the degree of sro

to be quite small compared to the sro state of the furnace cooled material.

Besides the difference in the degree of sro between the duplex annealed material and the furnace cooled metal, there must be another factor required to cause the metal to cleave in a "near basal" mode in salt water. Recall that it was shown earlier that the fractographic:metallographic crack paths in salt water were identical in the two 6Al-4V Ti ELI Grade heat treatment conditions (i.e., "near basal" cleavage). "Near basal" cleavage was also an important contributor* to crack advance at low ΔK when TL oriented samples were fatigue tested in lab air in either of the two heat treatment conditions. However, in the case of our lab air results, no difference in crack growth rate at any ΔK was discernible when Rex'l I and duplex annealed 6Al-4V Ti ELI Grade products were compared at any ΔK. A major difference between the 6Al-4V Ti ELI Grade da/dn

---

*as Bowen (Reference 8) points out for 6Al-4V Ti ELI Grade metal, crack growth advance in TL oriented samples of basal transverse textured metal at ΔK's > 17 Ksi $\sqrt{in.}$ is a complex admixture of $\{11\bar{2}1\}$ twinning and <c+a> slip. At significantly lower ΔK in lab air, we find "near basal" cleavage playing a large role as well but some fraction of crack advance continues to occur via Bowen's previously identified mode. Compare Figures 12(a) and 14(a) & (b) with Figure 13(a).

tests conducted in lab air and salt water was the amount of hydrogen available to enter the plastic zone surrounding the propagating crack. Essentially the salt water environment represents an extremely large source of hydrogen compared with the 20 ppm of hydrogen that was available when this metal cracked in lab air. It is for this reason probably that vacuum degassing the 6Al-4V Ti ELI Grade metal produced no further decrease in the metals da/dn rate in salt water (see Figure 21). Based on the present effort, one can postulate, therefore, that if a substantial quantity of hydrogen is present in the 6Al-4V Ti alloy, the fractographic result expected upon the application loads normal to $(0001)_\alpha$ is "near basal" cleavage. Fractographically, our lab air da/dn samples showed "near basal" cleavage to cover a major fraction of Figures 12(a) and 14(a) & (b). By contrast in Figure 18, evidence of all other fracture modes are gone and the fracture face consists of 100% "near basal" cleavage. This alteration provides additional support to the concept that one role of the saline solution is to supply large quantities of hydrogen to the crack tip plastic zone. In agreement with this postulate connecting hydrides and "near basal" cleavage Paton and Spurling (Reference 18) have shown that in a Ti-6.6 wt% Al binary alloy, low hydrogen supersaturation concentration (at least down to 100 ppm by wt.) will lead to hydride platelet precipitation on the basal plane. Moreover, such hydride precipitation will occur preferentially in the area of high residual stress. The fracture of such hydride particles,

habited on the basal plane as it were, would be expected to occur by a cleavage mode.

A major question still remains as to why the presence of a significantly higher degree of sro in the slowly cooled metal should result in such a large degree of crack growth acceleration in salt water (and/or lab air, if one considers the Lewis et al results as well) if the principal fractographic mode is "near basal" cleavage in both heat treatment conditions. A possible answer to this question is suggested by Paton and Spurling's observation that in order to precipitate a hydride platelet on the basal plane, basal slip bands are formed which emanate from the tips of these platelets "in order to provide an accomodation mechanism for the large (~18%) misfit of the hydrides in their titanium matrix." If the degree of local or short range order is high enough, the ability of these accomodation basal slip bands to form is restricted, Since a Ti hydride platelet is ~18% larger by volume than the alpha phase matrix in which it must form, restricting or preventing the formation of accomodation basal slip bands at the edge of the platelets leaves the lattice badly distorted in this region. Moreover, the distortion of the alpha phase matrix at the platelet edge takes the form of residual tension normal to the basal plane (balanced by compression on the face of the particle). A crack approaching such a configuration is accelerated through this region because relief of this lattice distortion will act as an additional source

of crack propagation energy (over and above that supplied by the externally applied strain field).

The above hypothesis emphasizes that fatigue crack growth rate acceleration on $(0001)_\alpha$ in both salt water and lab air in $\alpha + \beta$ alloys requires the simultaneous presence of both hydrogen and some reasonable degree of short range order in the α phase. While substantial evidence now exists to support this thesis, several experiments come to mind which should be done to continue to build confidence in this crack growth acceleration mechanicsm.

- Lab air da/dn tests in alpha rich Ti alloys on $(0001)_\alpha$: $\langle 10\bar{1}0\rangle_\alpha$ as a function of oxygen level aluminum level, hydrogen level and the degree of sro (e.g., as can be varied by duplex annealing).
- Salt water environmental testing of $(0001)_\alpha$: $\langle 10\bar{1}0\rangle_\alpha$ fatigue crack growth rates as a function of degrees of sro at oxygen and aluminum levels equivalent to those employed here in 6Al-4V Ti Standard Grade, etc.

It should be noted that since sro plays an important role in this hypothesis, one should not be surprised if the minimum stabilization temperature in the duplex anneal (i.e., 1400°F in the case of 6Al-4V Ti ELI Grade) required to minimize the rate of "near basal" cleavage varied with alloy chemistry (i.e., oxygen level, aluminum level, etc.). For example, 6Al-2Sn-4Zr-6Mo Ti in this study was stabilized at 1200°F prior to rapid cooling. This stabilization

temperature was chosen based on William's observation that this is the lowest temperature at which any α_2 present in the alloy from the previous heat treatment step of slow cooling from 1700°F will rapidly dissolve (J. C. Williams, Carnegie-Mellon University, Private Communication, 1976). As Christian points out, however, sro can be very intense just above the order:disorder transformation temperature (Reference 16). Thus, although the 6Al-2Sn-4Zr-6Mo Ti was subjected to a "duplex" heat treatment, the stabilization temperature in the treatment was such as to magnify the rate of growth of a "near basal" cleavage crack under the proposed hypothesis rather than minimize it. Of course, one expects that the worst possible case here would be one where α_2, itself, was extensively present and hydrogen was available at the crack tip as could well have been the case in the Lewis et al study.

Completer verification of our proposed model for the acceleration of "near basal" cleavage fatigue crack growth has real practical as well as academic importance at this time. Firstly, from an engineering data perspective, this form of accelerated growth is the only significant type available in equiaxed two phase $\alpha + \beta$ microstructures. Recall, that fatigue growth on $(10\bar{1}0)_\alpha : \langle 0001 \rangle_\alpha$ for example, is quite insensitive to the details of alloy chemistry and thermal practice in lab air and only mildly so in salt water when compared to the alterations possible on $(0001)_\alpha \langle 10\bar{1}0 \rangle_\alpha$ oriented

samples when these same parameters are varied. Secondly, a significant fraction of aerospace Ti hardware is fabricated such that it is used in a slowly cooled $\alpha + \beta$ equiaxed condition (from above 1300 ^{o}F). Moreover, current specification requirements for hydrogen content are set at 125 ppm by weight as a maximum (i.e., well in excess of the level of hydrogen present in any of the metals studied here) and no controls exist with respect to the allowed intensity of preferred basal poles. Trends toward the use of such slowly cooled metal are increasing with the introduction of such cost saving manufacturing processes as diffusion bonding, superplastic forming and isothermal forging. The common denominator of all three of the above processes is that they are used to generate precisely dimensioned structural components at elevated temperatures (in the case of 6Al-4V Ti, at >>1300^{o}F). Since rapidly cooling precisely dimensioned structural components or "net parts" requires expensive tooling if extensive warpage is to be avoided, the aerospace industry is going to be loathe to consider such an additional thermal process step unless sufficient incentive is provided. A potential method for avoiding the need to rapidly cool a reasonable fraction of such hardware would be to vacuum anneal the raw stock at about 1550^{o}F prior to producing the "net shape" assuming the material's hardware useage would not involve exposure to saline water. Requiring Ti raw material producers to supply metal with a

random array of basal poles represents only a partial solution to the problem of da/dn acceleration assuming the producers know how to do this on a commercial basis and were willing to guarantee such a product. This approach would certainly lessen the da/dn acceleration observed in slow cooled metal by averaging rates on the prism and basal planes in some complex fashion but should not be expected to remove it.

Let us turn our attention to fatigue crack growth on $(10\bar{1}0)_\alpha$: $\langle 0001 \rangle_\alpha$ in lab air. As noted earlier in connection with Figure 29, fatigue crack growth over the ΔK range 10 Ksi $\sqrt{in.}$ - 45 Ksi $\sqrt{in.}$ is relatively insensitive to alloy chemistry details. This result is in keeping with Bowen's approach (Reference 8) that crack growth above 20 Ksi $\sqrt{in.}$ can be accounted for in terms of a combination of $\langle c+a \rangle_\alpha$ slip generating striated fatigue and monotonic fracture (ductile tear and shear). Essentially our crack growth and fractographic results extend Bowen's hypothesis to crack growth rates which are a factor of 10 lower than his observations. Of importance here is the point that forcing a significant portion of the crack advance to occur monotonically at da/dn rates as low as 7×10^{-7} inches/cycle (see Figure 12(b)) should lead to this orientation exhibiting a higher ΔK threshold level than would otherwise be expected if crack advance was totally striated as was argued in the Introduction of Part III. A higher ΔK threshold, in turn,

should result in this orientation exhibiting a higher degree of fatigue crack growth retardation during variable load amplitude testing for reasons cited earlier than would orientations where growth occurs in a totally striated fashion.

One of the more surprising observations in this study was the incidence of some type of prism cleavage at low ΔK in salt water (see Figure 25). This cleavage did not appear to cause any major acceleration of crack growth which, in turn, varied as a function of final thermal processing or alloy chemistry at least based on the preliminary observations made during the current study. At high ΔK in salt water, this orientation exhibited striated fatigue (see Figure 26) and thus one can state that whatever mechanism generates this type of cleavage failure, it is only important at low ΔK and only generates a modest degree of acceleration with respect to lab air da/dn data. Certainly more effort is needed here as well.

Finally, some comments should be offered with regard to the frequency dependence of the fatigue crack growth rates we

observed in both test orientations in saline water. As Dawson and Pelloux point out the shift of growth rate with frequency (say from 20 hertz to 2 hertz) is complex (Reference 9). The results we obtained here for both test orientations in terms of the shift of growth rate with frequency alteration in salt water agree rather well with their earlier results. This is rather impressive since the mechanisms controlling the acceleration (salt water vs lab air) we observed in the two orientations are more than likely governed by different microscopic processes once the ΔK frequency;conbination is such that the Dawson and Pelloux "passivating film" remains ruptured throughout a majority of the load cycle.

In discussing our current results for fatigue crack growth on $(0001)_\alpha : \langle 10\bar{1}0 \rangle_\alpha$, we proposed that the same model for "near basal" cleavage governed growth rate accelerations in lab air and salt water. In this model, the saline environment played an important role as a source of hydrogen which could readily be diffused into the plastic zone at the crack tip and thus effectively raise the hydrogen concentration of the metal on a local basis. In the lab air tests, the only source of hydrogen is whatever is dissolved in the metal to start. Unfortunately no da/dn tests were run as a function of load cycle frequency in lab air in this effort to

determine whether a comparable shift in crack growth on $(0001)_\alpha$: $\langle 10\bar{1}0\rangle_\alpha$ exists in lab air with alterations in load cycle frequency. It should be recalled that enough Ti alloy da/dn testing has been done by various investigators over an extensive period of time that it is generally accepted that shifts in da/dn with load cycle frequency alterations will be small in lab air (compared to what is observed from time to time in salt water), if they exist at all. If the proposed model of "near basal" cleavage crack growth acceleration does apply equally in lab air and a saline environment, one must explain why the da/dn frequency shift in an enert environment such as lab air would be expected to be much smaller than is observed in an aqueous saline environment. In this regard, if one tests in lab air, the only hydrogen participating in the process is already dissolved in the metal. At $70^{\circ}F$ hydrogen can diffuse on the order of a 0.1μ per second in pure titanium (Reference 19) or more than 3 times the rate of crack advance for the conditions of 20 cps and 1×10^{-6} inches/cycle. Thus, dissolved hydrogen should be readily available to the crack tip. In the case of salt water testing, the saline solution is expected to supply a large quantity of hydrogen according to our model. The large da/dn frequency shifts observed in salt water could well be tied up with the rates at which one or more of the various chemical/electrochemical processes occur which control liberation of hydrogen, diffusion of it through the liquid phase, absorption

of it at liquid:metal interface, etc. Finally, some data do exist which suggests that there is a modest shift in da/dn in lab air with frequency for $(0001)_\alpha$: $\langle \bar{1}2\bar{1}0 \rangle_\alpha$ oriented samples. Working with part through cracked samples of strongly basal transverse textured 6Al-4V Ti in high humidity air (>85%), Pettit et al (Reference 2) reported at a ΔK = 10 Ksi$\sqrt{in}$. that da/dn in humid air shifted from 7×10^{-7} inches/cycle at 10 hertz to 4×10^{-6} inches/cycle at 0.1 hertz (R = 0.1). The metal contained 100 ppm of hydrogen.

CONCLUSIONS

(1) Crack growth velocities induced by either static or fatigue loading in recrystallized 6Al-4V Ti and 6Al-2Sn-4Zr-6Mo Ti alloys are a strong function of alpha phase crystallography, final thermal practice and detailed alloy chemistry.

(2) Working with strongly basal transverse textured versions of both generic alloy compositions, two crystallographically distinct modes of cleavage fracture have been identified during fatigue at low ΔK. These are (1) the well known "near basal" cleavage and (2) cleavage on or near the prism plane of the alpha phase.

(3) The velocity of cracks propagating via a "near basal" cleavage mode is very sensitive to minor changes in final thermal processing and alloy chemistry. Combinations of such small changes can alter the observed crack growth rates by a factor of 100 during fatigue in 3.5% NaCl in H_2O.

(4) In contrast to the extreme velocity sensitivity of "near basal" cleavage to minor metallurgical changes, prism cleavage is virtually insensitive to such changes.

(5) "Near basal" cleavage could be readily induced by statically loading a cracked $(0001)_\alpha$: $<10\bar{1}0>_\alpha$ oriented sample of either 6Al-4V Ti or 6Al-2Sn-4Zr-6Mo Ti in 3.5% NaCl in H_2O. The same fracture mode also occurred during the static loading of similarly oriented samples of 6Al-2Sn-4Zr-6Mo Ti in lab air.

(6) Prism cleavage was never observed during static loading of cracked $(10\bar{1}0)_\alpha$: $<0001>_\alpha$ oriented samples of either alloy in this program in either lab air or 3.5% NaCl in H_2O. In fact, cracks could not be induced to grow statically in this orientation in either alloy in lab air or 3.5% NaCl in H_2O even at loadings equivalent to 80% of their mixed mode fracture toughness.

(7) A model is proposed to account for "near basal" cleavage crack growth observed under static and fatigue loadings in lab air and 3.5% NaCl in H_2O environments which predicts that the velocity of such "near basal" cleavage cracks is a product of:

f (hydrogen concentration) X g (short/long range ordering of Al and O in the alpha phase)

(8) The metallurgical origins of prism cleavage are unclear at this time. Prism cleavage has been observed during the 3.5% NaCl in H_2O fatigue crack growth testing of 6Al-4V Ti and in lab air during similar tests with 6Al-2Sn-4Zr-6Mo Ti. In no case when it was observed was there any marked acceleration of crack growth rate associated with its occurrence.

(9) From an engineering perspective, if our "near basal" cleavage model is correct and there truly is a strong dependence of "near basal" cleavage velocities on degree of short/long range Al + O ordering in the alpha phase, then one expects the fatigue crack growth rates (in lab air and salt water) of all $\alpha + \beta$ Ti alloys will be very sensitive functions of the final cooling rate the product sees the last time it is heated to a temperature in the range $1000^{\circ}F$ - $1300^{\circ}F$ as has been seen here in the case of 6Al-4V Ti ELI Grade. For example, this alloy composition cracked 10 times faster at 2 hertz in 3.5 NaCl in H_2O when it was furnace cooled through this temperature region ($<100^{\circ}F/hr.$) than when it was air cooled through this same temperature range ($>2000^{\circ}F/hr.$).

(10) Several new cost saving Ti fabrication methods (diffusion bonding, superplastic forming and isothermal forging) effect their cost saving by producing a virtually "net part" through metal flow above 1400°F in the case of 6Al-4V Ti. These parts are then slowly cooled in their tooling to room temperature and then used in this final heat treatment state. Recognizing the potential problems that could arise as these novel manufacturing practices are adopted for use in the aerospace industry, recommendations are presented for their avoidance and specific tasks are suggested for research in this important area.

REFERENCES

1. J. C. Chesnutt, J. D. Frandsen, A. W. Thompson; "Influence of Metallurgical Factors on the Fatigue Crack Growth Rate in Alpha-Beta Ti Alloys" Interim Reports on USAF Contract F33615-74-C-5067, 1974 - present.

2. D. E. Pettit, W. E. Krupp, J. T. Ryder and D. W. Hoeppner; "Investigation of the Effects of Stress and Chemical Environments on the Prediction of Fracture in Aircraft Structural Materials" AFML-TR-74-183, Dec., 1974.

3. L. R. Hall, R. W. Finger and W. F. Spurr; "Corrosion Fatigue Crack Growth in Aircraft Structural Materials", AFML-TR-73-204, Sept., 1973.

4. G. R. Yoder, L. A. Cooley and T. W. Crooker; "A Transition to Enhanced Fatigue Crack Propagation Resistance in a β-Annealed Ti 6Al-4V Alloy of Commercial Purity", Second Int'l Conf. on Mech. Behavior of Materials, Boston, Mass.; 16-20 Aug., 1976.

5. M. J. Harrigan, M. P. Kaplan, and A. W. Sommer, Fracture Prevention and Control", D. W. Hoeppner, Editor, Mater./ Metalwork Tech. Ser., No. 3 ASM, 1974, pg. 225.

6. M. J. Blackburn and J. C. Williams; "Metallurgical Aspects of SCC in Ti Alloys" Ohio State University Conference on Fundamentals of SCC, Col. Ohio, 1967.

7. M. J. Harrigan, A. W. Sommer, P. A. Reimers and G. A. Alers; "The Effect of Rolling Texture on the Fracture Mechanics Properties of 6Al-2Sn-4Zr-6Mo Ti Alloys", 2nd Int'l Conf. on Titanium, May, 1972; Plenum Press, N.Y., N.Y., J. Jaffee and H. Burte, Editors.

8. A. W. Bowen; "Some Relationships Between Crystallography and Stage II Fatigue Crack Growth in a 6Al-4V Alloy" Royal Aircraft Establishment Tech. Rep't 74132; Farnborough, U.K., Nov., 1974.

9. D. B. Dawson and R. M. Pelloux; Met. Trans 5; 723; Mar., 1974.

10. D. A. Meyn; Met. Trans., 5, 2405, Nov., 1974

REFERENCES (Cont.)

11. J. A. Hall, C. M. Pierce, D. L. Ruckle and R. A. Sprague; Mat. Sci, Eng.; 1972, 9, pg. 197-210.

12. J. Y. Lim, C. J. McMahon, Jr., D. Pope and J. C. Williams, Met. Trans.; 1976, 78, pg. 139.

13. G. Welsch, G. Lutjering, K. Gazioglu, and W. Bunk; Presentation to Fall AIME Meeting, 1976 entitled "Mechanical Properties Correlated to Microstructural Phenomena of Age Hardened 6Al-4V Ti," Neagara Falls, N. Y., Sept., 1976.

14. S. Fujishiro; AFML/WPAFB, Private Communication, June, 1976.

15. R. A. Swalin; Chap.9 in "Thermodynamics of Solids"; John Wiley and Sons; 1962.

16. J. W. Christian; Chap. 6 in "The Theory of Transformation in Metals and Alloys", Int'l Series of Monographs on Metal Physics and Physical Metallurgy"; Pergamon Press, London, England; 1965.

17. R. E. Lewis, J. G. Bjeletich, T. M. Morton and F. A. Crossley; ASTM STP 601, 371, June, 1976.

18. N. E. Paton and R. A. Spurling, "Hydride Habit Planes in Titanium-Aluminum Alloys:, Rockwell Int'l Science Center, Thousand Oaks, Ca; Submitted to Met. Trans., April, 1976.

19. P. Tung and A. W. Sommer, Acta Metallurgica 22, 191, 1974